NISTIR 6399

Deterioration of Iowa Highway Concrete Pavements: A Petrographic Study

FINAL REPORT
HR-1065

Paul E. Stutzman

Building and Fire Research Laboratory
Gaithersburg, Maryland 20899

NIST

United States Department of Commerce
Technology Administration
National Institute of Standards and Technology

NISTIR 6399

Deterioration of Iowa Highway Concrete Pavements: A Petrographic Study

Paul E. Stutzman

December, 1999

Building and Fire Research Laboratory
National Institute of Standards and Technology
Gaithersburg, MD 20899

National Institute of Standards and Technology
William M. Daley, *Secretary*
Technology Administration
Dr. Cheryl L. Shavers, *Under Secretary of Commerce for Technology*
National Institute of Standards and Technology
Ray Kammer, *Director*

Executive Summary

Major highway concrete pavements in Iowa have exhibited premature deterioration. The cause(s) of the deterioration has been the subject of much controversy. Various investigators have used different methods to characterize the processes and have arrived at different interpretations. The deterioration has been attributed to effects of ettringite formation (including delayed ettringite formation), alkali-silica expansive reactions, and to frost attack, or some combination of them. Evidence for all three processes have been reported. While one or more of these processes is likely to be the cause of the deterioration, the possibility that there may be other deleterious processes should be considered.

Highway pavements included in this study were constructed in the mid-1980s as non-reinforced, dual-lane, roads ranging in thickness between 200 mm and 300 mm, with skewed joints reinforced with dowels. Deterioration was initially recognized with a darkening of joint regions, which occurred for some pavements as soon as four years after construction. Pavement condition ranges from severe damage to none, and there appeared to be no unequivocal materials or processing variables correlated with failure.

Based upon visual examinations, petrographic evaluation and application of materials models the deterioration of concrete highway pavements in Iowa appear related to a freeze-thaw failure of the coarse aggregate and mortar. For concrete cores extracted from sections showing no apparent, to minor damage, cracking is initially noted in the coarse aggregate, and then in the mortar. Crack patterns sub-parallel to the concrete surface transecting the mortar fraction and the coarse aggregate are indicative of freeze-thaw damage.

The entrained air void system was marginal to substandard, according to guidelines in ACI 212.3R (Chapter 2), and filling of some of the finer-sized voids by ettringite further degraded the air void system. The filling increases the void spacing factor and decreases specific surface values beyond those considered necessary for concrete to have adequate durability when exposed to freeze-thaw conditions. The formation of secondary ettringite within the entrained air voids probably reflects a relatively high degree of concrete saturation causing the smaller voids to fill with pore solution when the concrete freezes.

Freeze-thaw cracking of aggregate may be related to both the high degree of saturation and the loss of the adjacent air void system as no correlation between aggregate texture and cracking was noted. Modeling simulations of deterioration processes indicate that cracking may be explained by both aggregate and paste expansions.

The original air void system parameters generally appear to be uniform from top to base of the concrete. The excessive vibration, considered by some to be contributory [9], appears to not have adversely affected the entrained air void system. Specimens taken from the visible "vibrator trails", which mark the insertion points of an immersion probe vibrator, show a marked increase in the air void spacing factor to a depth of about 15 cm.

Measurement of the void filling shows it to be either uniform or, in some cases, increasing with depth, suggesting that the degradation is not a “top down” process by infiltration of gypsum-contaminated road salt solutions. These trends may also reflect an influence of surface drying and / or a source of water at the base of the slabs.

Microcracking is common in most of the cores occurring as vertical surface cracks extending 10 mm to 20 mm into the core. These cracks may be found both exclusively in the cement paste and also in the paste and coarse aggregates, and may be drying shrinkage-related and / or due to freeze-thaw cycling. Cracks along the vibration trails appear to be drying shrinkage cracks resulting from increased shrinkage potential of the mortar-rich vibration trail regions relative to the bulk concrete.

Other failure processes proposed include alkali-silica reaction (ASR) and delayed ettringite formation (DEF). ASR affects the shale and an occasional quartz sand grain in the fine aggregate, but is not deemed to be a significant cause of the deterioration. The field survey found no evidence of permanent expansion such as closure of joints, blowups, nor gel efflorescence. Significant cracking associated with ASR may occasionally be found when large (5mm) shale aggregates are located in the upper-most 20 mm of the concrete. Delayed ettringite formation was not deemed likely as no evidence of a uniform paste expansion away from aggregates was observed, no massive agglomerations of ettringite in the paste, near aggregates, or in cracks, and no filling of the capillary pore system was observed. The lack of observed expansion, as mentioned above, is also evidence against this mode of deterioration.

The utilization of fly ash does not appear to have affected the deterioration as all pavements with or without fly ash exhibiting substantial damage also exhibit significant filling of the entrained air void system, and specimens containing fly ash from sound pavements do not have significant filling.

US 20 pavements are among some of the best and worst performing pavements in this study. A set of specimens, reportedly containing the same materials (including fly ash) and the same mix design, exhibit opposite performance. Cores from the undamaged stretch of the road appear to have a smaller coarse aggregate maximum size and a more uniform aggregate gradation. These cores contain an entrained air content almost double, and a spacing factor half that of the failed pavement. The additional air volume may account for the improvement in spacing factor and resulted in an air system adequate for freeze-thaw protection. However, specific surface values still indicate a coarse-sized entrained air void system. The change in aggregate gradation may have altered the mixture rheology facilitating development of an improved entrained air void system.

The influence of the mixture design, mixing, and placing must be evaluated with respect to development of an adequate entrained air void system, concrete homogeneity, long-term drying shrinkage, and microcracking. A high-sand mix may have contributed to the field-observed harsh mixture characteristics and exacerbate concrete heterogeneity, difficulty in developing an adequate entrained air void system, poor consolidation potential, and increased drying shrinkage and cracking.

Finally, the availability of moisture, in particular to the base of the pavement slab, must also be considered, as the secondary precipitation of ettringite in entrained air voids indicates they were at least partially filled with some pore solution at times. Freeze-thaw failure of concrete occurs when a critical level of saturation is reached. Water available at the base of the slabs, in joints, and cracks may have been wicked into the slabs to a point of critical saturation.

Abstract

Major highway concrete pavements in Iowa have exhibited premature deterioration attributed to effects of ettringite formation, alkali-silica expansive reactions, and to frost attack, or some combination of them. These pavements were constructed in the mid-1980s as non-reinforced, dual-lane, roads ranging in thickness between 200 mm and 300 mm, with skewed joints reinforced with dowels. Deterioration was initially recognized with a darkening of joint regions, which occurred for some pavements as soon as four years after construction. Pavement condition ranges from severe damage to none, and there appeared to be no unequivocal materials or processing variables correlated with failure.

Based upon visual examinations, petrographic evaluation, and application of materials models, the deterioration of concrete highway pavements in Iowa appear related to a freeze-thaw failure of the coarse aggregate and the mortar. Crack patterns sub-parallel to the concrete surface transecting the mortar fraction and the coarse aggregate are indicative of freeze-thaw damage of both the mortar and aggregate. The entrained air void system was marginal to substandard, and filling of some of the finer-sized voids by ettringite appears to have further degraded the air void system. The formation of secondary ettringite within the entrained air voids probably reflects a relatively high degree of concrete saturation causing the smaller voids to be filled with pore solution when the concrete freezes. Alkali-silica reaction (ASR) affects some quartz and shale in the fine aggregate, but is not considered to be a significant cause of the deterioration. Delayed ettringite formation was not deemed likely as no evidence of a uniform paste expansion was observed. The lack of field-observed expansion is also evidence against the ASR and DEF modes of deterioration. The utilization of fly ash does not appear to have affected the deterioration as all pavements with or without fly ash exhibiting substantial damage also exhibit significant filling of the entrained air void system, and specimens containing fly ash from sound pavements do not have significant filling.

The influence of the mixture design, mixing, and placing must be evaluated with respect to development of an adequate entrained air void system, concrete homogeneity, long-term drying shrinkage, and microcracking. A high-sand mix may have contributed to the difficult mixture characteristics noted upon placement and exacerbate concrete heterogeneity problems, difficulty in developing an adequate entrained air void system, poor consolidation potential, and increased drying shrinkage and cracking. Finally, the availability of moisture must also be considered, as the secondary precipitation of ettringite in entrained air voids indicates they were at least partially filled with pore solution at times. Water availability at the base of the slabs, in joints, and cracks may have provided a means for absorbing water to a point of critical saturation.

Table of Contents

Executive Summary v

Abstract vii

1. INTRODUCTION 1

1.1 Background 1
1.2 Objective of the Study and Project Plans 1
1.3 Previous Studies 2

2. TECHNICAL APPROACH 4

2.1 Field Observations of Pavements 4
2.2 Analysis of Concrete Mixture Design 8
2.3 Cement Composition Analyses 10
2.4 Specimen Preparation 12
2.5 Air Void System Analysis 12

3. RESULTS 13

3.1 Air Void Analysis 13
3.2 Petrographic Analysis 16
3.2.1 Iowa 175 Test Road 16
3.2.2 Iowa 175 Cores 17
3.2.3.1 Site Description US 20, Mile 134.4 22
3.2.3.2 Core Descriptions 22
3.2.3.2 US 20 Location 2, Webster County 29
3.2.3.2.1 Core Descriptions 29
3.2.3.3 US 20, Webster County Location 3 37
3.2.3.3.1 Core Descriptions 37
3.3 Iowa I-35, Story County 50
3.4 Iowa I-80 58

4. DISCUSSION AND CONCLUSIONS 61
4.1 Primary Cause of Pavement Deterioration 61
4.2 The Significance of Secondary Ettringite 61
4.3 Freezing and Thawing 63
4.4 Microcracking 65
4.5 Alkali-Aggregate Reaction 66
4.6 Delayed Ettringite Formation 66
4.7 Fly Ash 66

5. ACKNOWLEDGEMENTS 67

6. REFERENCES 69

List of Figures

Figure 1. Onset of pavement deterioration is visible as a slight darkening of the concrete in the transverse joint region (top, I-80) and in pavements with advanced deterioration, a tightly-closed pattern cracking (bottom, US 20). Some of these pavements also have vibrator trails. 5
Figure 2. Map cracking oriented in the longitudinal direction of the pavement, interconnected by slightly finer cracks perpendicular to pavement direction becomes more prominent with progression of deterioration (top). Advanced degradation shows cracking paralleling the transverse joint and road edge, and along cracks within vibrator trails. The degradation would be characterized initially as "low" severity according to the SHRP Distress Identification Manual [17] and "moderate" as the deterioration progresses....6
Figure 3. Pavements exhibiting severe deterioration show significant pattern cracking (here accentuated by moisture along the crack), cracking along joints, spalling along joint edges and white efflorescence. Open joints and lack of displacement along pavement slabs provides evidence against permanent expansive processes such as alkali-aggregate reaction and sulfate attack. 7
Figure 4. Concrete materials proportions, by mass, for selected sections of Iowa US 20....8
Figure 5. Aggregate gradation plots showing coarse, fine, and combined aggregate gradation and the lack of particles in the intermediate size range. 9
Figure 6. Optimum aggregate chart plots of Iowa pavement mix designs fall into the gap-graded region and indicate likely difficulties in workability [20]. 10
Figure 7. Cement compositions, expressed as mass percent, from chemical analyses from the Iowa DOT database and using a modified Bogue calculation described in Taylor [22]. The y-axis has been expanded to more clearly illustrate total silicates and other phases....11
Figure 8. Potassium permanganate and barium chloride staining colors sulfate phases purple facilitating their identification. This allows discrimination of both the original and effective entrained air void systems. 13
Figure 9: Iowa 175 Core 2 shows some aggregate / mortar segregation and cracking located near the core base (base to the right). 18
Figure 10. Iowa 175 Core 2 surface microstructure. Slight discoloration in the upper mortar indicates approximate depth of carbonation. Micrograph field width: 14 mm 18
Figure 11. Iowa 175 Core 2 base mortar microstructure exhibiting partial filling of the entrained air void system. Micrograph field width: 4 mm 19
Figure 12. Iowa 175 Core 2 base microstructure exhibits cracking in the mortar and coarse aggregate. Micrograph field width: 14 mm. 19
Figure 13. Iowa 175 Core 2 air void and materials distribution plots. A decrease in air near the surface may reflect the loss of entrapped air. The blue triangles represent an air void parameter estimate for the original concrete; the red box represents that value as affected by void filling, if present. 20
Figure 14. Core 7 (road surface is to the left) exhibits cracking of coarse aggregate, vertical cracks from the surface that are either drying shrinkage or freeze thaw-related. Segregation of mortar and coarse aggregate is visible in the whole core cross section (upper image) and the upper-core microstructure (lower). 23
Figure 15. Core 8 exhibits less cracking but does have surface cracking to depths of 20 mm. Some of these cracks as seen in the lower image (13 mm field width) are associated with cracking within the coarse aggregate. 24

Figure 16. Cracking (red) and ASR (yellow) in Core 7 as observed using SEM. Cracking of aggregate is common. Surface cracks appear carbonated and terminate in both the mortar and the coarse aggregate. Micrograph field width is approximately 10 cm....25
Figure 17. Filling of the smaller entrained air voids (purple) has significantly increased the air void spacing factor while only slightly decreasing the total entrained air void volume for both Cores 7 and 8. Field width: 4 mm. 25
Figure 18: Air void distribution, spacing factors, and concrete component distribution versus depth for Core 7. The red boxes represent the current value, the blue triangle, the original value, and the red line in the spacing factor plot denotes the ASTM C 457 recommended limit for freeze-thaw protection....26
Figure 19: Air void distribution and spacing factors versus depth, and concrete component distribution for Core 8, mid-panel. 27
Figure 20. Core 13 cross sections show segregation within the concrete and only minor cracking of the mortar and coarse aggregate. 30
Figure 21. Core 14 exhibits some cracking of both the paste and coarse aggregate and some mortar / aggregate segregation in middle. 31
Figure 22. Clustering of air voids may indicate difficulties in mixing and development of a properly sized, disseminated entrained air void system. Field: 7 mm....32
Figure 23. A SEM image of Core 13 paste shows ettringite-filled entrained air voids, the irregularly-shaped capillary voids (black), and a reactive shale grain in the lower-left. Note absence of cracking outside of this shale grain and lack of paste / aggregate gaps that would be typical of an overall paste expansion. Field: 200 μm. 32
Figure 24. X-ray images corresponding to image in Figure 23. While the shale has undergone alkali-silica reaction, no cracking is apparent within the paste. Common locations of aluminum, sulfur and calcium in the X-ray images delineate ettringite. .33
Figure 25. Air void distribution and spacing factors versus depth, and concrete component distribution for Core 13. The air volume appears uniform with depth while the spacing factor appears substandard in the upper 100 mm. Filling has resulted in a slight increase in the spacing factor. 34
Figure 26. Air void distribution and spacing factors versus depth, and concrete component distribution for Core 14. The total air volume appears similar to that of Core 13 from the joint and appears uniform with depth (deviations from the median probably reflect entrapped air voids). The spacing factor appears marginal to sub-standard at depths below 6 cm, and filling of the smaller entrained air voids has resulted in an increase in void spacing factor. 35
Figure 27. Core 18 contains about 12 % entrained air volume and a spacing factor of 0.08 mm. Aggregate gradation appears more uniform, and possibly smaller maximum size than the degraded pavement concretes. Low specific surface and common entrapped air voids are features common to other cores in this study. 38
Figure 28. Air void and component distribution plots for core 18. Little loss of air void volume is evident with only a slight, uniform loss of air void spacing factor. Component distribution appears uniform from top to bottom....39
Figure 29. Core 18 mortar microstructure includes numerous shale fragments that appear to have undergone alkali-silica reaction, however little cracking of the mortar was evident. SEM examination indicated that some of the reaction product permeated the paste filling the capillary voids adjacent to the shale. Field width: 10 mm....40

Figure 30. Friedel's salt in hardened paste is identified here using X-ray microanalysis. It appears to be a primary hydration product in the paste throughout the cores, suggesting that it may be a result of the presence of chlorides in the original mix as opposed to the infiltration of road salts. 40
Figure 31. SEM of Core 18 shows an air void partially filled with ettringite (lower-right) and partially reacted fly ash particles (circular). X-ray element distribution (lower image) shows regions of high sulfur and aluminum that delineate locations of ettringite. Regions of chlorine and aluminum delineate regions of chloroaluminate. Field width: 75 μm. 41
Figure 32. Core 19 exhibits extensive cracking of both the paste and coarse aggregate. Cracks trending parallel to the pavement surface (to the left) intersect perpendicular cracks; features typical of freeze-thaw cracking. The oblique view of the upper portion of core 19 shows cracking in both the surface (polished for clarity) and cross-section orientations....43
Figure 33. SEM image of a surface crack (road surface is at the top, 5 mm field width) extending through the paste portion of the mortar and terminating in a coarse aggregate. 44
Figure 34. Back scattered electron image of Core 19 paste microstructure showing ASR-affected shale (left) and fly ash (circular). X-ray image regions of high sulfur (yellow) and intermediate aluminum (purple) mark locations of ettringite while regions of high chlorine (lower left image) denote locations of chloroaluminate. 45
Figure 35. Core 19 (left) appears to have a finer-sized sand and possibly a larger maximum coarse aggregate size when compared to Core 18 (right)....46
Figure 36. Core 19 data show a decrease in spacing factor with depth and possibly a trend to an increased loss of spacing factor with depth. The component distribution plot shows a possible increase in aggregate and decrease in paste in the upper half of the core. 47
Figure 37. Top portion of core 19 with cracks (red) and ASR-affected shale grain (yellow) shows cracking through both the cement paste and coarse aggregate. A color-coded stress image resulting from a simulation of aggregate expansion showing regions of high stresses in red correlates well with some, but not all of the observed cracking...49
Figure 38. Cores 11, joint (top) and 12, mid-panel (bottom) cross section with horizontal crack in lower-most third. Some segregation is visible in both cores. 52
Figure 39. Surface cracking in Core 11 to about 20 mm passes through both the mortar and coarse aggregate. Lower image shows minor surface carbonation and cracking within the mortar. Field width 8 mm. 53
Figure 40. Surface crack in core 12 (approx. center-left) appears to be entirely within the mortar, and the lower image shows the crack plane through mortar highlighted using ink. 8 mm field width. 54
Figure 41: Core 11 air void parameters and component distribution show a loss of air void spacing yet relatively uniform air void volume and materials distribution. 55
Figure 42. Core 12 air void volume and spacing parameters, and component distribution shows an increased degree of entrained air void filling with depth. 56
Figure 43. Core 29 cracking near surface passes through both the mortar and coarse aggregate. Cracking also follows close along paste-aggregate interface and is typical of a shrinkage crack. Cracking in aggregate and in the mortar at depth may reflect freeze-thaw damage, as the air void system in the upper half of this core is much poorer than that in the lower half. 59

Figure 44. Core 29, centered on a well-defined vibration trail exhibits a significant increase in spacing factor in the upper half. This probably represents the zone of influence of the immersion vibrator probe. Note that the spacing factor is generally not satisfactory at any depth. 60

List of Tables

Table 1. Cores Selected for Linear Traverse Analysis: C 457, Modified Point Count 14
Table 2. ASTM C-457 Modified Point Count Results of Original and Effective Entrained Air Void Parameters. 15
Table 3. Iowa 175, West of Ellsworth, Iowa: Materials and Properties [28] 16
Table 4. US 20 Location 1, Webster County: Materials and Properties [28]. 21
Table 5. US 20 Location 2, Webster County: Materials and Properties [28]. 28
Table 6. US 20 Location 3, Webster County: Materials and Properties [28]. 36
Table 7. I-35 Story County Location 5: Materials and Properties [28]. 51
Table 8. I-80, Milepost 210.40: Materials and Properties [28]. 57

1. INTRODUCTION

1.1 Background

Major highway concrete pavements in Iowa have exhibited premature deterioration. The Iowa Department of Transportation (DOT) has responsibility for determining the cause of the deterioration and implementing measures for avoiding similar future problems. The cause(s) of the deterioration has been the subject of much controversy. Various investigators have used different methods to characterize the processes and have arrived at different interpretations. The deterioration has been attributed to effects of ettringite formation (including delayed ettringite formation), alkali-silica expansive reactions, and to frost attack, or some combination of them. Evidence for all three processes have been reported. While one or more of these processes is likely to be the cause of the deterioration, the possibility that there may be other deleterious processes should be considered.

1.2 Objective of the Study and Project Plans

The objective of this study is to identify probable processes responsible for premature deterioration of the concrete pavement of selected major state highways in Iowa and, if possible, to determine the major causes of the premature deterioration of concrete pavements.

Our project consists of three major tasks outlined in a research plan which has been developed in collaboration with the Iowa DOT. The first task consisted of field inspections of deteriorated concrete and collection of as much information as available on the pavement projects such as the concrete mix designs and constituent materials, the mixing, consolidation and curing of concretes, test records, and inspection reports. Specimens of both deteriorated and un-distressed pavements, constructed from the same concretes, have been collected.

In the second task, the concrete specimens were subjected to petrographic examination using visible light microscopy and scanning electron microscopy coupled with image analysis, and X-ray powder diffraction analysis. The intent of these investigations was to identify the major degradation process(es) causing premature deterioration of the pavement and if more than one major process was identified, assess their relative contributions.

Task three involved the attempt to identify the causes of deterioration by application of microstructure simulation, hydration simulation, and micro-mechanical models developed at NIST. Through a combination of backscattered electron and X-ray imaging, the microstructure of the distressed concretes was established. Segmenting images into constituent phases and "healing" the cracks via image processing provides a starting microstructure for operation of the models. Modeling of deterioration processes involves selected expansion of phases in accordance with proposed deterioration mechanisms. Analysis of the stress fields after a series of expansion cycles formed a basis for predicting the crack patterns associated with the different modes of deterioration. Comparison of the predicted stress fields and resulting crack patterns provided additional information regarding the potential mode(s) of deterioration.

1.3 Previous Studies

Highway pavements in this study were constructed in the mid-1980s as non-reinforced, dual-lane, roads ranging in thickness between 200 mm and 300 mm, with skewed joints reinforced with dowels. Deterioration was initially recognized by Iowa DOT staff as a darkening of joint regions, which occurred for some pavements as soon as four years after construction. Pavement condition ranges from severe damage to none, and there appeared to be no unequivocal materials or processing variables correlated with failure.

Numerous studies of cores from these pavements have produced a variety, and some conflicting, opinions as to the causes of the deterioration, and the significance of microstructural features. Jones [1] examined cores drilled from US 20 in Webster County and found low air contents in regions where cracking was occurring. He speculated that the paver vibration and supplemental vibration around joint regions might be responsible for the low air void content leaving the pavements vulnerable to freeze-thaw damage. Ouyang [2] examined Wisconsin and Iowa pavements and concluded that internal and external sulfate attack and freeze-thaw attack were the most probable causes for premature deterioration of the US 20 pavements. He also felt that improper construction methods resulted in a low air content in the surface layer of the pavements. He noted that deposits of ettringite in the entrained air voids may have reduced resistance to sulfate attack and to freeze-thaw damage, and that freeze-thaw cracking could have facilitated the transport of external sulfate ions into the pavements.

Pitt et al. [3] examined the role of sulfate impurities originating from deicing salts on the durability of Portland cement mortar and pavements. They speculated that deicing salt impurities may have contributed to early pavement failures previously attributed to D-cracking. They note that concrete incorporating aggregate that passed freeze-thaw tests can exhibit failure in the field. These failures were observed to be especially severe in joint areas, and may actually have been the result of sulfate attack, even though the crack patterns appeared similar to that of D-cracking. Specimens exposed to gypsum-containing brines appeared to deteriorate more rapidly compared to those exposed to pure water. They observed an increase in ettringite and Friedel's salt after exposure to deicing salts. It was thought that these phases filled voids making the mortars more vulnerable to freeze-thaw cycling damage.

Stark [4] concluded that the expansion caused by alkali-silica reaction (ASR) was the cause of the pavement deterioration. He felt that the ASR reaction was associated with chert and shales in the coarse sand sizes and that the problem pavements incorporated high alkali cements and Class C fly ash. Similarly, Thalow [5] found alkali-silica reactivity involving chert in the sand fraction and concluded that it was the primary cause of deterioration. He considered the filling of the entrained air voids to reflect water saturation. Evidence of an overall paste expansion, possibly indicating a delayed ettringite formation, was not found. Kofoed [6] examined a set of cores and found alkali-silica reaction involving shale in the sand and a poor entrained air void system and concluded that both ASR-related expansion and freeze thaw cycling led to cracking. In contrast to these findings, Marks [7] tested properties of selected Iowa sands used in construction and noted that while many failed the ASTM P-214 test (now ASTM C 1260 [8]), that in the past they had a good performance record in pavements.

Marks and Dubberke [9] observed the filling of entrained air voids with ettringite and felt that the voids would serve as a center-of-pressure as ettringite precipitation progressed, resulting in cracking. While no measurements were performed, they considered the volume of ettringite to be excessive and, that sodium chloride, likely from road salts, may have accelerated the deterioration by causing the ettringite to expand and then dissolve. This is in contrast to observations of Stark [10] finding ettringite to be stable in sodium chloride solutions, and that monosulfate appears to be converted to ettringite under such conditions. Schlorholtz and Amenson [11] determined that two or more deterioration processes were acting simultaneously. They concluded that freeze-thaw damage was most probable for the cracks in the cores extracted from I-35 and US 20. Alkali-silica reaction products were observed in all cores but were considered secondary in importance relative to the freeze-thaw processes. In regions showing less severe deterioration, damage was attributed to mixing or plastic concrete problems. D-cracking and marginal air void systems were also thought to be potential causes of deterioration.

Gress [12] noted a relationship between tine groove depth and distress. Regions with shallow tine depths and apparently poor finishability, generally denoted regions where distress was more likely. He considered these an indication of possible setting problems and that the loss of entrained air in these regions may be due to over vibration. Cracking was observed within the matrix with some cracks in the coarse aggregates and small entrained air voids were filled with what is thought to be ettringite. Empty cracks intersecting these filled voids led Gress to conclude that growth of ettringite in the voids created the pressure that cracked the concrete. Additionally, he felt these concretes contained "excessive ettringite", though no measurements were made.

Ouyang and Lane [13] examined freeze-thaw-cycled laboratory specimens prepared with and without Class C fly ash. They found a relationship between filling of entrained air voids and loss of freeze-thaw durability. They also felt that the degree of filling coincided with the length of moist curing prior to cycling, as well as the usage of Class C fly ash. This led to a subsequent study by Ouyang and Lane [14] where they devised an experimental program to examine the role of ettringite filling of entrained air voids and freeze-thaw durability in which a correlation between filling and freeze thaw performance was found. They felt that the filling was influenced by the period of moist curing and wet-dry test cycling, and by the materials used in the concretes. They proposed limits for materials in an effort to minimize the formation of ettringite.

A study by Northwestern University [15] of pavements from the Midwest, including those from Iowa, concluded that damage resulted from of multiple factors. They recommended investigation of the role of fly ash in pavements, avoidance of high alkali and high sulfate cements, the use of a permeable base, and also stressed the need to account for synergistic effects of combinations of variables in future testing.

2. TECHNICAL APPROACH

2.1 Field Observations of Pavements

A field examination of the pavements was organized by Vernon Marks of Iowa DOT. Site visits to pavements of Iowa US 20, Iowa 175, I-35, US 218, and I-80 allowed examination and designating coring locations. Sites were selected from pavements exhibiting no apparent deterioration, those slightly affected, and pavements with relatively severe damage. In the following paragraphs, the observations are summarized. More detailed observations are given in the results of petrographic examinations of specific cores.

In some cases, onset of pavement deterioration was visible as a slight darkening of the concrete in the transverse joint region. The darkening may reflect accumulation of dirt and other road debris and moisture migration within fine-sized cracks along the joints. Additional degradation resulted in development of cracking along the transverse joint and road edge, and along cracks parallel to vibrator trails (Figure 1). The degradation would be characterized initially as "low" severity according to the Strategic Highway Research Program (SHRP) Distress Identification Manual [16] and "moderate" as the deterioration progresses. The most severely deteriorated regions exhibited pattern cracking over the entire slab, more substantial darkening at joints, cracking paralleling joints and the road edge, along with minor spalling of concrete adjacent to the joint. Map cracking oriented in the longitudinal direction of the pavement, interconnected by slightly finer cracks perpendicular to pavement direction became more prominent with the progression of deterioration (Figure 2). Damage observed during the field examination does not exceed the "moderate" rating, although some of the sections of US 20 considered to be the most severely affected, were paved with an asphalt overlay at the time of the site visit.

Longitudinal cracks with widths ranging from less than 1 mm to 2 mm wide are present along some vibrator trails. Vibrator trails exhibit a slightly different texture, probably related to lack of coarse aggregate as observed in regions where the pavement surface had been ground. Gress [12] noted that the tining penetrated deeper across the vibrator trails. The cracking paralleling the longitudinal cracks may also be classified as "low" to "moderate" (Figure 3).

There was no evidence of any permanent volume change, deflection, closing / opening of joints, or tilting and shearing of slabs. All roads had a tined surface reportedly cut after the concrete had set [21] and the condition of the tine grooves varied from cleanly cut to having a torn appearance. The exposed pavement surfaces appeared satisfactory, though some surfaces reportedly experienced difficulty in finishing during the paving operation. Iowa DOT noted many of the mixes were "harsh" and were difficult to place [21]. Secondary deposits in the form of a white efflorescence (probably carbonated calcium hydroxide) were noted along US 20 on surfaces and in cracks within the spalling adjacent to the joints, but only in regions with the most severe deterioration.

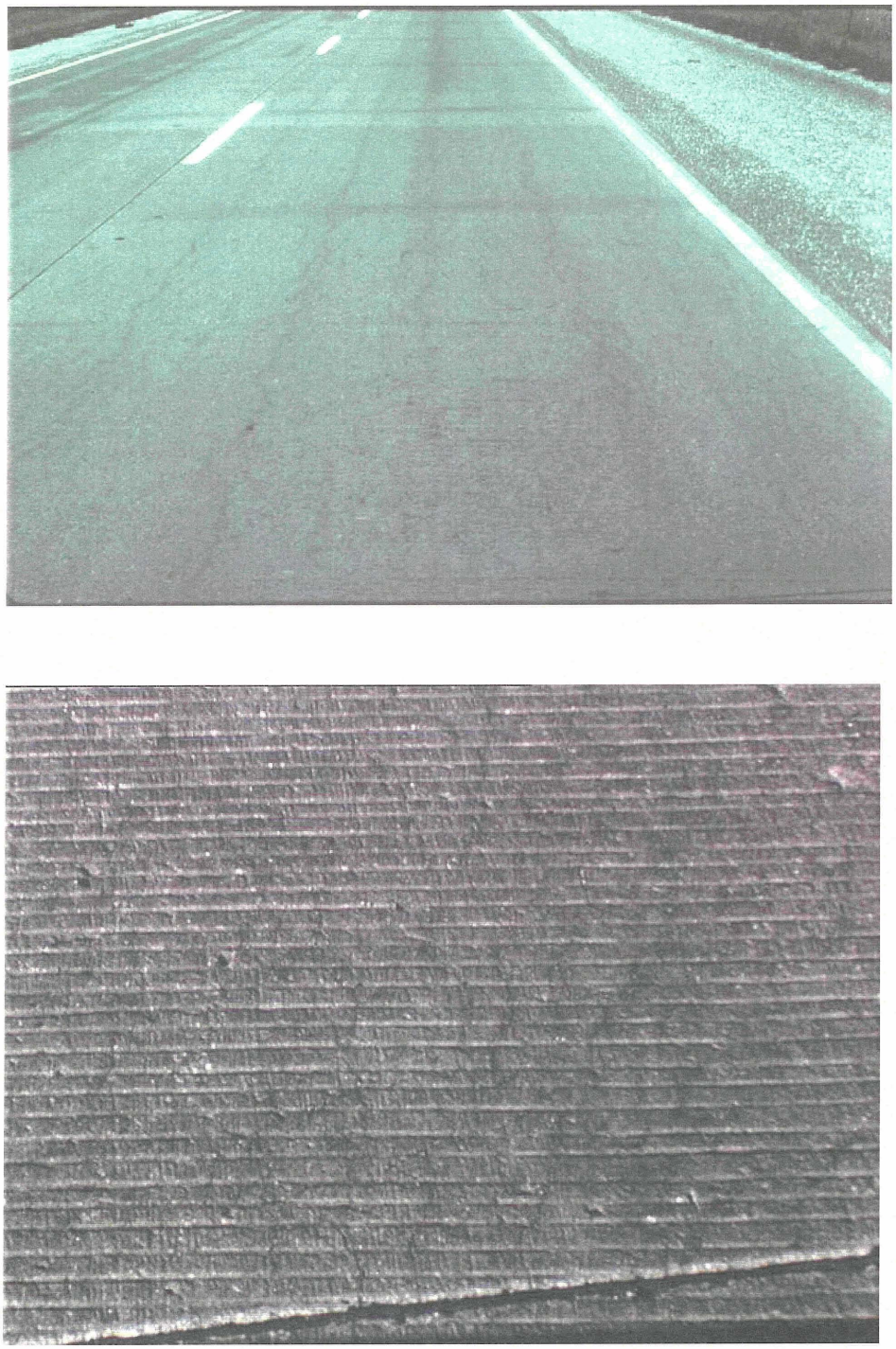

Figure 1. Onset of pavement deterioration is visible as a slight darkening of the concrete in the transverse joint region (top, I-80) and in pavements with advanced deterioration, a tightly-closed pattern cracking (bottom, US 20). Some of these pavements also have vibrator trails.

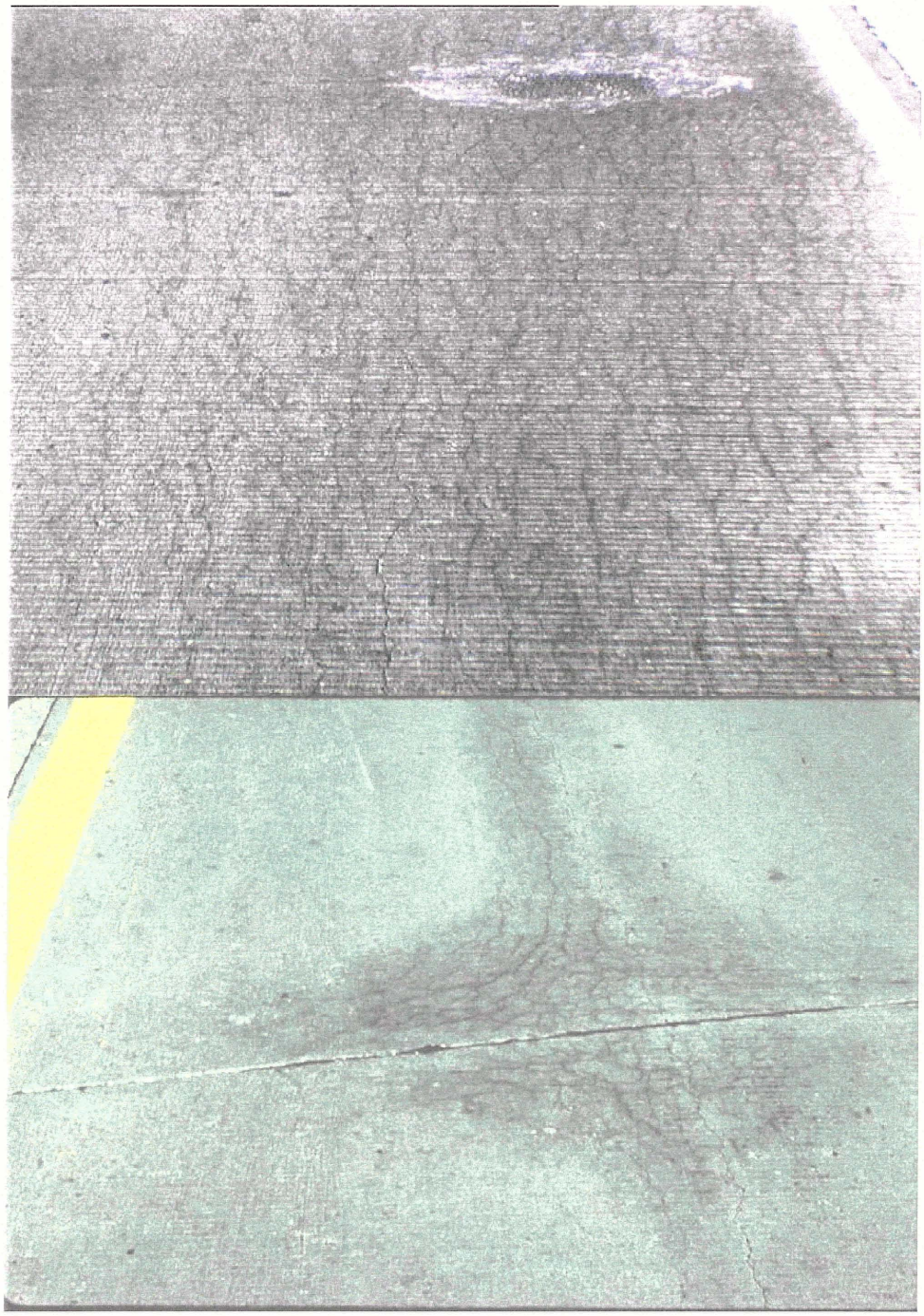

Figure 2. Map cracking oriented in the longitudinal direction of the pavement, interconnected by slightly finer cracks perpendicular to pavement direction becomes more prominent with progression of deterioration (top). Advanced degradation shows cracking paralleling the transverse joint and road edge, and along cracks within vibrator trails. The degradation would be characterized initially as "low" severity according to the SHRP Distress Identification Manual [17] and "moderate" as the deterioration progresses.

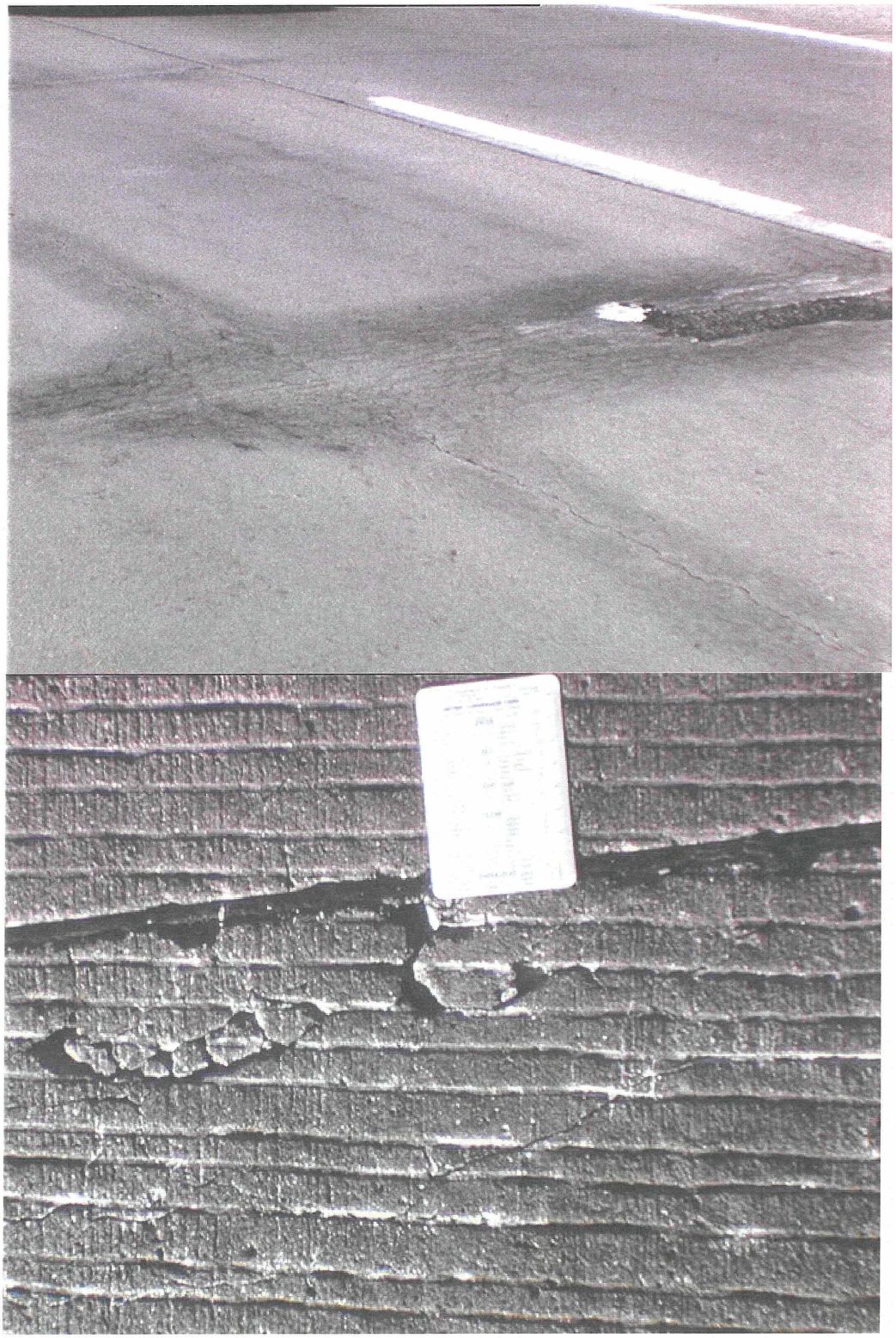

Figure 3. Pavements exhibiting severe deterioration show significant pattern cracking (here accentuated by moisture along the crack), cracking along joints, spalling along joint edges and white efflorescence. Open joints and lack of displacement along pavement slabs provides evidence against permanent expansive processes such as alkali-aggregate reaction and sulfate attack.

2.2 Analysis of Concrete Mixture Design

Figure 4 gives the concrete materials proportions from US 20 for mixes with and without fly ash while Figure 5 indicates the gap grading of the aggregates. Evaluation of the mix design by two separate internationally recognized engineers [18,19] found agreement in that the high sand content and gap-grading probably led to difficulties in workability and consolidation, and may have resulted in drying shrinkage problems. The aggregate distributions plotted on a Shilstone Coarseness Factor Chart [20] fall in a region reflecting gap-graded concrete and where workability difficulties may be present (Figure 6). The parallel blue lines on this chart define a region of optimum grading for low water demand and optimum response to vibration. While the potential difficulty in workability were not unexpected to the Iowa Department of Transportation staff [21], it is significant in that it may also affect the development of the entrained air void system during mixing. Failure to develop an adequate entrained air void system appears to be contributory to the deterioration of these pavements.

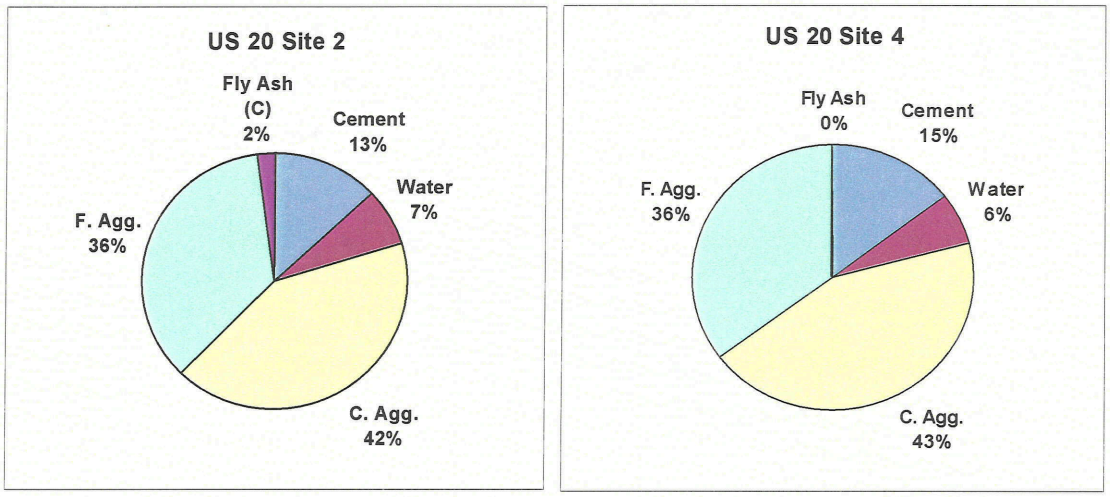

Figure 4. Concrete materials proportions, by mass, for selected sections of Iowa US 20.

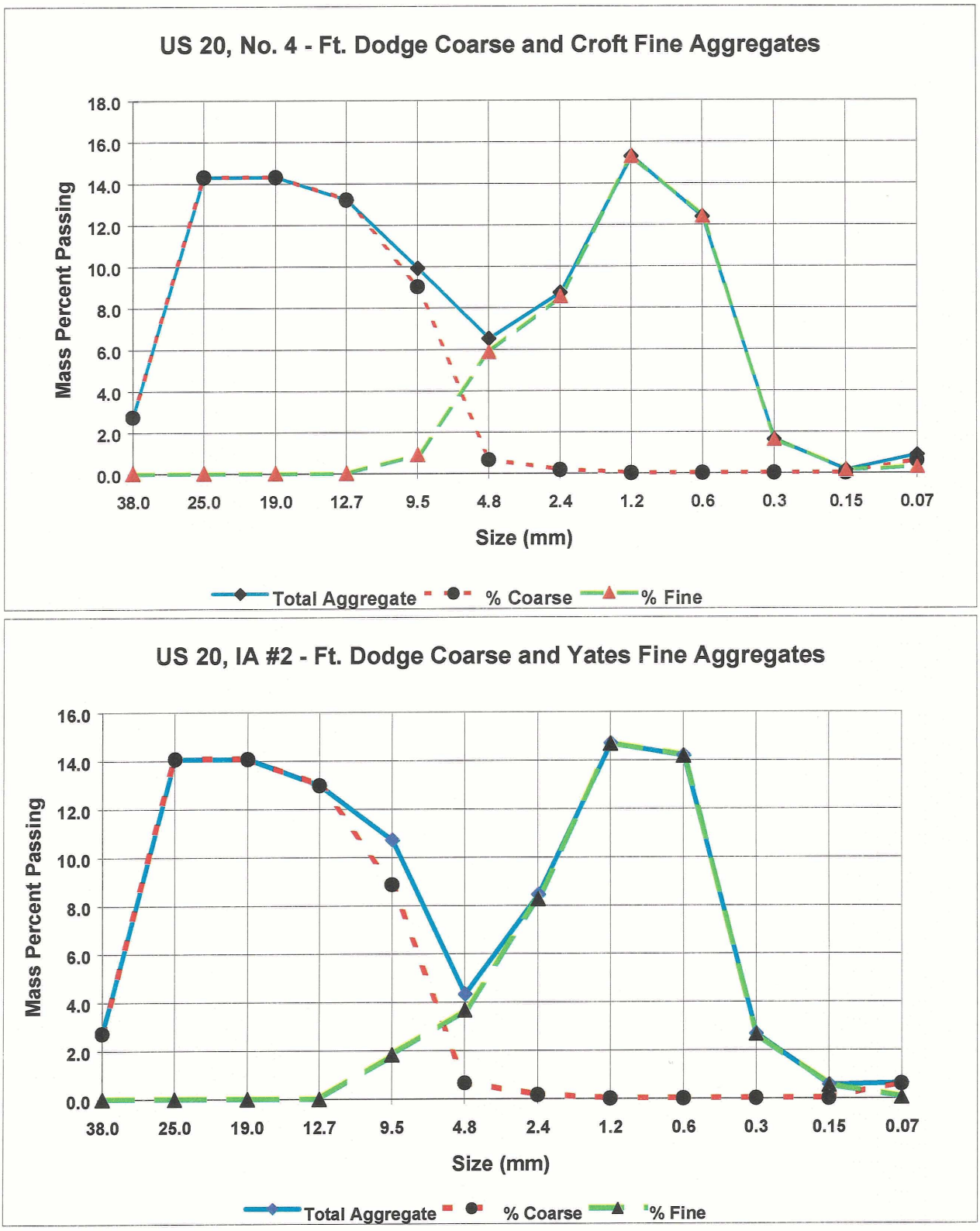

Figure 5. Aggregate gradation plots showing coarse, fine, and combined aggregate gradation and the lack of particles in the intermediate size range.

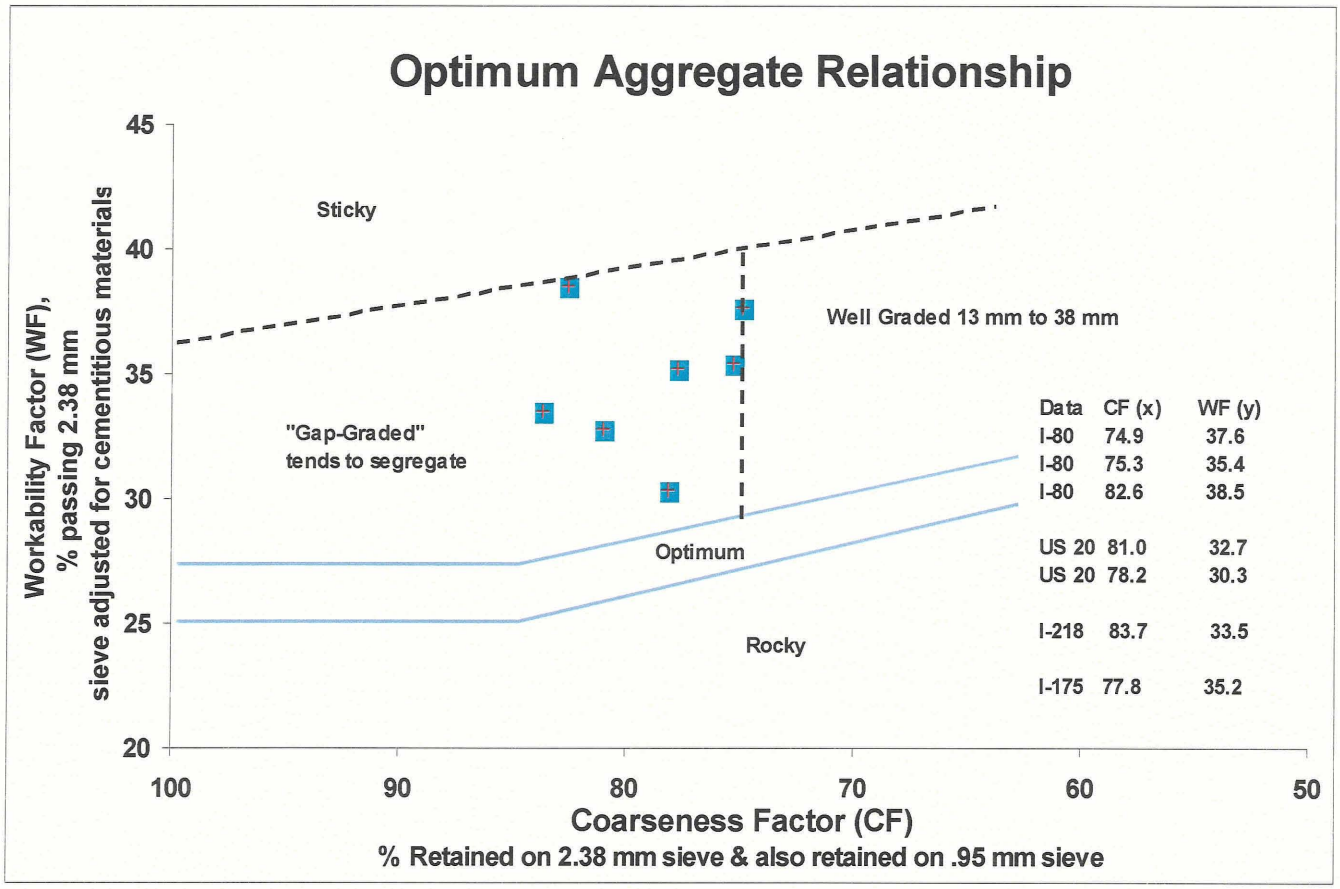

Figure 6. Optimum aggregate chart plots of Iowa pavement mix designs fall into the gap-graded region and indicate likely difficulties in workability [20].

2.3 Cement Composition Analyses

Estimates of cement compositions were made using a modified Bogue calculation described by Taylor [22]. Chemical data for these analyses were taken from the Iowa State University testing results provided in the Iowa Department of Transportation materials database. As data were not available, assumptions for free lime (0.3 %) were made for all estimates. These data show that, if one considers total silicates as a group, cement compositions appear generally uniform across the job interval. Variations in the silicate phase fractions may reflect deviations of the free lime content from that assumed in the calculations (Figure 7), errors in sampling, and analysis. These data were later used in conjunction with the mix design to estimate the potential volume of ettringite formation to test the hypothesis of excess ettringite formation. Data were not available to allow matching of cement analyses with pavement locations.

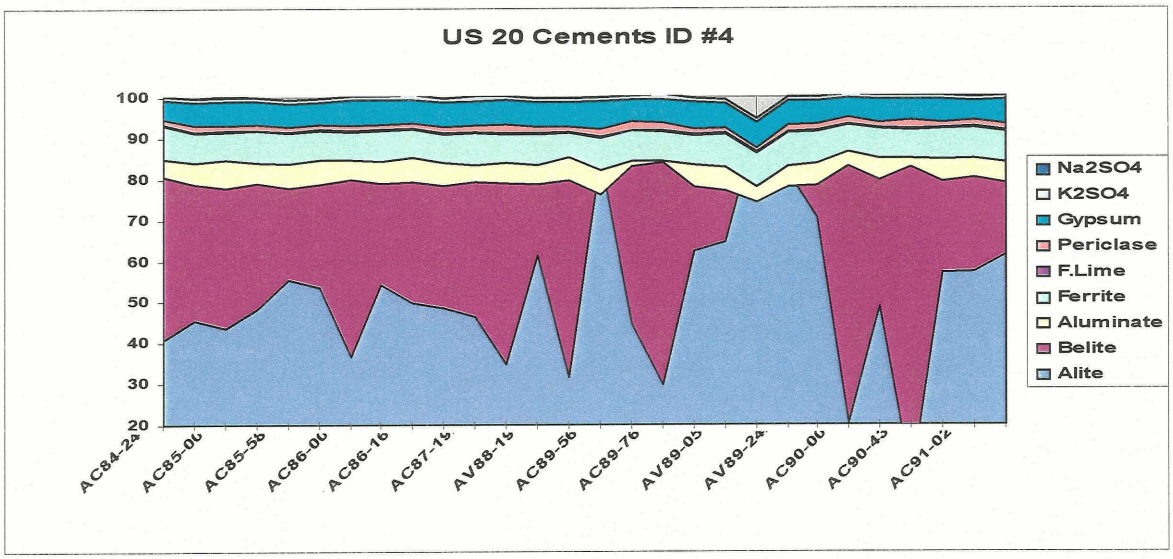

	C_3S	C_2S	C_3A	C_4AF	Free Lime	Periclase	Gypsum	K_2SO4	Na_2SO_4	Ckr. $CaSO_4$
Avg.	51.2	28.0	4.8	7.4	0.3	1.5	5.7	1.0	0.0	0.0
Stdev.	18.7	20.4	1.4	0.5	0.0	0.3	0.5	0.0	0.1	0.0

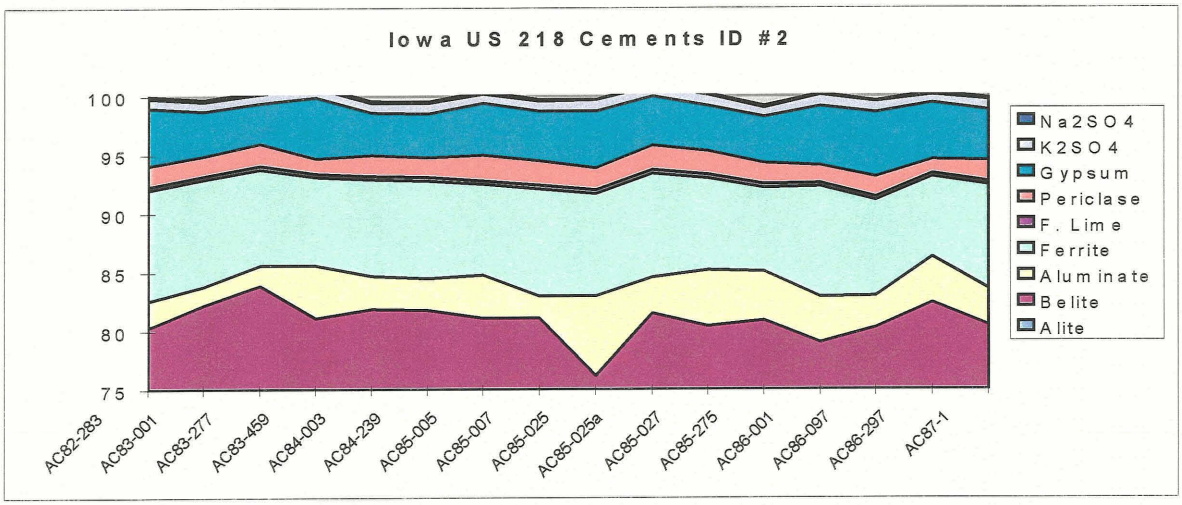

	C_3S	C_2S	C_3A	C_4AF	Free Lime	Periclase	Gypsum	K_2SO4	Na_2SO_4	Ckr. $CaSO_4$
Avg.	45.7	35.2	3.4	8.3	0.3	1.8	4.4	0.9	0.2	0.0
Stdev.	9.4	10.3	1.3	0.8	0.0	0.3	0.6	0.1	0.1	0.1

Figure 7. Cement compositions, expressed as mass percent, from chemical analyses from the Iowa DOT database and using a modified Bogue calculation described in Taylor [22]. The y-axis has been expanded to more clearly illustrate total silicates and other phases.

2.4 Specimen Preparation

A set of cores was prepared to allow examination of full-depth concrete cross sections of specimens from both the joint and mid-panel, outside of a wheel path, and both between and on vibrator trails. Examination of cores followed recommendations provided in ASTM C 856 [23], Standard Practice for Examination of Hardened Concrete, while procedures for preparation and examination may also be found in Walker [24].

Core numbers were logged upon receipt and core surfaces examined and described. Examination of the entire core allows description of the overall concrete condition, the coarse and fine aggregate characteristics, cement paste condition, qualitative assessment of entrapped and entrained air void system, cracking, and identification of any foreign objects. Photographing the prepared surfaces provided a record of the specimen condition.

Lapping provides a smooth surface necessary for examination of the concrete microstructure using a stereo microscope [23,24]. Cracks were marked using India ink and a draftsman's pen by touching the pen tip to the crack and allowing capillary suction to draw the ink along the crack plane [24]. This technique was also used to identify open aggregate cracks in the limestone coarse aggregate and shale in the sand. Selected cores were then marked for sampling for scanning electron microscopy (SEM). The cores were cut in half lengthwise and a slab approximately 15 mm was taken from the core center. The core slab was sectioned into four pieces and dried in an oven at 50 °C. After 48 h, these sections were imbedded using a low-viscosity epoxy in a low vacuum to assist in infiltration of the pore structure, and the epoxy was cured at 60 °C for 24 hours. The embedded specimens were then ground to expose the concrete face, and polished using a series of (6, 3, 1, and 0.25) μm diamond polish; the surfaces were cleaned using a lint-free cotton cloth. A thin carbon coating was deposited on the surface for conduction of excess SEM beam charge. The slabs were stored in a vacuum dessicator to protect them from laboratory humidity. Remnant core halves were lapped and polished similar to the procedure for petrographic analysis.

2.5 Air Void System Analysis

Characterization of the entrained air void system of selected cores was performed using the modified point count procedure of ASTM C 457 [25]. Data were obtained from a slab sawn from the center of each core, carefully smoothed and polished to present a surface suitable for microscopical examination. The prepared surface was then stained using a potassium permanganate, barium chloride stain per Poole and Thomas [26] to highlight air voids filled with ettringite (Figure 8). The point count was performed using a semi-automated linear traverse system [27] with an additional point count tabulator. Each data set represents a total traverse length of at least 2540 mm, in accordance with ASTM C 457 requirements. Uncertainties in the measurements are estimates of two standard deviations, corresponding to a 95 % level of confidence. The linear traverse analysis counted all voids, that is, all effective and those rendered ineffective due to filling.

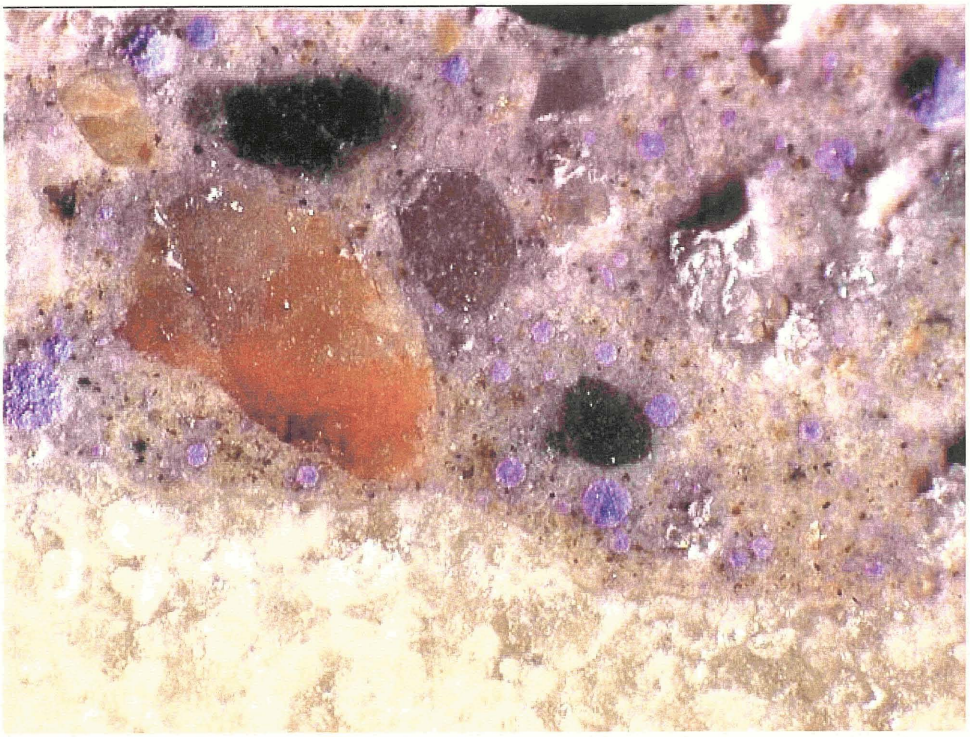

Figure 8. Potassium permanganate and barium chloride staining colors sulfate phases purple facilitating their identification. This allows discrimination of both the original and effective entrained air void systems.

The second tabulator was used to track the filled air voids, permitting recalculation of the data to reflect the effective entrained air void system. This facilitated counting of two air void systems, that of the concrete as placed, and that of the concrete at the time of sampling. These values differ because of the subsequent filling of some of the entrained air voids with ettringite. Criterion for distinction between an ineffective and effective void was that the void must appear completely filled. Voids rimmed or partially filled with secondary mineralization, and those with open cores were considered effective as entrained air voids.

3. RESULTS

3.1 Air Void Analysis

The cores selected for air void analysis are given in Table 1 along with their conditions based upon visual observations. Table 2 presents results of the air void analysis. Trends in total air and air void spacing as both original and effective values are plotted versus core depth and will be presented in the petrography section (section 3.2). Examination of these plots, as well as a plot of concrete component distribution proved helpful in understanding the deterioration of the pavements.

Table 1. Cores Selected for Linear Traverse Analysis: C 457, Modified Point Count

Core #	Road	Location	Condition, comments
2	Iowa 175	J	Test section, 15 % Class C fly ash, appears sound
11	I-35, Story	J	No vibrator trail evident, North-bound lane,
12	I-35, Story	M	Pattern cracking at mid-panel joints
7	US 20	JB	Mix 3, severe pattern and longitudinal cracking
8	US 20	MB	slight transverse cracking, joint spalling, popouts
13	US 20	JB	Mix 2, appears sound
14	US 20	MB	
18	US 20	JB	Mix 1, sound in this location
19	US 20	J	Mix 1, severe map cracking, cracking along joints, Paved over before site visit
29	I-80	MO	Longitudinal and slight pattern cracking

J = joint
M = midpanel
B = between vibrator trail
O = on vibrator trail

Specimens without a vibration trail code reflect the lack of a clearly discernable vibration trail at that location.

Table 2. ASTM C-457 Modified Point Count Results of Original and Effective Entrained Air Void Parameters.

Core	Air Content Orginal*	Effective	Volume Percent Paste	Aggregate	Paste/Air Ratio Org.	Eff.	Specific Surface (mm^{-1}) Org.	Eff.	Spacing Factor (mm) Org.	Eff.
2	11.9 ± 1.7	11.7 ± 1.6	21.2 ± 2.1	66.9 ± 2.7	1.8	1.8	17.5 ± 2.6	17.1 ± 2.6	0.10 ± .01	0.11 ±. 02
11	8.0 ± 1.7	6.0 ± 1.4	27.0 ± 2.4	65.4 ± 2.6	3.4	4.5	21.3 ± 3.8	15.2 ± 3.3	0.16 ± .03	0.30 ± .06
12	8.6 ± 1.4	7.9 ± 1.3	21.4 ± 2.1	67.3 ± 2.0	2.5	2.7	17.4 ± 3.1	10.1 ± 2.0	0.18 ± .03	0.34 ± .06
7	6.0 ± 1.0	4.3 ± 0.9	28.8 ± 2.0	65.2 ± 2.0	4.8	4.5	29.1 ± 4.9	9.0 ± 1.9	0.16 ± .03	0.74 ± .16
8	5.9 ± 1.2	4.6 ± 1.1	25.3 ± 2.3	68.9 ± 2.1	4.3	5.5	35.4 ± 7.4	21.1 ± 5.3	0.12 ± .03	0.26 ± .06
13	6.6 ± 0.9	6.2 ± 1.2	25.6 ± 2.3	67.9 ± 2.7	3.9	4.1	22.1 ± 4.6	18.4 ± 3.9	0.18 ± .04	0.22 ± .05
14	6.5 ± 1.2	6.3 ± 1.3	25.0 ± 2.3	68.2 ± 2.7	3.8	3.9	18.1 ± 3.8	17.3 ± 3.8	0.21 ± .04	0.23 ± .05
18	12.2 ± 1.7	12.0 ± 1.8	21.1 ± 2.1	67.6 ± 2.7	1.7	1.8	20.8 ± 3.1	18.5 ± 2.8	0.08 ± .01	0.09 ± .01
19	9.5 ± 1.5	7.9 ± 1.4	17.8 ± 2.0	72.0 ± 2.2	1.9	2.3	14.6 ± 2.6	7.7 ± 1.5	0.13 ± .02	0.29 ± .06
29	6.2 ± 1.2	6.2 ± 1.2	32.2 ± 2.3	61.2 ± 2.4	5.2	5.2	15.4 ± 3.4	14.3 ± 3.1	0.34 ± .07	0.36 ± .08

3.2 Petrographic Analysis

3.2.1 Iowa 175 Test Road

Iowa 175, west of the town of Ellsworth, is a test road with sections containing portland cement concrete, and concrete panels containing partial cement replacement by Class C or Class F fly ash. These pavements, constructed about 1981, have performed very well and exhibit no evidence of vibrator trails. This location was of interest as these concretes appear to be in excellent condition, yet are slightly older than those exhibiting problems, and used similar materials, including fly ashes. The materials and properties of the specimens taken from Iowa 175 were provided by the Iowa Department of Transportation and are given in table three.

Table 3. Iowa 175, West of Ellsworth, Iowa: Materials and Properties [28]

Cement:	Type I, 2.16 % SO_3, 0.35 % equivalent alkali
Coarse Aggregate:	Alden (Weaver) Limestone, open quarry, 1.5 % freeze-thaw loss, 2.7 % absorption, LA Abr. 40 % loss, durability factor 79
Fine Aggregate:	Ames sand
Admixtures:	AEA
Fly Ash:	Class C, 15 % replacement of cement 1.65 % SO_3, 1.46 % equivalent alkali, 0.20 % loss on ignition

Concrete Batch Mass / m^3 (IDOT A-3 Mix)

Cement	278 kg	0.49 w/s	Slump: 90 mm to30 mm, avg. 50 mm
Water	161		Air: 7.8 % to 5.4 %, avg. 6.6 %
Fly Ash	49		
C. Agg.	973		Slipform paver - spreader used
F. Agg.	844		Temperature: 32 to 7 (°C), no precipitation, clear
WR	0		Mix Characteristics: no reported problems
AEA no value provided			27.1 MPa compressive strength

Cores:

No.	Mile Post	Location	Vibrator Trail Designation	Condition/Comments
2	224+95	Joint	2j	Excellent Condition

3.2.2 Iowa 175 Cores

Iowa 175 cores appear mostly sound with few cracks, strong paste and aggregate, clean saw cuts in preparation, good paste / aggregate bonding. Their surfaces exhibit a rounded-edged tining with possible minor freeze-thaw-related spalling of the concrete surface. Coarse aggregate is a crushed limestone and the sand is a blend of quartz, feldspar, and shale. Occasional cracking related to alkali-silica reactivity of the shale fragments was observed. This cracking appears minor and is seldom greater than a few tenths of a millimeter in length. Lateral segregation of coarse aggregate and mortar are seen in Core 2 as mortar-rich regions (Figure 9). The cement paste from Core 2 is slightly darker than that from cores extracted from other sections of the I-175 test road and probably reflects color influence of the Class C fly ash. The paste is even-colored, appears strong, with no evidence of bleeding, and carbonation depths of a few millimeters (Figure 9, Figure 10). Entrapped air voids are common, especially in the center of the core where void diameters approach 20 mm. Entrapped air voids were less common in Cores 4 and 6. The entrained air void systems appear adequate, though some filling of the voids is apparent near the core base (Figure 11). Cracking is confined to the base region of the core, and traverses the core through both coarse aggregate and paste (Figure 12). Examination of the air void data presented in (Table 2) and a graphical depiction presented in Figure 13 shows that the air void spacing factor is within the range recommended for durability in moderate and severe environments. The decrease in total air near the surface probably reflects the influence of consolidation vibration on the removal of entrapped air. Loss of some of the air void system was noted with the filling of some of the air voids with ettringite, primarily near the base of the core. The large, open fracture in the base of Core 2 transecting both coarse aggregate and paste is within the region where this filling occurs and, while the spacing factor is still sufficient for freezing and thawing durability according to ACI 201, the cracking appears to be freeze-thaw-related. Therefore, this may indicate a high degree of concrete saturation at the base of this pavement.

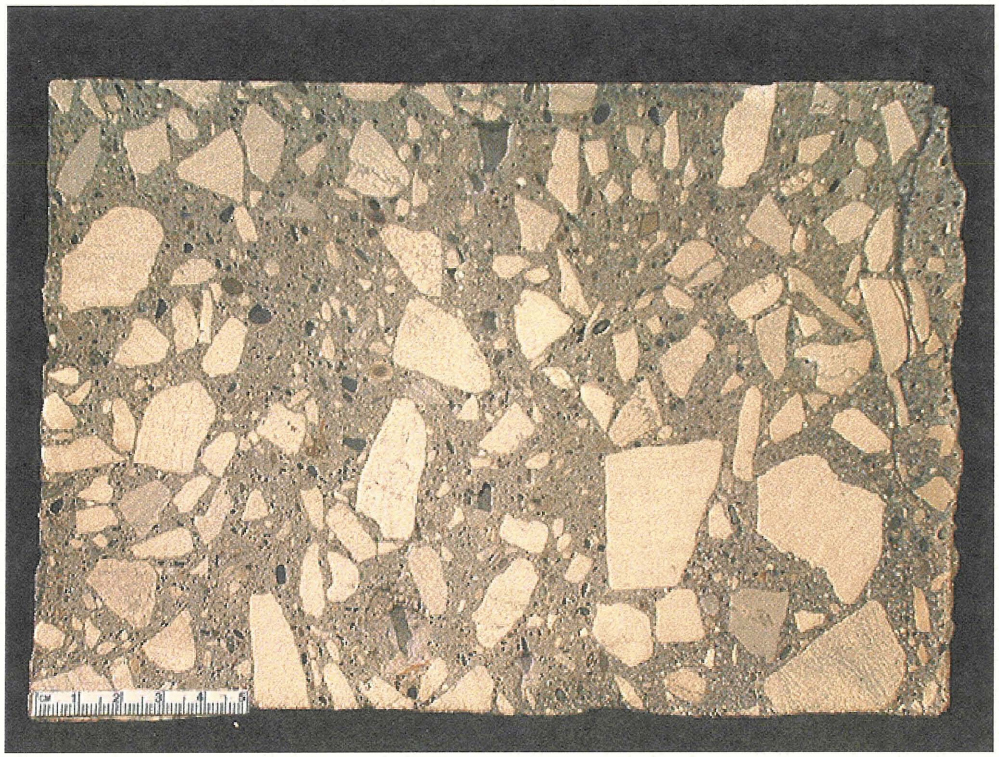

Figure 9: Iowa 175 Core 2 shows some aggregate / mortar segregation and cracking located near the core base (base to the right).

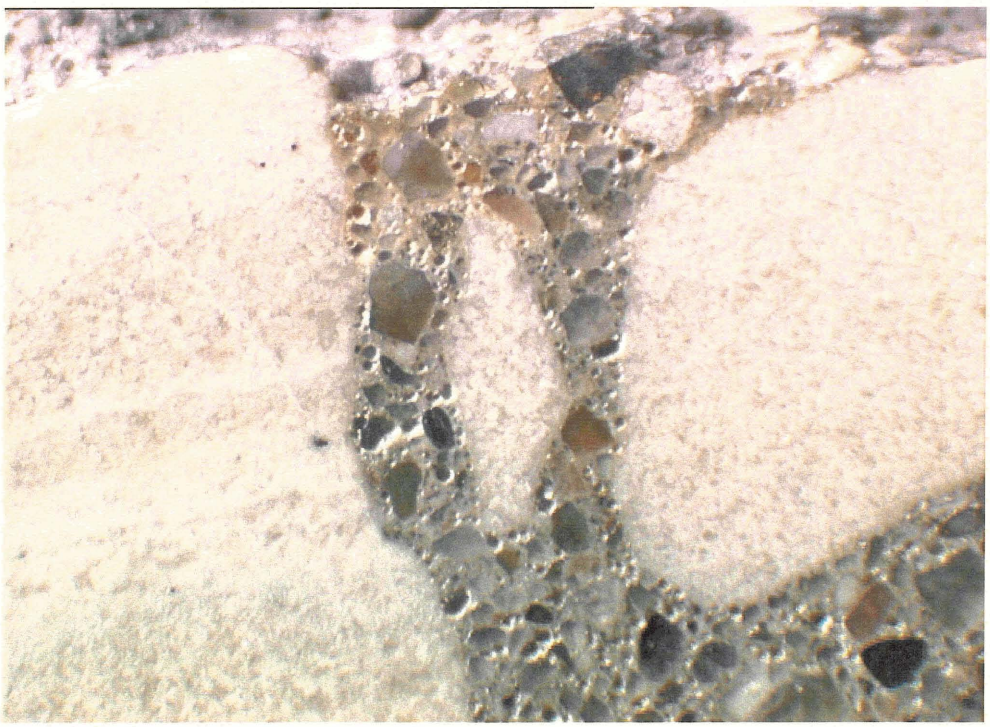

Figure 10. Iowa 175 Core 2 surface microstructure. Slight discoloration in the upper mortar indicates approximate depth of carbonation. Micrograph field width: 14 mm

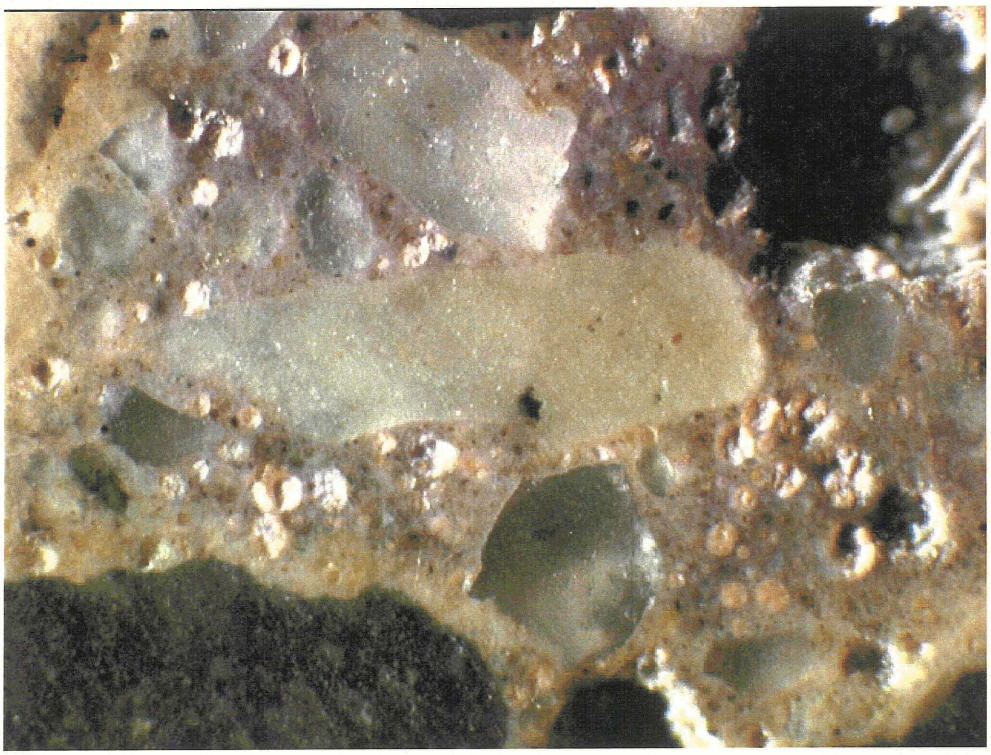

Figure 11. Iowa 175 Core 2 base mortar microstructure exhibiting partial filling of the entrained air void system. Micrograph field width: 4 mm

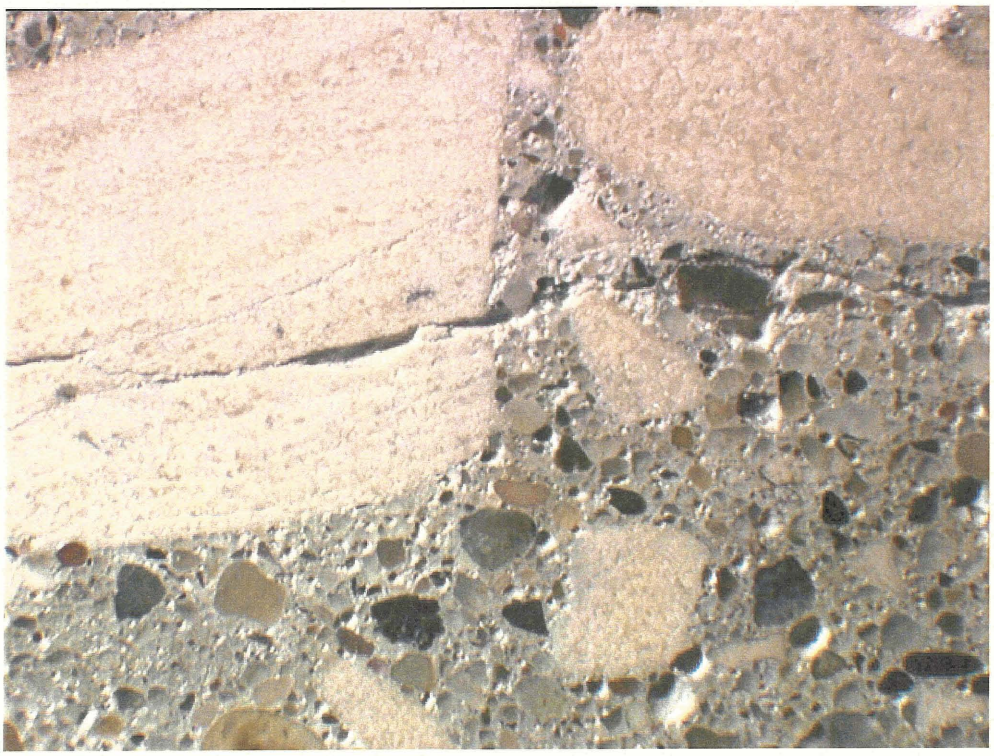

Figure 12. Iowa 175 Core 2 base microstructure exhibits cracking in the mortar and coarse aggregate. Micrograph field width: 14 mm.

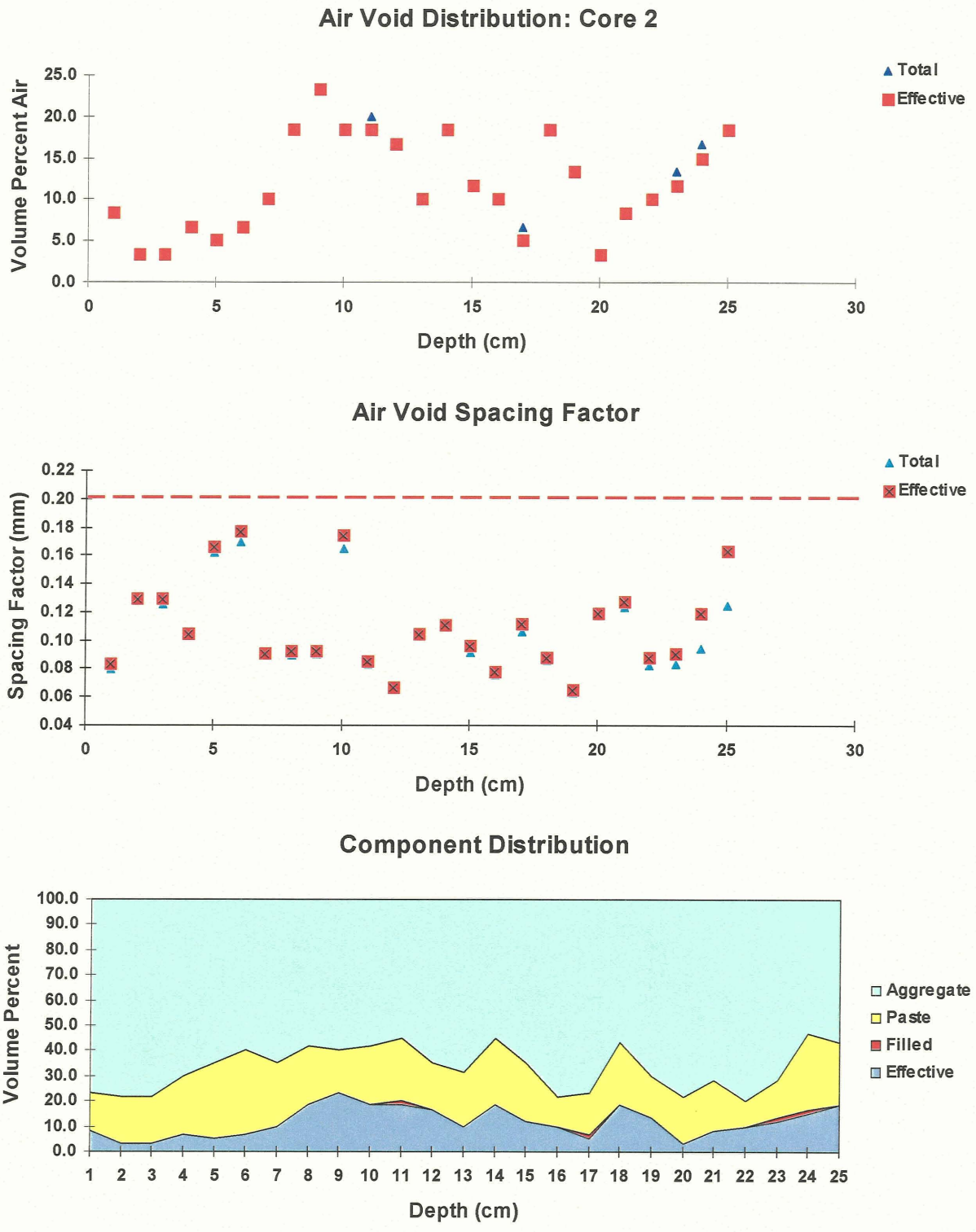

Figure 13. Iowa 175 Core 2 air void and materials distribution plots. A decrease in air near the surface may reflect the loss of entrapped air. The blue triangles represent an air void parameter estimate for the original concrete; the red box represents that value as affected by void filling, if present.

3.2.3 US 20, Webster County

US 20 provided a set of specimens that represented the best- and poorest-performing pavements, concretes with and without fly ash replacement of the cement, and pavements using a single mix design exhibiting opposite performance characteristics. Four sampling sites were identified with the assistance of Iowa DOT to facilitate comparison of poorly-performing with sound pavements. Materials and properties information (Table 4) was taken from IDOT reports supplied to the Pooled Pavement Study by Northwestern University [28].

Table 4. US 20 Location 1, Webster County: Materials and Properties [28].

Cement:	Type I 3.5 % SO_3, 0.77 % equivalent alkali,
Coarse Aggregate:	Ft. Dodge Limestone, Gilmore City bed, ledge 36-42 1 % Freeze-thaw loss, 0.9 % absorption., LA abrasion 28 % loss, durability factor 94
Fine Aggregate:	Yates sand
Admixtures:	AEA (air entraining admixture)
Fly Ash:	Class C, 3.23% SO_3, 2.95% equivalent alkali, 0.28% loss on ignition

Concrete Batch Mass / m^3

Cement	274 kg	0.48 w/s	Slump: 50 mm to 44 mm, avg. 46 mm
Water	160		Air: 7.8 % to 6.0 %, avg. 6.7 %
Fly Ash	46		
C. Agg.	980		slipform paver with spreader
F. Agg.	821		Temp: 31 to 10 (°C), no precipitation, clear/sunny
WR	na		Mix Characteristics: Harsh
AEA no value			31 MPa compressive strength

(IDOT Mix 3 - actual material mass estimated from mass proportions [28]
Completed 5/86, deterioration noted 1990

Cores

No.	Mile Post	Location	Vibrator Trail	Designation	Condition
7	134.4	Joint	Between	7jb	severe pattern, parallel to
8	134.4	Midpanel	Between	8mb	joints, and longitudinal cracking

3.2.3.1 Site Description US 20, Mile 134.4

Sampling location IDOT site 2 was located at milepost 134.4 in the west-bound lane of US 20 in Webster county. Pavements exhibit cracks paralleling the transverse joints, severe mid-panel pattern cracking, joint spalling, popouts, and longitudinal cracking along vibration trials.

3.2.3.2 Core Descriptions

Cores 7 and 8 exhibit a white exhudation from some large shale fragments indicating some alkali-aggregate reaction, though no significant cracking was observed. Large (to 30 mm) entrapped air voids were common. The top surface appears rough with uneven tining grooves. The paste appears strong and cuts cleanly, and the paste / aggregate bond appears strong. The coarse aggregate is a crushed limestone that exhibits some internal cracking, and the sand is silicious and angular. The larger-sized sand particles appear more rounded and contain some shale grains. Segregation is common with a lack of coarse aggregate in the upper third of the core (Figures 14, 15). The partial loss of the core in the upper image of Figure 14 resulted from the core transecting a joint dowel (circular void). Surface cracking terminating in both limestone aggregate and paste is common (Figure 16). These cracks were empty and closed, and were identified through a subtle change in paste coloration due to carbonation along the crack plane. Entrained air void system analysis indicates a lower volume of air near the concrete surface and a significant loss of entrained air void capacity due to filling with ettringite (Figure 17, Table 2). The total air volume decreased from 5.9 % to 4.6 % while the spacing factor has increased from 0.12 mm to 0.26 mm. The loss of the smaller entrained air voids is reflected by the change in specific surface from 35 mm^{-1} to 21 mm^{-1}. The increased spacing factor is in excess of that recommended in ACI 201 for freeze-thaw protection.

Graphical representation of the total air, spacing factors, and component distribution (Figure 18, Figure 19) illustrates the alteration of the air void system resulting from the ettringite filling. Air distribution, as measured by total air volume, appears uniform from the core top to base. Core 7 may show a slight decrease in air in the upper 50 mm, possibly reflecting the elimination of entrapped air in the upper-most portion of the concrete. This also indicates that, outside the immediate regions if the immersion vibrators, the air void spacing factors do not appear to be adversely affected. The decrease in ettringite precipitation near the surface (upper 5 mm) may reflect the influence of surface drying. At greater depths, filling of voids appears uniform from both a total air void volume and loss of spacing factor. Component distribution appears uniform indicating no apparent vertical segregation of materials due to vibration.

SEM examination found no evidence of an overall paste expansion typified by gaps around aggregates. Some cracking was seen within aggregates but similar to the other specimens, there does not appear to be any relation to their rock texture. Rims on outer surfaces of sand-sized chert grains may indicate ASR reactivity but little, if any, cracking appears associated with these grains.

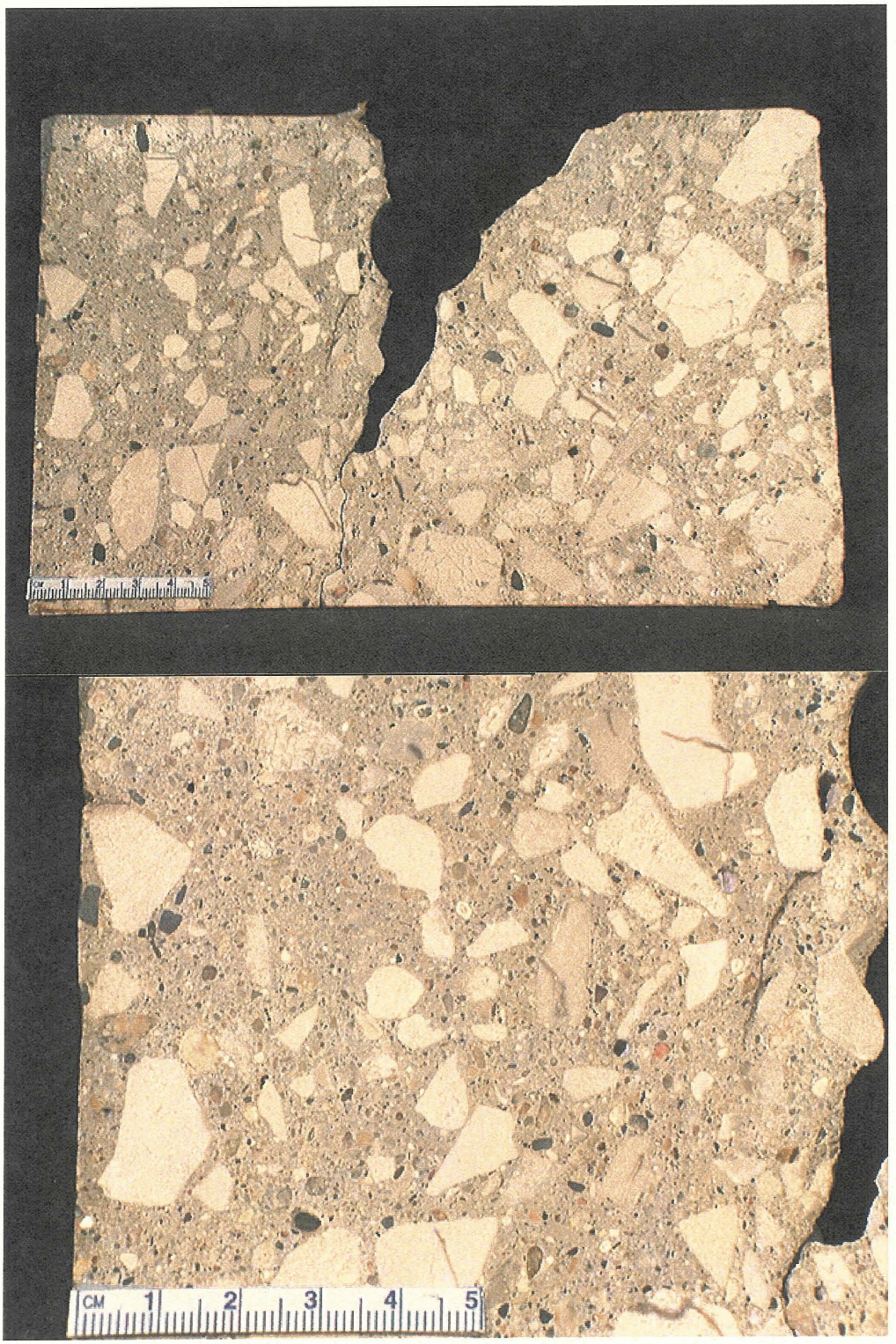

Figure 14. Core 7 (road surface is to the left) exhibits cracking of coarse aggregate, vertical cracks from the surface that are either drying shrinkage or freeze thaw-related. Segregation of mortar and coarse aggregate is visible in the whole core cross section (upper image) and the upper-core microstructure (lower).

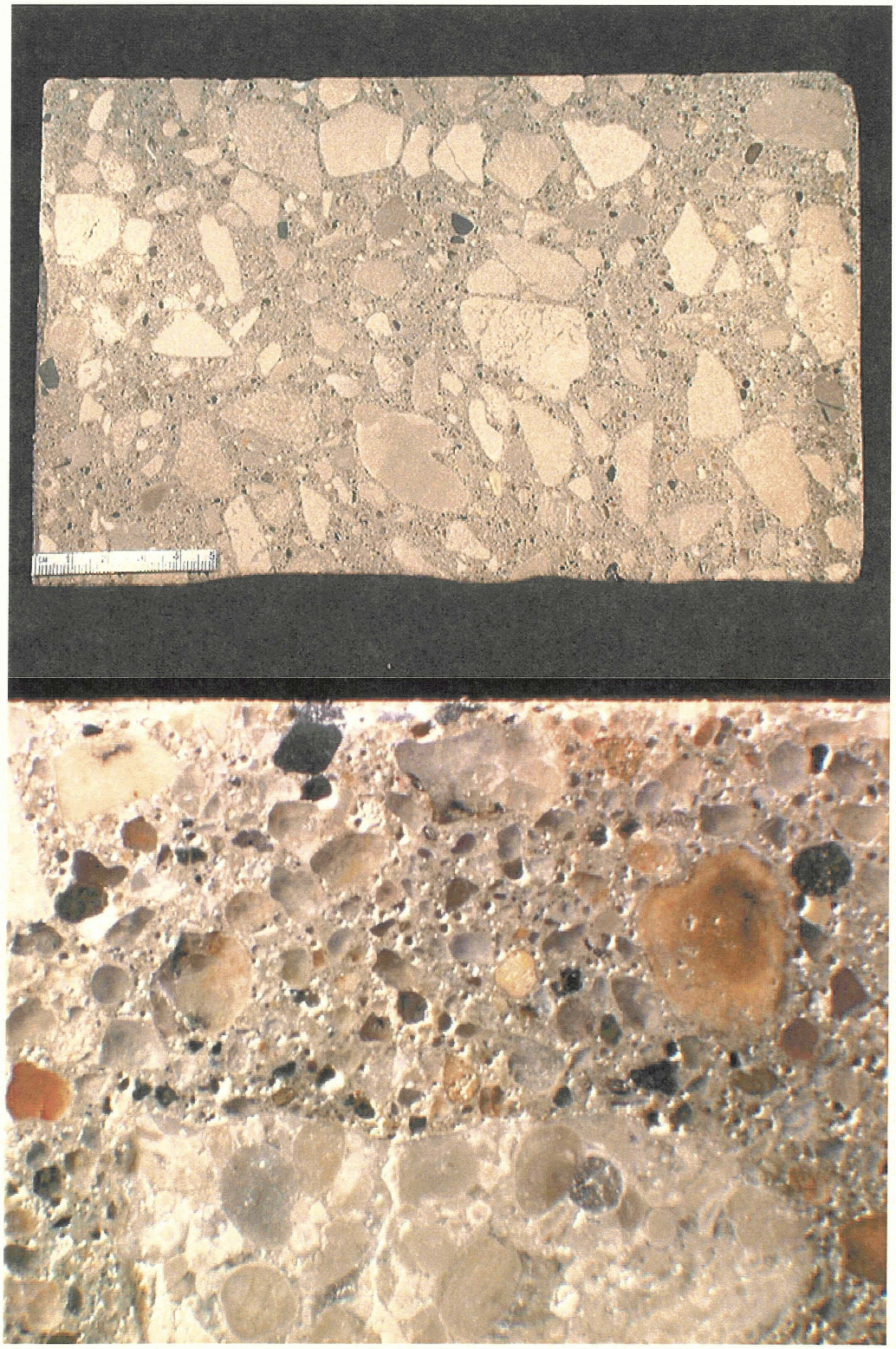

Figure 15. Core 8 exhibits less cracking but does have surface cracking to depths of 20 mm. Some of these cracks as seen in the lower image (13 mm field width) are associated with cracking within the coarse aggregate.

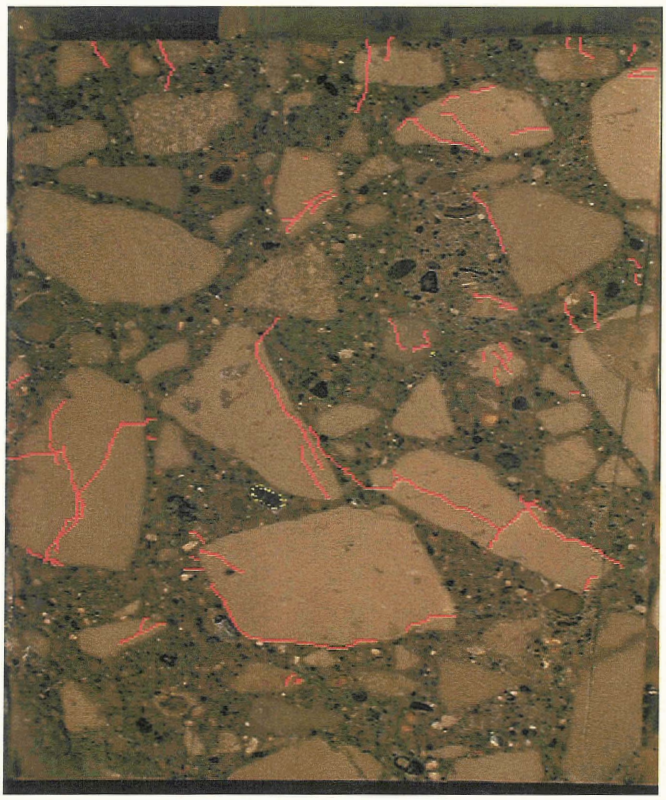

Figure 16. Cracking (red) and ASR (yellow) in Core 7 as observed using SEM. Cracking of aggregate is common. Surface cracks appear carbonated and terminate in both the mortar and the coarse aggregate. Micrograph field width is approximately 10 cm.

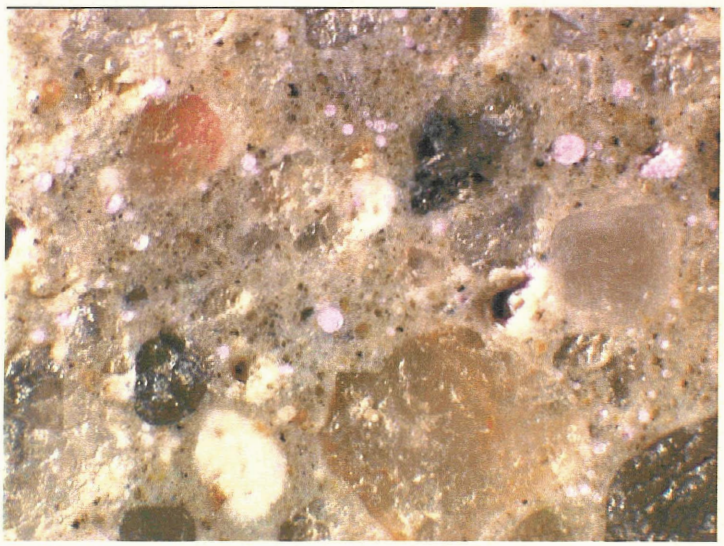

Figure 17. Filling of the smaller entrained air voids (purple) has significantly increased the air void spacing factor while only slightly decreasing the total entrained air void volume for both Cores 7 and 8. Field width: 4 mm.

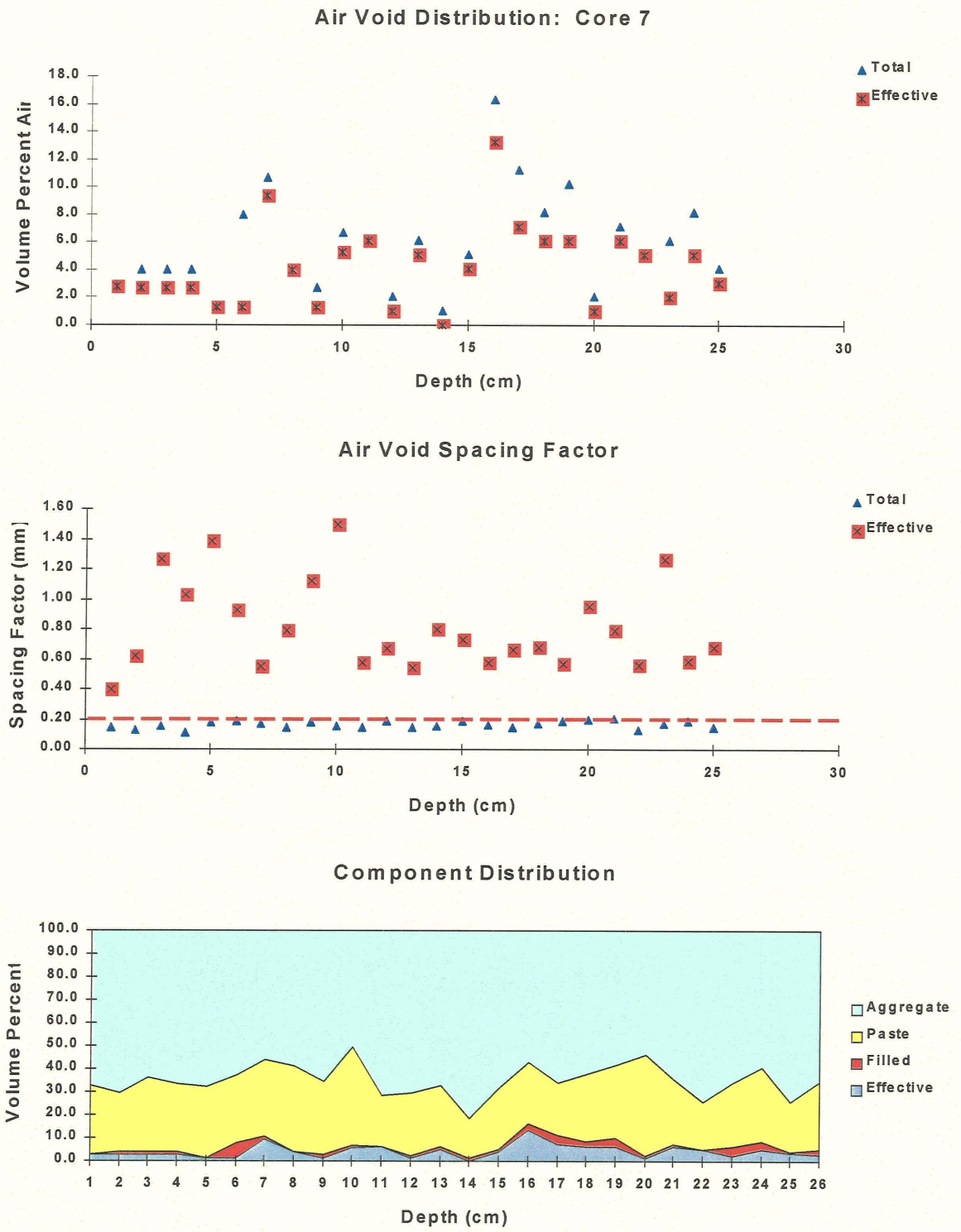

Figure 18: Air void distribution, spacing factors, and concrete component distribution versus depth for Core 7. The red boxes represent the current value, the blue triangle, the original value, and the red line in the spacing factor plot denotes the ASTM C 457 recommended limit for freeze-thaw protection.

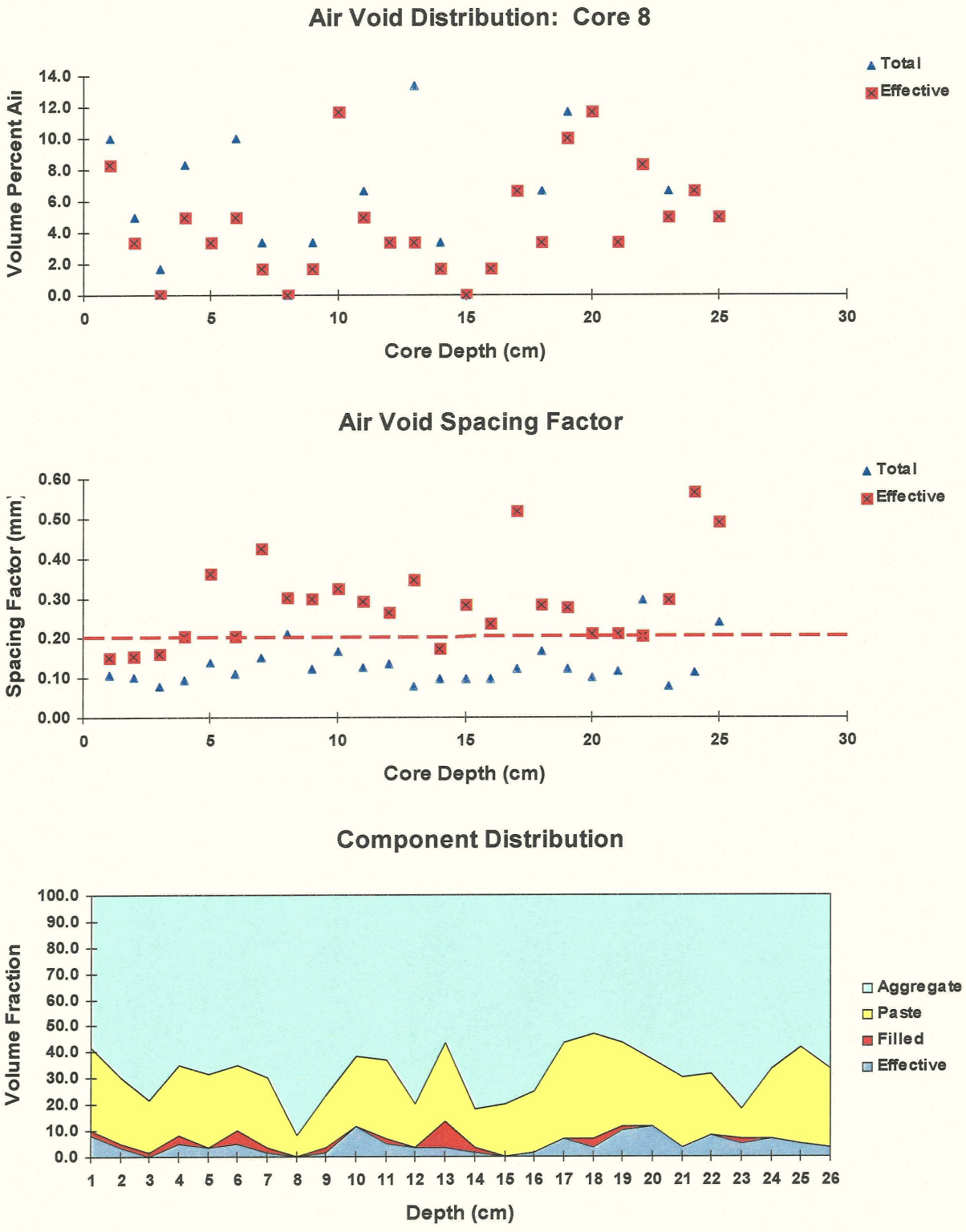

Figure 19: Air void distribution and spacing factors versus depth, and concrete component distribution for Core 8, mid-panel.

Table 5. US 20 Location 2, Webster County: Materials and Properties [28].

Cement:	Type I, 3.5 % SO_3, 0.77 % equivalent alkali,
Coarse Aggregate:	Fort Dodge Limestone, Gilmore City < 1% FT Loss, 0.9 % absorption, LA abrasion 28 % loss, durability factor 94
Fine Aggeregate:	Croft sand
Admixtures:	WR, AEA

No Fly Ash

Concrete Batch Mass / m^3 (IDOT Mix #2)

Cement	340 kg	0.40 w/s	Slump: 50 mm to 40 mm, avg. 46 mm
Water	136		Air: 7.5 % to 5.6 %, avg. 6.5 %
Fly Ash	0		
C.Agg.	1009		Slipform paver with spreader
F.Agg.	825		Temp: 23 to 24 (°C), no precipitation, clear/mild
WR	0		Mix Chara: no data
AEA no value			31 MPa compressive strength

Cores:

No.	Mile	Location	Vibrator Trail	Designation	Condition
13	127	Joint	Between	13jb	appears sound
14	127	Midpanel	Between	14mb	same

3.2.3.2 US 20 Location 2, Webster County

Cores 13 and 14 are from a section of US 20 placed in late 1986 that still appears sound. This pavement used a concrete mix design without fly ash replacement of cement. This sampling site was selected as the use of fly ash was considered to be a potential source of the durability difficulties and therefore provides a reference from which to compare to pavements that incorporated fly ash.

3.2.3.2.1 Core Descriptions

Cross sections of the cores are presented in Figures 20 and 21. The cores exhibit a rough-textured tined surface with an occasional white efflorescence along the core exterior that appears related to shale fragments. The concrete appears sound and strong, it cuts cleanly and has good cement / aggregate bonding. The cement paste is a uniform gray and exhibits only a thin carbonation layer near the core surface. The coarse aggregate is a limestone up to 40 mm in cross section, and the fine aggregate is a silicious sand. Some cracking occured in the coarse aggregate. Shale particles in the sand appear to have undergone some alkali-silica reaction but cracking associated with this reaction appears limited. Sand-sized shale grains at the core surface occasionally exhibit minor popouts. Some cracking was noted at the top surface about 4 mm in length traversing both paste and an occasional sand grain, with some cracking terminating in a limestone coarse aggregate. Segregation of mortar and coarse aggregate is apparent within the cores. Segregation near the surface was not observed. Entrapped air voids as large as 12 mm occur in the lower half of the core. Clustering of entrained air voids in paste, and also along aggregate boundaries is common (Figure 22). The entrained air void system is marginal to substandard with respect to spacing factor, and has been altered slightly due to filling with ettringite. The spacing factor values, especially when examined across the core, are often in excess of those recommended for freeze-thaw resistance (Table 2). SEM imaging of a mid-core paste region (Figure 23) shows the filling of some air voids. Some of the smaller, irregularly shaped capillary voids (black regions) were probably locations of monosulfate that decomposed, serving as the source material for the ettringite. X-ray imaging of the same field (Figure 24) highlights the ettringite locations using its characteristic X-ray signature of high sulfur, intermediate aluminum, and intermediate calcium. Additionally, the reacted shale in the lower-left does not have any associated cracking. Air void volume and spacing factor plots indicate a relatively uniform air volume from top to the base, while the spacing factor appears marginal to about 100 mm below the surface (Figure 25, Figure 26). Void filling, as shown by the spacing factor plot, appears uniform from top to bottom. The component distribution plot also indicates a uniform material distribution, with possibly a slight increase in aggregate with depth. The entrained air void system is substandard when considering the specific surface (Table 2), void distribution, and possibly spacing factor. The poor air void system and the mortar / coarse aggregate segregation throughout the core may reflect the harshness of the mix, incomplete mixing, and so, difficulties in achieving dispersion of the air entraining agent and the ability to generate a good entrained air void system.

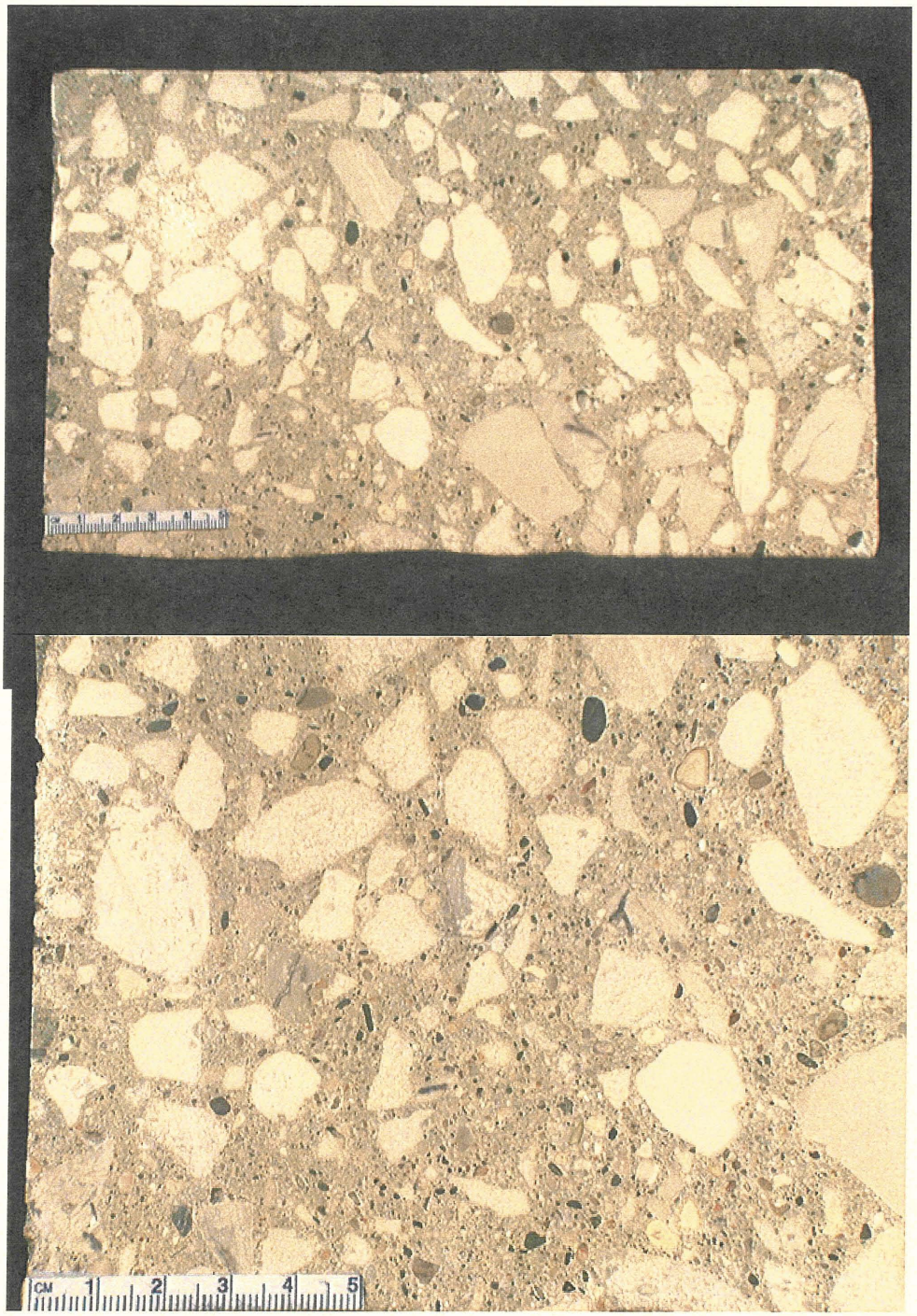

Figure 20. Core 13 cross sections show segregation within the concrete and only minor cracking of the mortar and coarse aggregate.

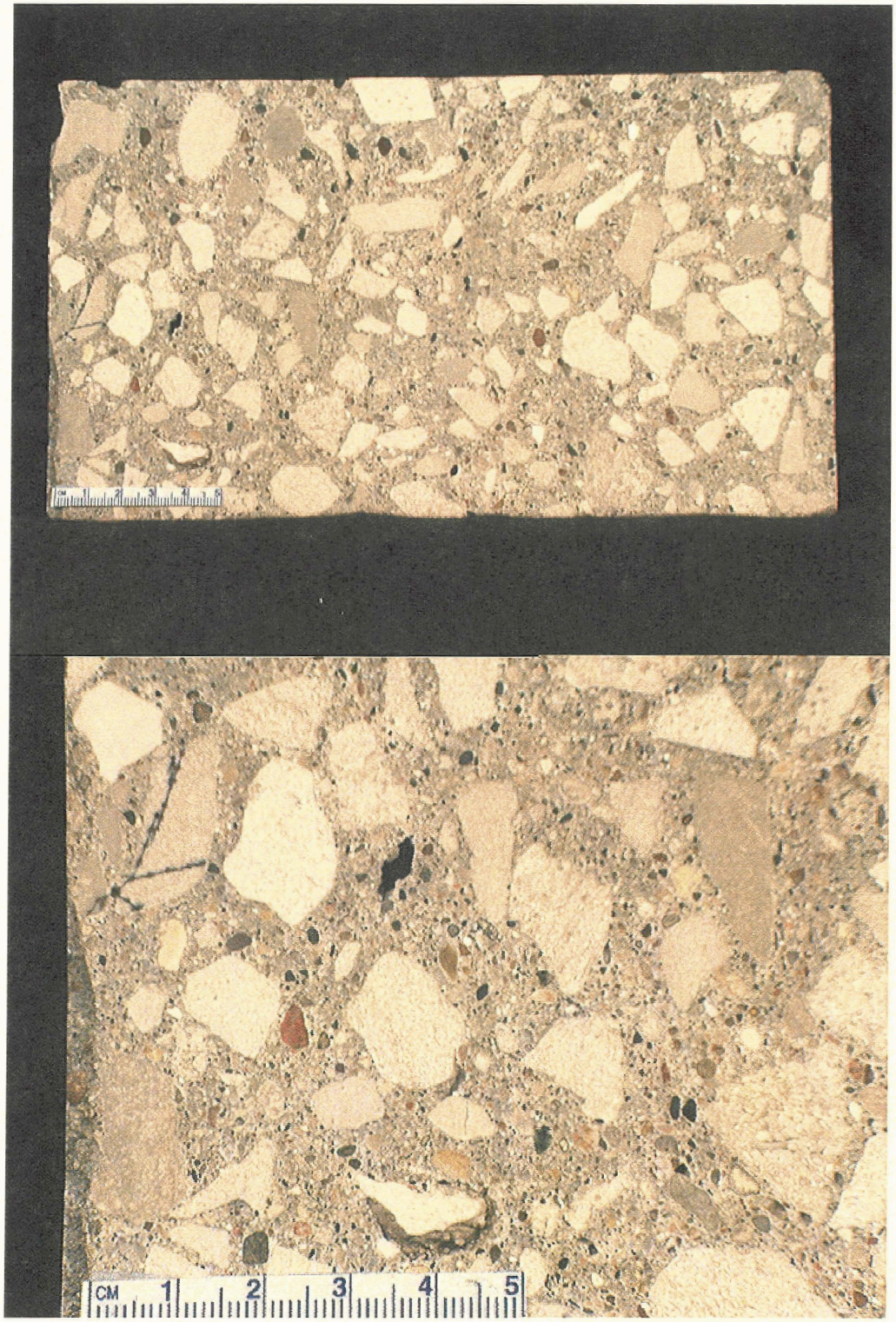

Figure 21. Core 14 exhibits some cracking of both the paste and coarse aggregate and some mortar / aggregate segregation in middle.

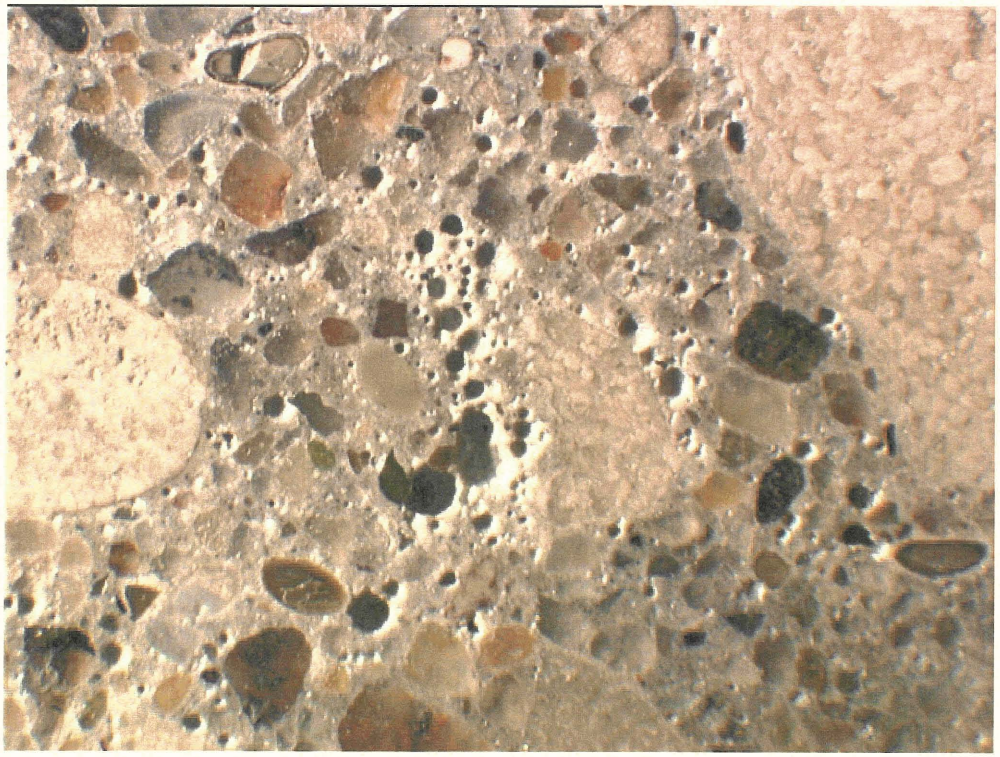

Figure 22. Clustering of air voids may indicate difficulties in mixing and development of a properly sized, disseminated entrained air void system. Field: 7 mm.

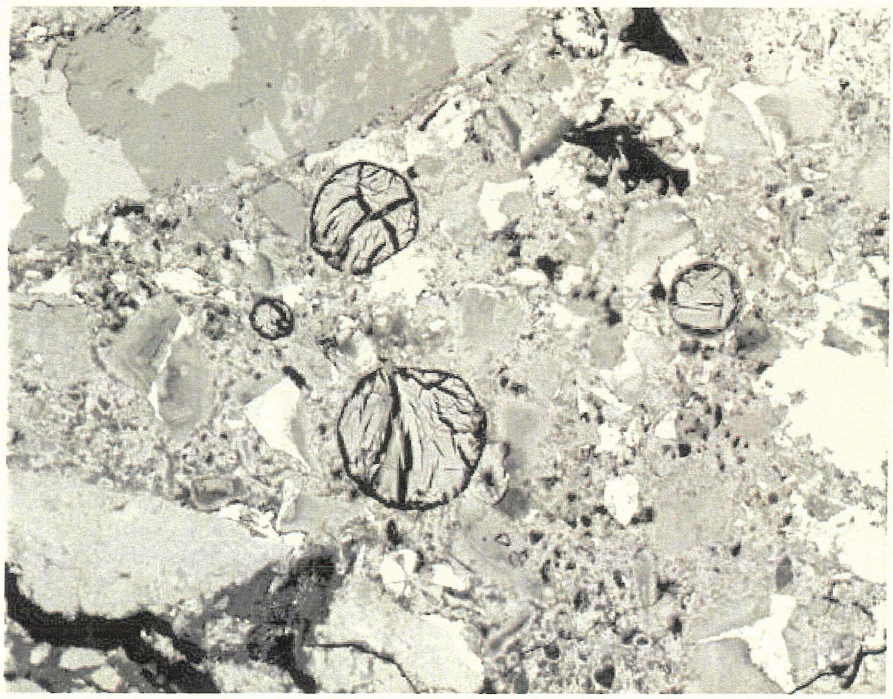

Figure 23. A SEM image of Core 13 paste shows ettringite-filled entrained air voids, the irregularly-shaped capillary voids (black), and a reactive shale grain in the lower-left. Note absence of cracking outside of this shale grain and lack of paste / aggregate gaps that would be typical of an overall paste expansion. Field: 200 μm.

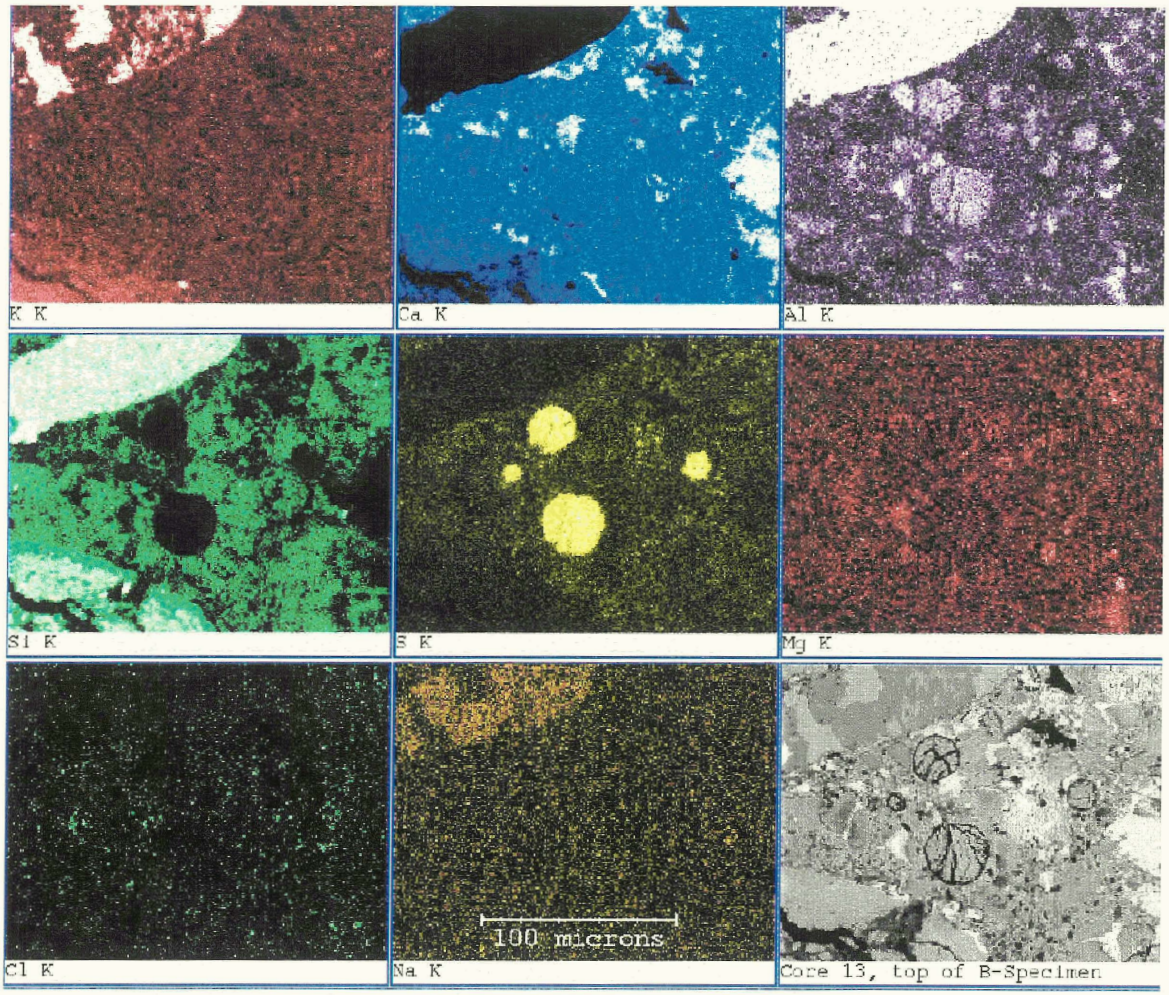

Figure 24. X-ray images corresponding to image in Figure 23. While the shale has undergone alkali-silica reaction, no cracking is apparent within the paste. Common locations of aluminum, sulfur and calcium in the X-ray images delineate ettringite.

The difference between these cores and those from pavements incorporating fly ash is the increased clustering of entrained air voids. The filling of entrained air voids, as seen in these specimens, is not a feature unique to the fly ash-containing concrete pavements. The entrained air void system may also be considered to be marginal to sub-standard. Subsequent filling of the air voids with ettringite resulted in a decrease in total air volume and an increase in spacing factors. While these pavements appear sound, the air void data would indicate that they would exhibit deterioration as time progresses.

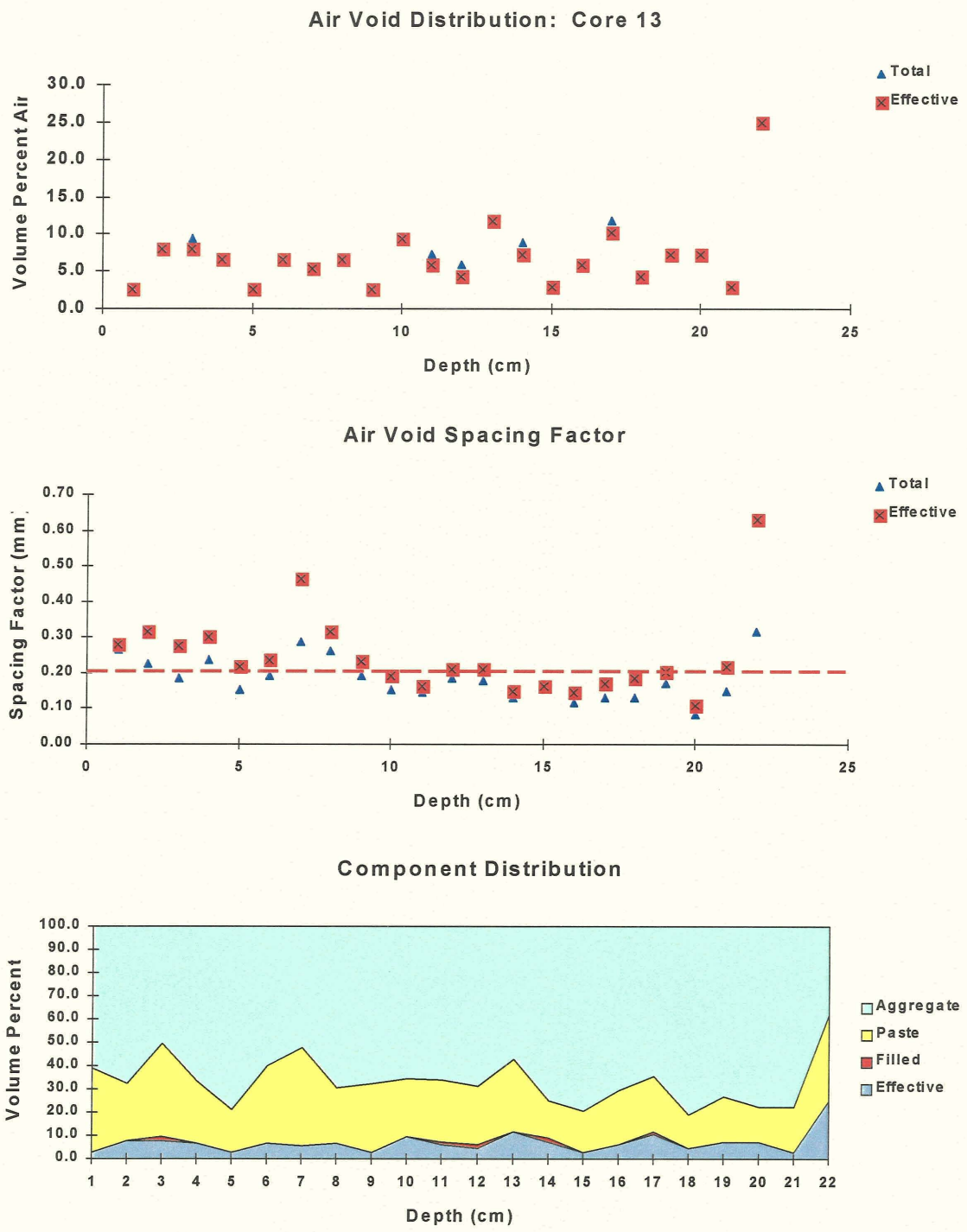

Figure 25. Air void distribution and spacing factors versus depth, and concrete component distribution for Core 13. The air volume appears uniform with depth while the spacing factor appears substandard in the upper 100 mm. Filling has resulted in a slight increase in the spacing factor.

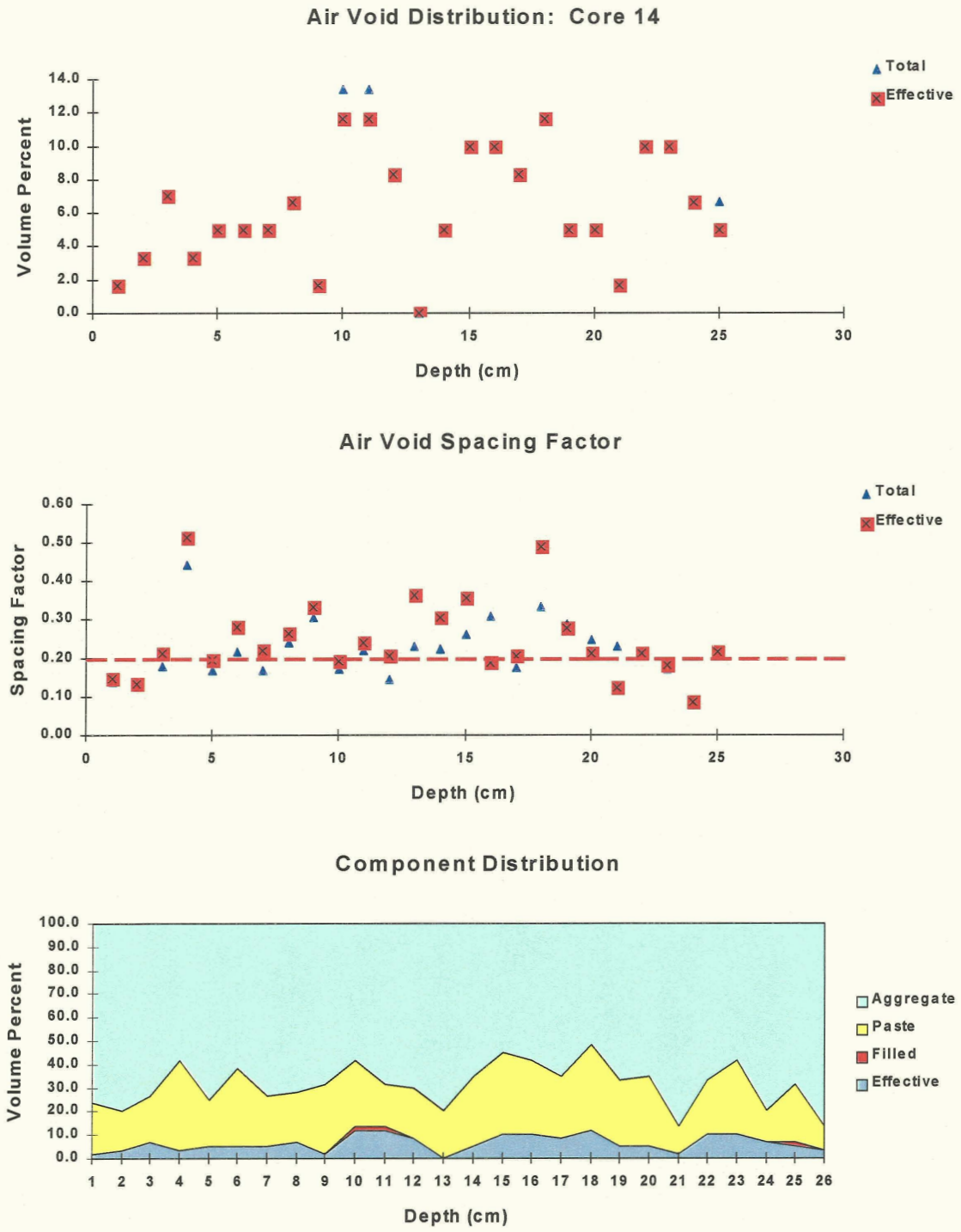

Figure 26. Air void distribution and spacing factors versus depth, and concrete component distribution for Core 14. The total air volume appears similar to that of Core 13 from the joint and appears uniform with depth (deviations from the median probably reflect entrapped air voids). The spacing factor appears marginal to sub-standard at depths below 6 cm, and filling of the smaller entrained air voids has resulted in an increase in void spacing factor.

Table 6. US 20 Location 3, Webster County: Materials and Properties [28].

Cement:	Type I, 3.5 % SO_3, 0.77 % equivalent alkali,
Coarse Aggregate:	Fort Dodge Limestone, Gilmore City < 1 % FT Loss, 0.9 % absorption, LA abrasion 28 % loss, durability factor 94
Fine Aggregate:	Croft Sand
Admixtures:	WR, AEA
Fly Ash:	Class C: 3.62 % SO_3, 3.73 % equivalent alkali, 0.45 % loss on ignition

Concrete Batch Mass / m^3

Cement	274	Slump: 50 mm to 38 mm, avg. 43 mm
Water	160	Air: 6 % to 7.2 %, avg. 6.6 %
Fly Ash	46	
C.Agg.	980	Slipform paver, spreader
F.Agg.	821	Placing conditions: 29 °C, clear/sunny
WR	7	Mix Characteristics: very harsh
AEA	no value	31 MPa compressive strength

Cores:

No.	Mile Post	Location	Vibrator Trail	Designation	Condition/Comments
18	124	Joint	Between	18jb	appears sound
19	125.55	Joint	Between	19jb	severe cracking bituminous overlay

3.2.3.3 US 20, Webster County Location 3

Cores from this sampling site were extracted from US 20, west bound. This pavement was placed using IDOT concrete Mix 1 containing a class C fly ash. Cores from mile 124 (Core 18) were extracted from a short segment that was closed to traffic and not salted for at least the first year. This pavement exhibits no evidence of distress and led to speculation that deicing salts may be significant in the degradation [21].. In contrast, specimens from Mile 125.55 (Core 19) are severely damaged, showing longitudinal cracking along vibrator paths, cracks paralleling transverse joints, and map cracking. The distress was first noted in 1990, about four years after placement, and the crack density appears to decrease with distance from edges and joints.

3.2.3.3.1 Core Descriptions

Core 18 (Figure 27), from a sound pavement at mile 124.4, is approximately 300 mm in length and appears different from Core 19 in that it seems to have a more uniform aggregate gradation, and a substantially better entrained air void system. The concrete appeared sound, though some microcracking was evident in the outer few millimeters under SEM examination. The concrete cut cleanly and exhibits good aggregate - paste bonding. Occasionally, a millimeter-sized void filled with alkali-silica reaction gel was seen, but little cracking was observed adjacent to the gel.

The cement paste is a uniform gray and appears strong and carbonation is limited to a thin layer at the wearing surface. Entrapped air voids as large as 10 mm are common throughout the core. The entrained air void system appears adequate and fairly uniform from top to base, although some filling of the voids by ettringite is present throughout the core. Linear traverse analysis (Table 2) indicates the original and effective air void characteristics as changing little, though some ettringite filling has occurred and the specific surface is lower than that recommended in ASTM C 457. The spacing factor is within that recommended for freeze-thaw durability. This may have been achieved as a result of the relatively high total air volume. Graphical representation of the air void characteristics and concrete composition shows a uniform distribution of entrained air, spacing factor, and component distribution (Figure 28). While much less pronounced than at other sampling locations, the loss of entrained air voids due to filling appears to be uniform with depth, and the decrease in specific surface values indicate a coarsening of the void system. Shale fragments show evidence of alkali-silica reactivity, but little significant cracking is present (Figure 29). No evidence of any overall paste expansion was observed. X-ray imaging revealed a significant amount of chlorine in discrete regions. These regions appear to be the phase chloroaluminate, or Friedel's salt ($C_3A{\cdot}CaCl_2{\cdot}10H_2O$) (Figures 30, 31). The presence of Friedel's salt is not unique to these cores, nor to any specific locations within the core. This mode of occurrence suggests that the chloride may have been present in the plastic concrete, possibly as an accelerator.

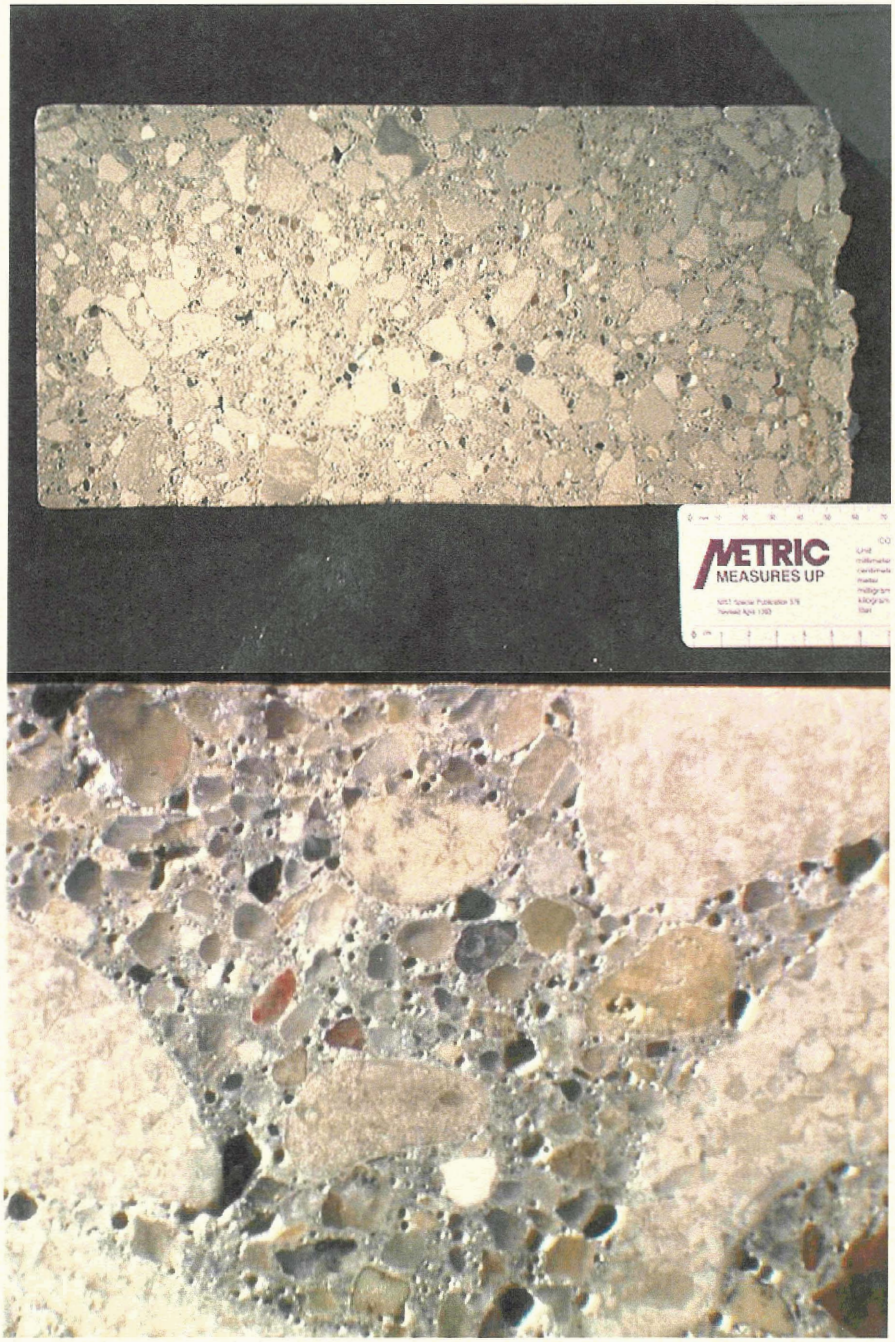

Figure 27. Core 18 contains about 12 % entrained air volume and a spacing factor of 0.08 mm. Aggregate gradation appears more uniform, and possibly smaller maximum size than the degraded pavement concretes. Low specific surface and common entrapped air voids are features common to other cores in this study.

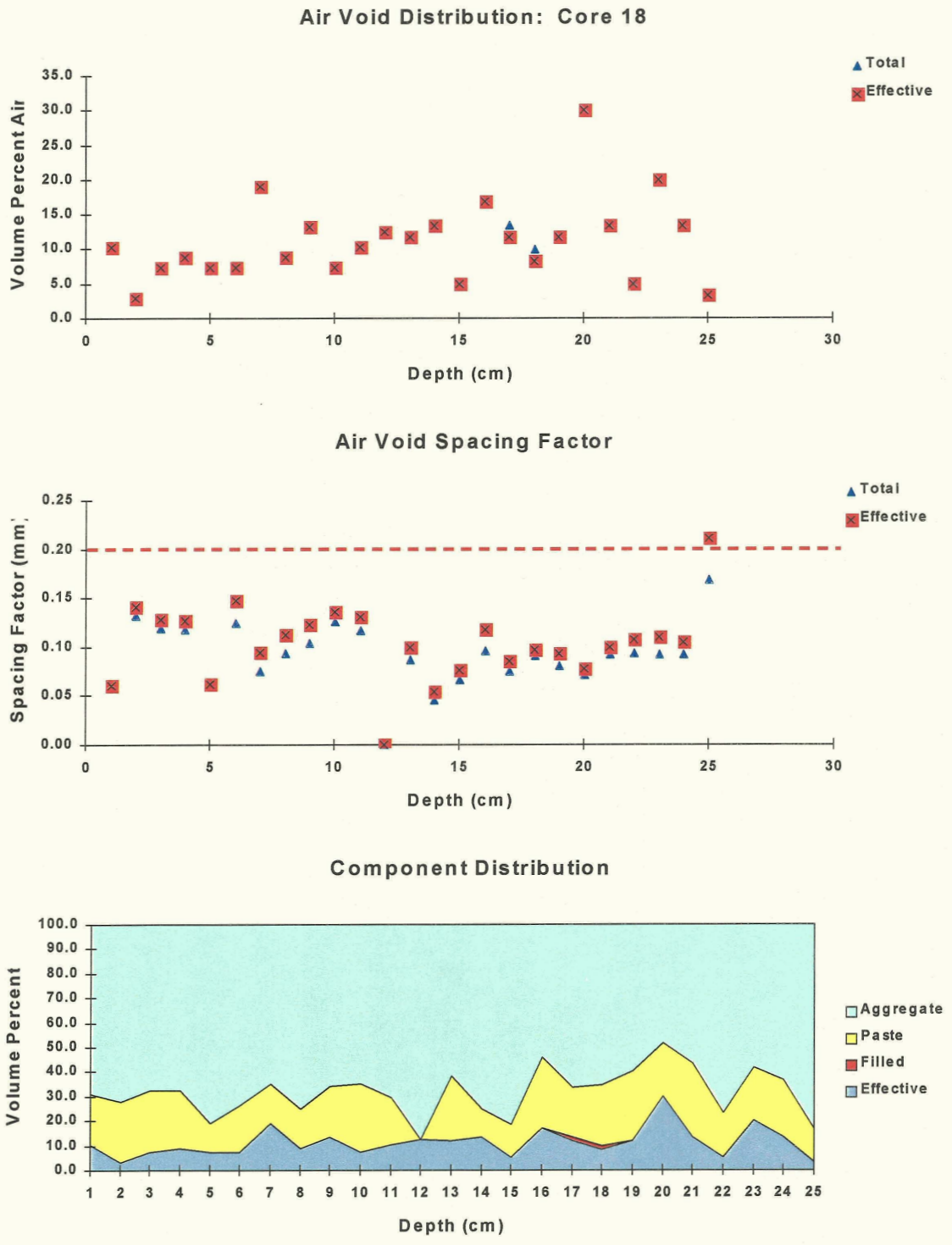

Figure 28. Air void and component distribution plots for core 18. Little loss of air void volume is evident with only a slight, uniform loss of air void spacing factor. Component distribution appears uniform from top to bottom.

Figure 29. Core 18 mortar microstructure includes numerous shale fragments that appear to have undergone alkali-silica reaction, however little cracking of the mortar was evident. SEM examination indicated that some of the reaction product permeated the paste filling the capillary voids adjacent to the shale. Field width: 10 mm.

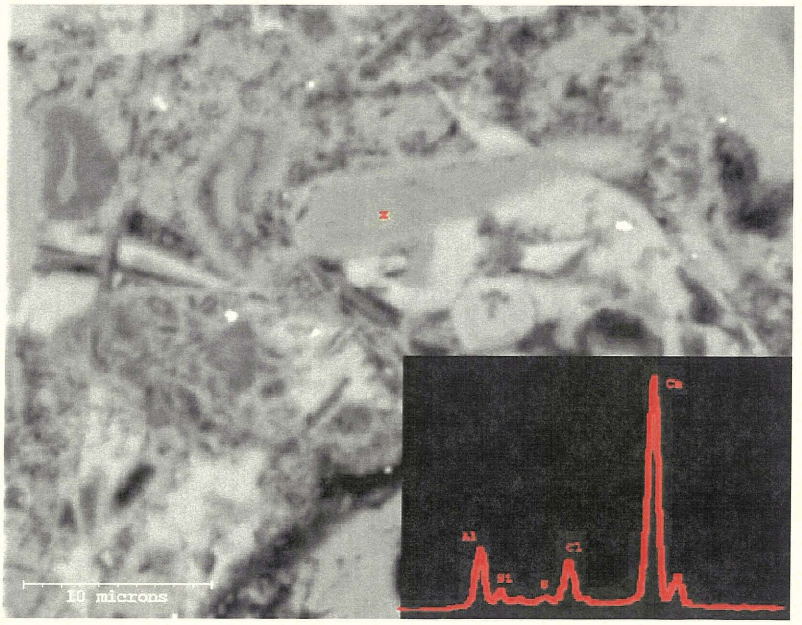

Figure 30. Friedel's salt in hardened paste is identified here using X-ray microanalysis. It appears to be a primary hydration product in the paste throughout the cores, suggesting that it may be a result of the presence of chlorides in the original mix as opposed to the infiltration of road salts.

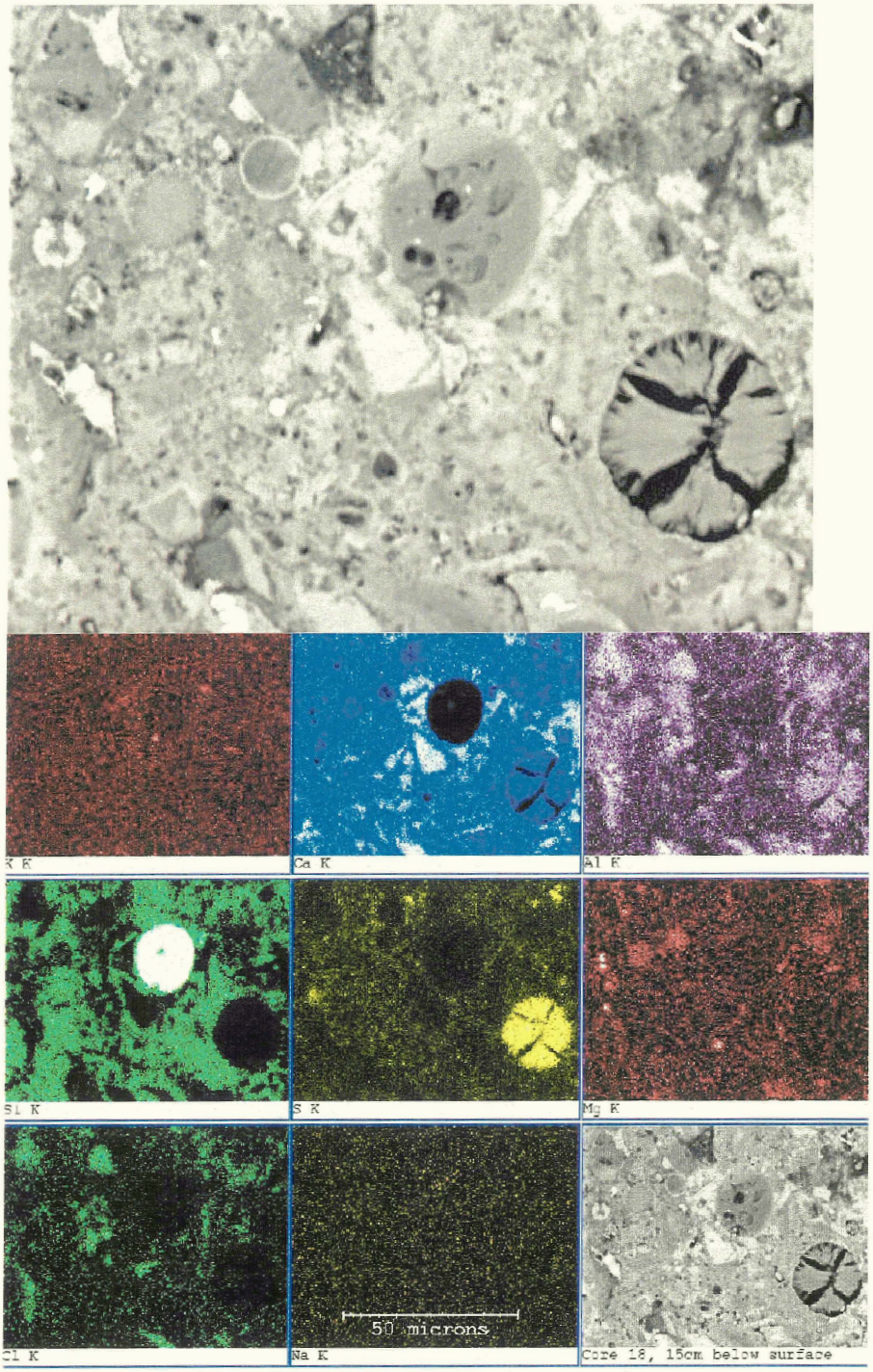

Figure 31. SEM of Core 18 shows an air void partially filled with ettringite (lower-right) and partially reacted fly ash particles (circular). X-ray element distribution (lower image) shows regions of high sulfur and aluminum that delineate locations of ettringite. Regions of chlorine and aluminum delineate regions of chloroaluminate. Field width: 75 μm.

Core 19, from Mile 125.5 on US 20 is from a pavement reportedly containing the same materials and mixture design as for Core 18. Pavements in this location have performed poorly and show extensive deterioration. These sites present an opportunity to compare sound vs. poorly performing concrete with similar, if not the same, materials, proportioning, and placement history.

Core 19 was extracted from the joint region of a pavement. This section of US 20 exhibited the greatest amount of cracking of sampling sites in this study. The core exhibits medium and fine open cracks throughout trending sub-parallel to the road surface (Figure 32). Vertical cracks appear to pass around aggregates and many surface cracks also pass through the coarse aggregate (Figure 33). Cracking within the aggregate is common and may often be traced into the mortar. The coarse aggregate often exhibited a de-lamination of the outer portions of the aggregate, much like the peeling of an onion skin. This feature is similar to that seen in aggregate from a laboratory-prepared concrete beam with known freeze thaw-susceptible aggregates. Damage in the mid-panel cores from this location occurs as cracking sub-parallel to the surface and cracking in aggregates. The mid-panel specimens show slightly less damage further from the surface. All cores cut cleanly and, aside from the cracking, appear sound and strong. Reactive shale in the sand fraction is present and a gel filling in voids adjacent to the shale is occasionally found. Cracking associated with these fragments appears to be very fine and limited in extent. The cement - aggregate bond appears strong. The cement paste is a uniform gray with no evidence of bleeding and only a few millimeters of carbonation along the road surface. Entrapped air voids to 10 mm are common throughout each of the cores.

Figure 34 shows SEM images of the cement paste from Core 19. The upper, backscattered electron, image shows a region that includes a shale grain (left side), and hydration products, fly ash (circular), and pores (black). Alkali-silica reaction gel within the aggregate may be located using the potassium X-ray image (upper-left of the nine image series) yet no cracking is seen within the paste. Ettringite in the cement paste may be identified by its platy parting and by the combined X-ray images of intermediate aluminum, high sulfur, and intermediate calcium intensities. The occurrence of ettringite within the cement paste is common and may be either primary or a replacement of monosulfate. The gaps surrounding the ettringite grains are, in part, shrinkage phenomena due to the microscope vacuum but may also be a result of dissolution. The relatively large, irregular-shaped pores (black) may indicate dissolution of monosulfate and calcium hydroxide. Field examinations of this pavement did not find any evidence of overall expansion, making the occurrence of ettringite apparently innocuous. Regions of the chlorine (lower-left) and intermediate-intensity aluminum images delineate chloroaluminate, or Friedel's salt.

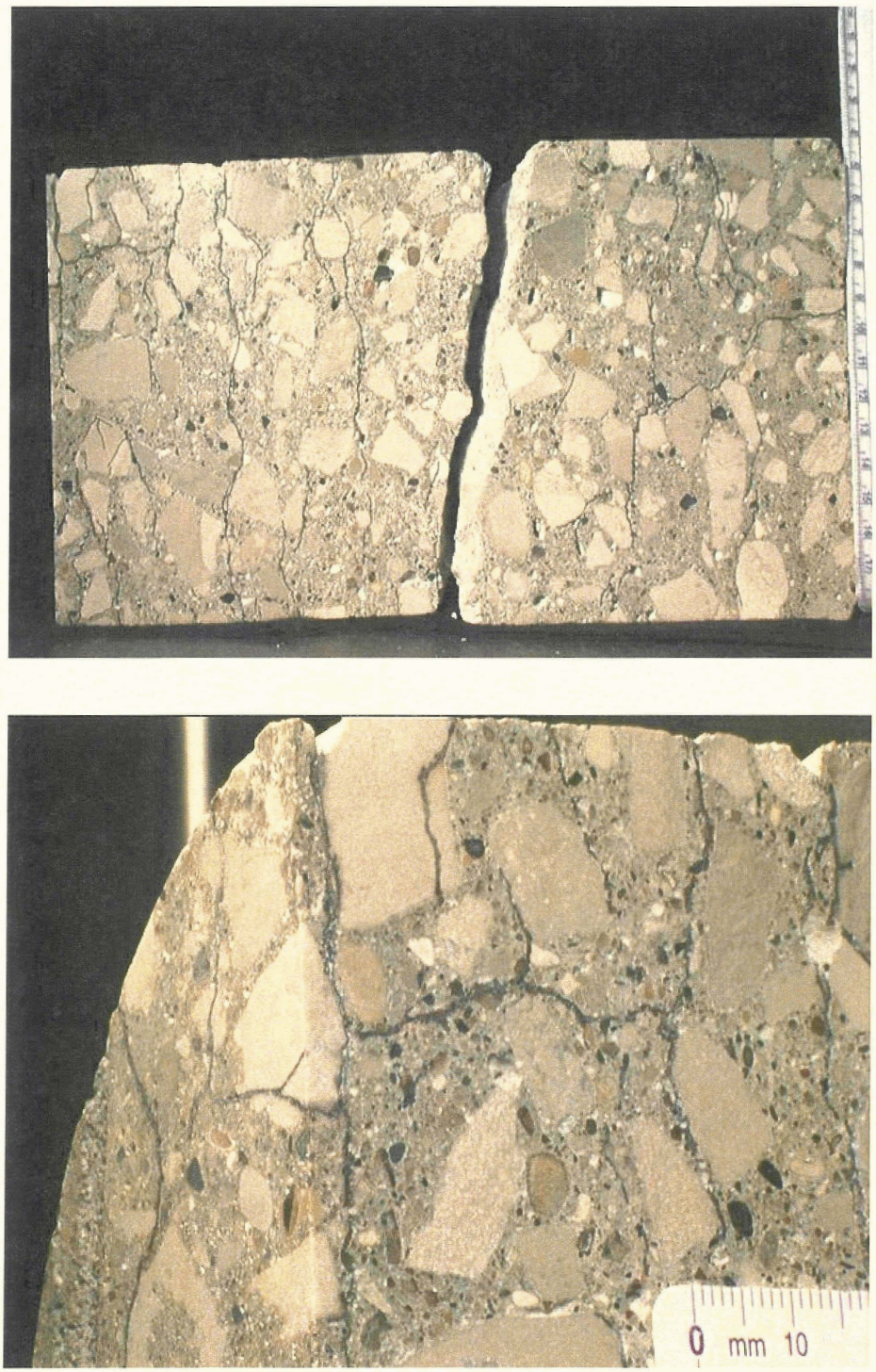

Figure 32. Core 19 exhibits extensive cracking of both the paste and coarse aggregate. Cracks trending parallel to the pavement surface (to the left) intersect perpendicular cracks; features typical of freeze-thaw cracking. The oblique view of the upper portion of core 19 shows cracking in both the surface (polished for clarity) and cross-section orientations.

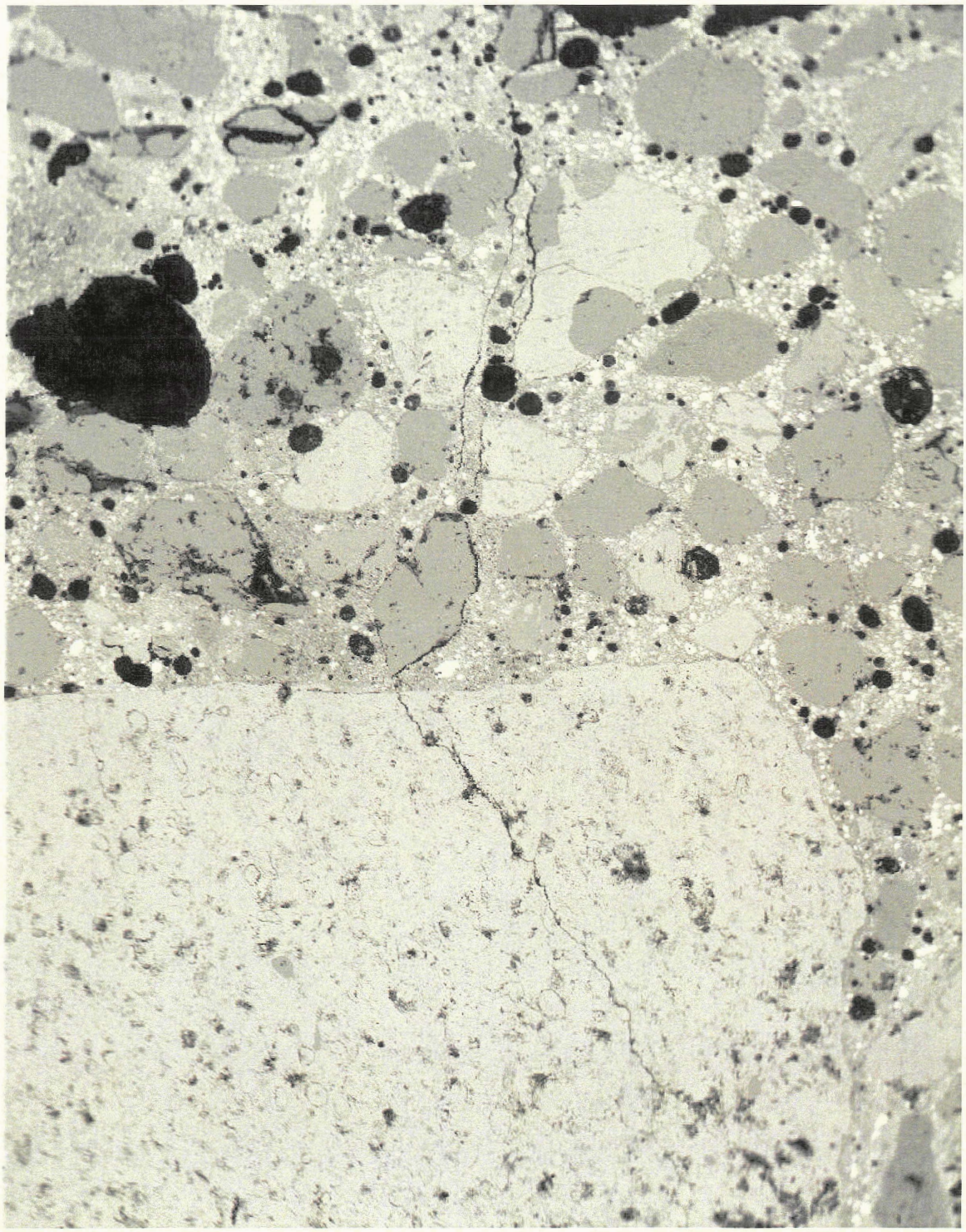

Figure 33. SEM image of a surface crack (road surface is at the top, 5 mm field width) extending through the paste portion of the mortar and terminating in a coarse aggregate.

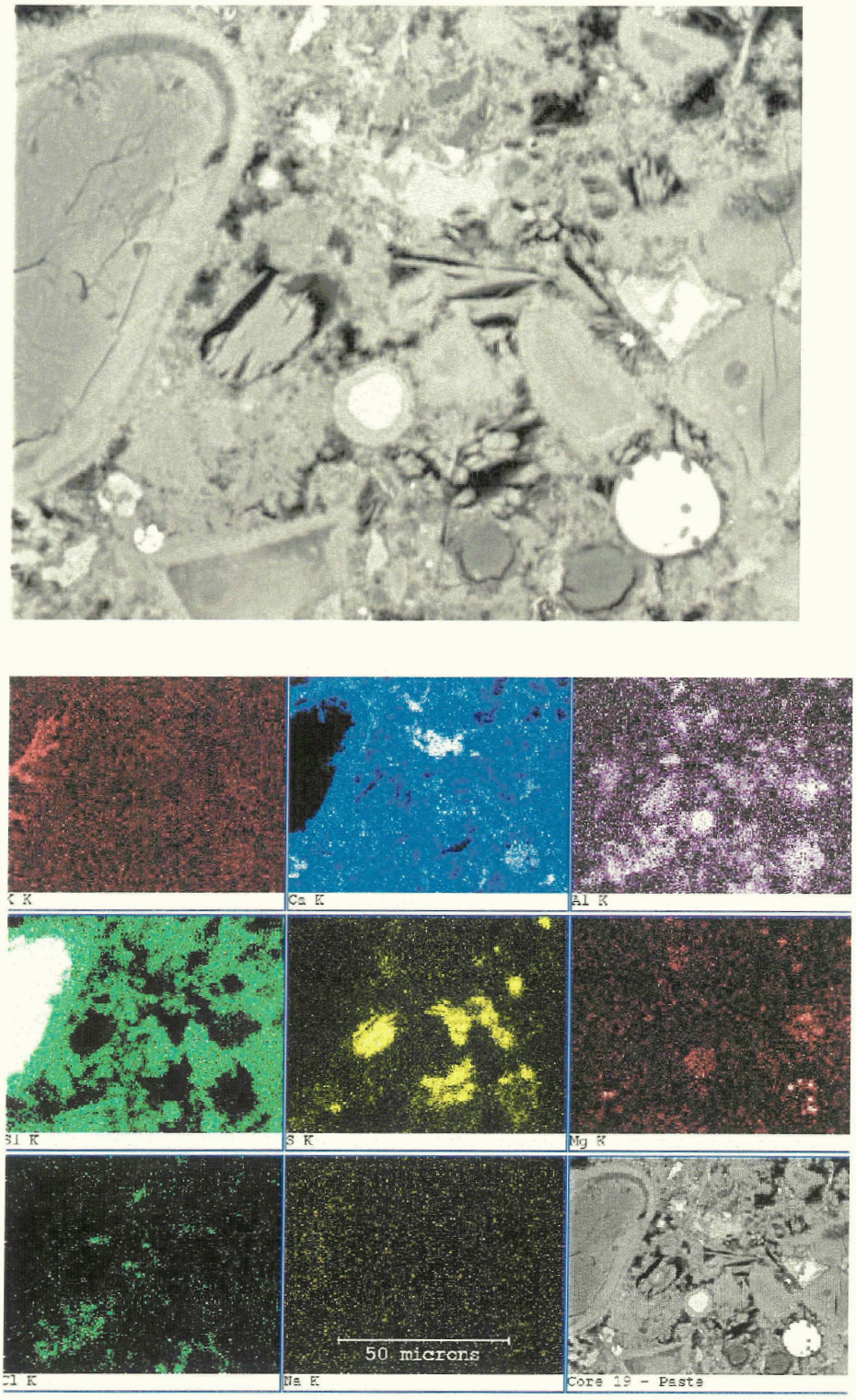

Figure 34. Back scattered electron image of Core 19 paste microstructure showing ASR-affected shale (left) and fly ash (circular). X-ray image regions of high sulfur (yellow) and intermediate aluminum (purple) mark locations of ettringite while regions of high chlorine (lower left image) denote locations of chloroaluminate.

Air void analysis (Table 2) show that total air decreased 1.6 % and the spacing factor more than doubled to 0.29 mm, while the specific surface dropped indicating a substantial coarsening of the effective entrained air void size distribution. The specific surface value of 14.67 is much lower than the recommended interval of between 23.6 and 43.3 indicating an air void size distribution much coarser than that recommended by ASTM C 457 [44].

Visual examination of Cores 18 and 19 found a likely difference in aggregate grading (Figure 35) with Core 18 appearing to have a more uniform, and perhaps smaller, aggregate gradation. The apparent change in aggregate gradation may have affected the development of the higher-volume entrained air void system in Core 18. However, specific surface values indicate a coarse air void size distribution.

Graphical representation of the air void and component distributions indicates a decrease in spacing factor and an increase in cement paste content with depth (Figure 36). The spacing factors for both the total (original) and effective systems fall beyond that necessary for frost protection at depths greater than 150 mm.

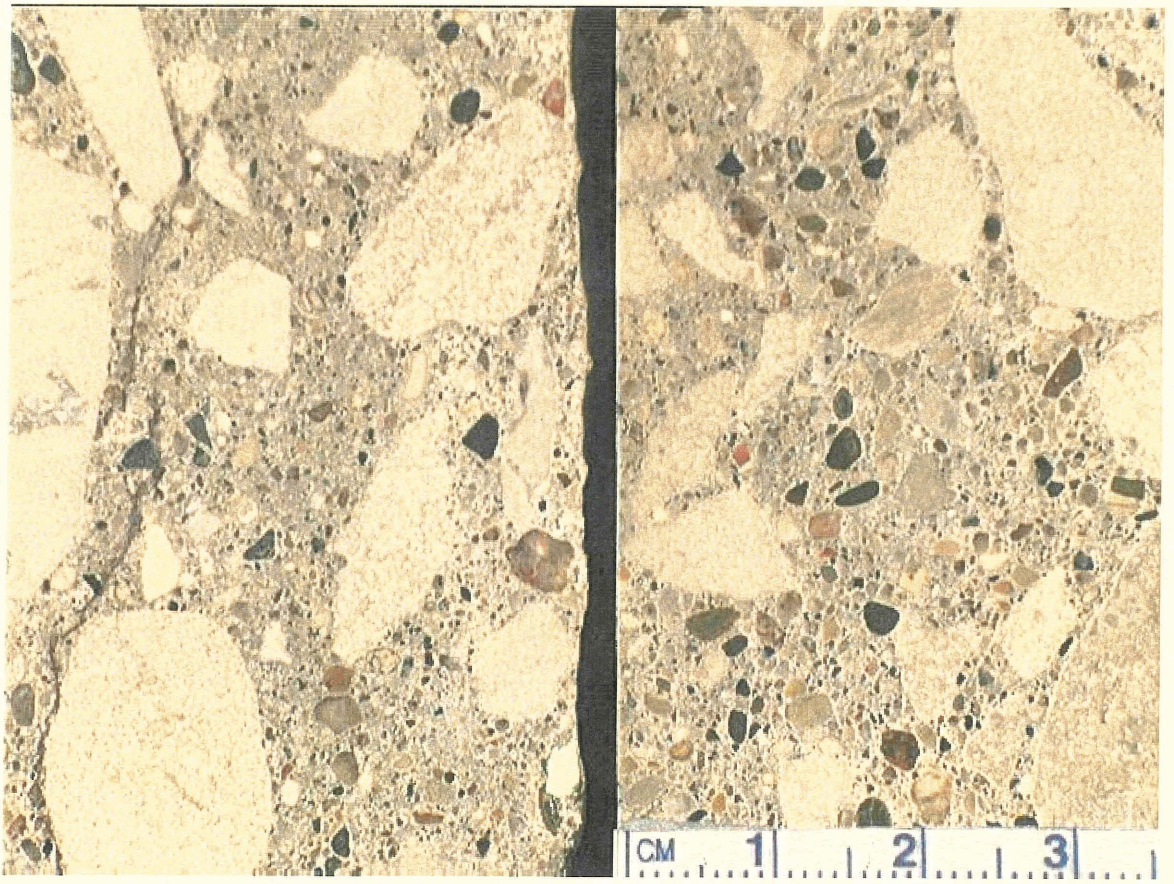

Figure 35. Core 19 (left) appears to have a finer-sized sand and possibly a larger maximum coarse aggregate size when compared to Core 18 (right).

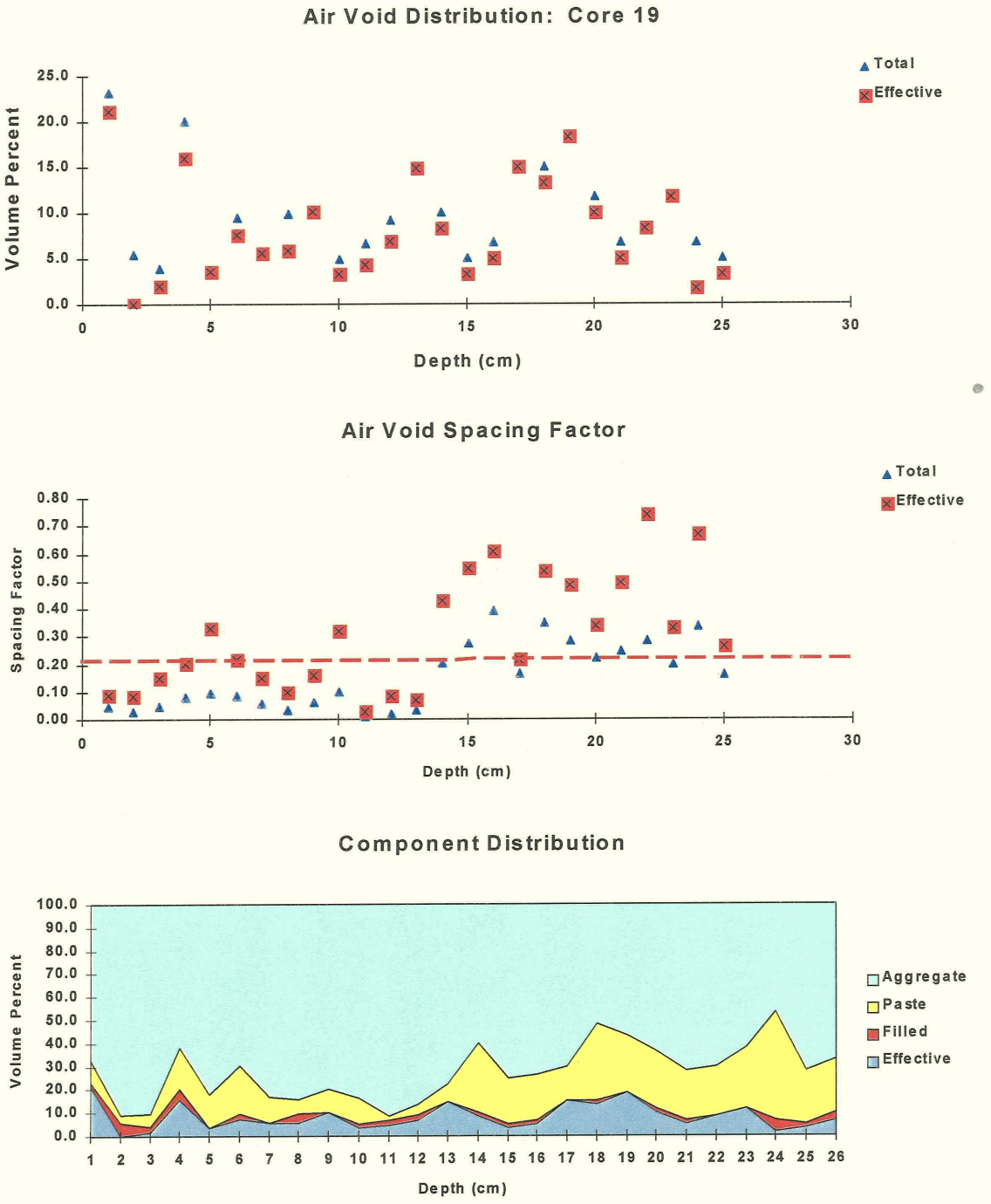

Figure 36. Core 19 data show a decrease in spacing factor with depth and possibly a trend to an increased loss of spacing factor with depth. The component distribution plot shows a possible increase in aggregate and decrease in paste in the upper half of the core.

Figure 37 shows the results of modeling aggregate expansion to simulate freeze-thaw failure of the coarse aggregate. Using a finite element program on the digital images, selected components of that image, such as the aggregate or the paste, are allowed to expand. Other components in the concrete serve to restrain this expansion, giving rise to stresses in the concrete. To simulate the field conditions, the section was surrounded on three sides by an effective material having the same material properties as the bulk concrete, while the upper surface was free to expand. This technique is still in development and is limited in that it uses a linear elastic finite element algorithm. Only stress analysis is considered, and the code uses finite-sized, 2-dimensional images. However, it should provide some insight as to how differing deterioration modes may affect the crack patterns [29,30].

The upper image is of the specimen examined in the electron microscope. Cracking (red) and ASR-affected shales (yellow) have been highlighted to provide a clearer picture of their occurrence within the concrete. The model was configured such that the core section was surrounded by similar material and only the top surface was free to move. In this example, expansion of the aggregate produced the color-coded stress image where intensity increases with a color change from black to yellow to red. High stress regions occur in the paste where two aggregates lie within close proximity, and within the aggregates. Many of these sites are also locations of cracking. However, not all of the cracks may be explained using this simulation, so aggregate expansion can explain only some of these cracks. Simulations where the paste was allowed to expand, such as in freeze-thaw cycling of paste, also showed high stresses in regions of cracking.

This data indicates that both coarse aggregate expansion and paste expansion may explain many of the cracks in this specimen. As no alkali-aggregate reaction products are associated with cracking in the coarse aggregate, these cracks must be attributed to freezing of water within the aggregate pore system. The paste expansion must be a result of freezing as the lack of evidence of a permanent expansion and lack of paste-aggregate interfacial zone gaps eliminates the overall, uniform paste expansion of delayed ettringite formation. Additionally, if the relatively coarser-sized pore systems of the aggregate are critically saturated, then the paste pore systems must also be saturated.

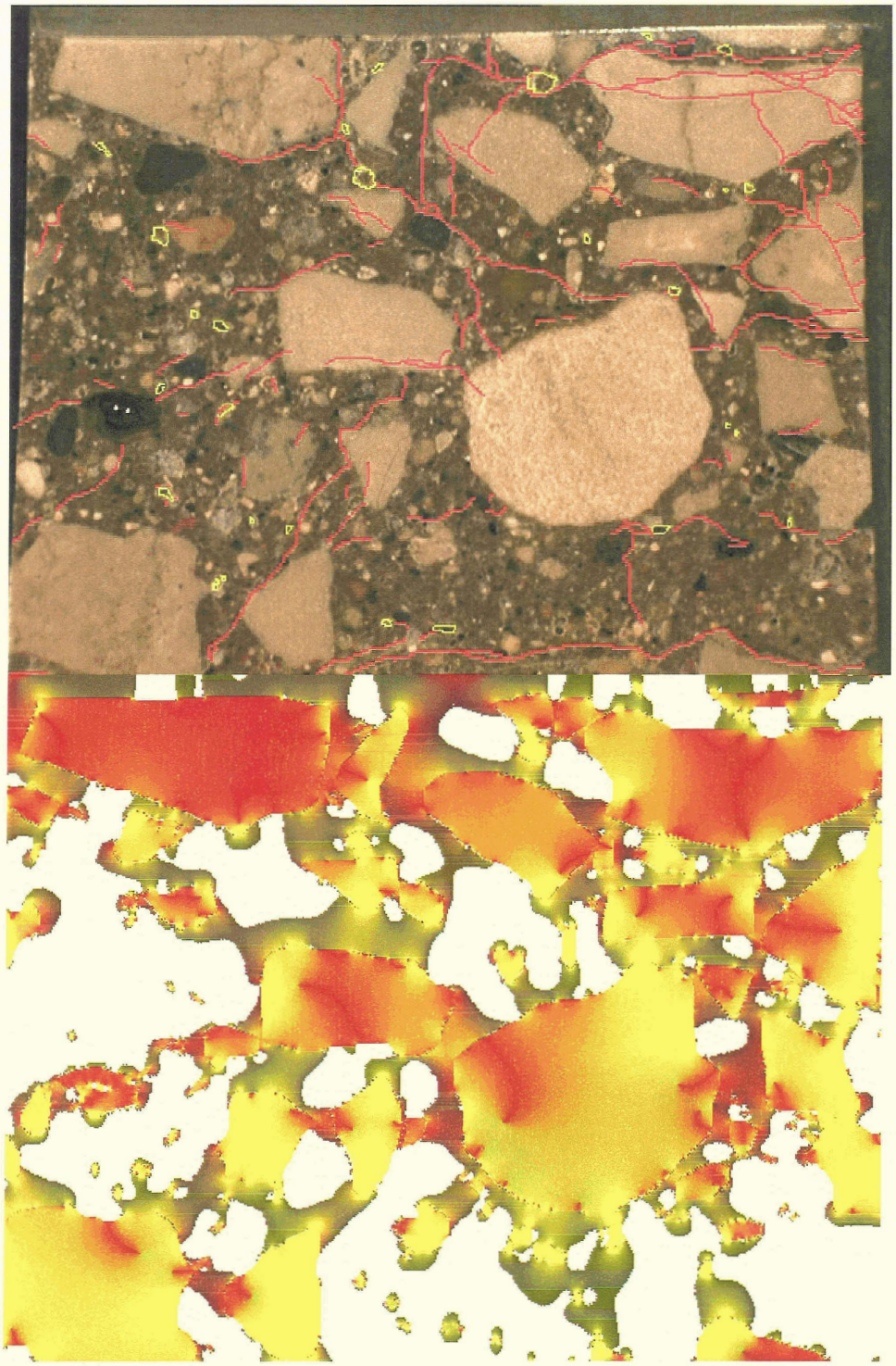

Figure 37. Top portion of core 19 with cracks (red) and ASR-affected shale grain (yellow) shows cracking through both the cement paste and coarse aggregate. A color-coded stress image resulting from a simulation of aggregate expansion showing regions of high stresses in red correlates well with some, but not all of the observed cracking.

3.3 Iowa I-35, Story County

Iowa I-35, Story County at mile post 122.1 (Table 7) exhibits longitudinal cracking and joint staining, along with pattern cracking at mid-panel joints. These pavements exhibits spotty damage that is less well-developed, and, according to Iowa DOT, were slower to show deterioration.

Concrete appears sound, well-proportioned, uniform, cuts cleanly with a strong appearing cement paste-aggregate bond (Figure 38). A single horizontal crack was found in the lower-third of the Core 11. The coarse aggregate consists of an angular crushed limestone predominantly of a grainstone texture. These specimens appear to have a finer coarse aggregate size and more uniform aggregate size distribution compared to those from US 20. The fine aggregate is composed of angular, silicious sand with a small proportion of oblate shale grains of up to 5 mm in size. The cement paste appears uniform and gray with carbonation limited to the outer few millimeters of mortar. Entrapped air voids were common in the regions about 4 cm above and below the surfaces. Vertical cracks from the surface were common and appear to terminate both within the mortar and a coarse aggregate (Figures 39, 40).

The entrained air void system (Table 2) was measured at 8 % to 9 % air by volume, with a spacing factor of 0.16 mm to 0.18 mm, and specific surface of 17 mm^{-1} to 21 mm^{-1}. These values are within recommended limits with the exception of the specific surface. Filling of some of the voids by ettringite results in a doubling of the spacing factors to 0.30 mm and 0.32 mm, a decrease in specific surface, and a loss of 2 % air volume for the joint core. This was the greatest volume loss for the set examined in this study. The original air void systems for cores 11 and 12 appear uniform with depth. Filling, in contrast, appears uniform for core 11 (Figure 41), but increases with depth for Core 12 (Figure 42), the mid-panel specimen. This may reflect the availability of water at the joint as compared to the mid-panel. The increased filling with depth may reflect a source of water beneath the slab or the effects of surface drying.

Table 7. I-35 Story County Location 5: Materials and Properties [28].

Cement:	Type I, 3.15 % SO_3, 0.63 % equivalent alkali
Coarse Aggregate:	Alden, open quarry, limestone, 1.50 % freeze-thaw loss, 2.70 % absorption LA Abr. 40 % loss, durability factor 79
Fine Aggregate:	Hallet (Ames pit)
Admixtures:	WR, AEA
Fly Ash:	Class C, 3.36 % SO_3, 2.87 % equivalent alkali, 0.33 % loss on ignition

Concrete Batch Mass / m^3

Cement	303	Slump: 76 mm to 19 mm, avg. 48 mm
Water	150	Air: 8 % to 5.3 %, avg. 6.1 %
Fly Ash	52	
C.Agg.	946	slipform paver, with spreader
F.Agg.	828	Temp: 32 °C, no precipitation, cloudy / cool
WR	No Value	Mix Characteristics: no problems
AEA	no value	33 MPa Compressive strength

actual material mass estimated from mass proportions [28]

Cores:

No.	Mile	Location	Vibrator Trail	Designation	Condition
11	122.1	Joint	not visible	11j	minor pattern cracking, joint staining, and longitudinal cracking
12	122.1	Midpanel		12m	

Figure 38. Cores 11, joint (top) and 12, mid-panel (bottom) cross section with horizontal crack in lower-most third. Some segregation is visible in both cores.

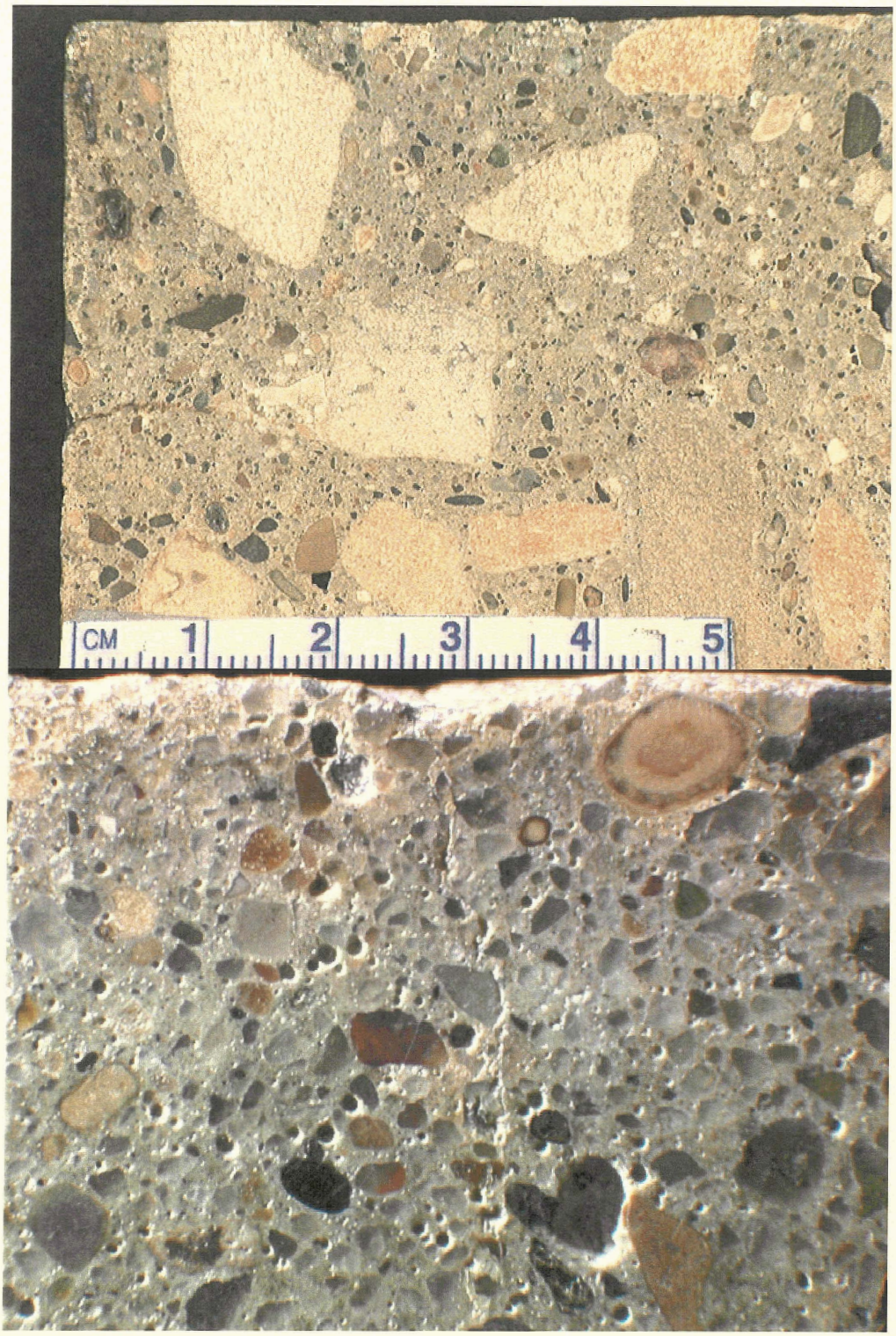

Figure 39. Surface cracking in Core 11 to about 20 mm passes through both the mortar and coarse aggregate. Lower image shows minor surface carbonation and cracking within the mortar. Field width 8 mm.

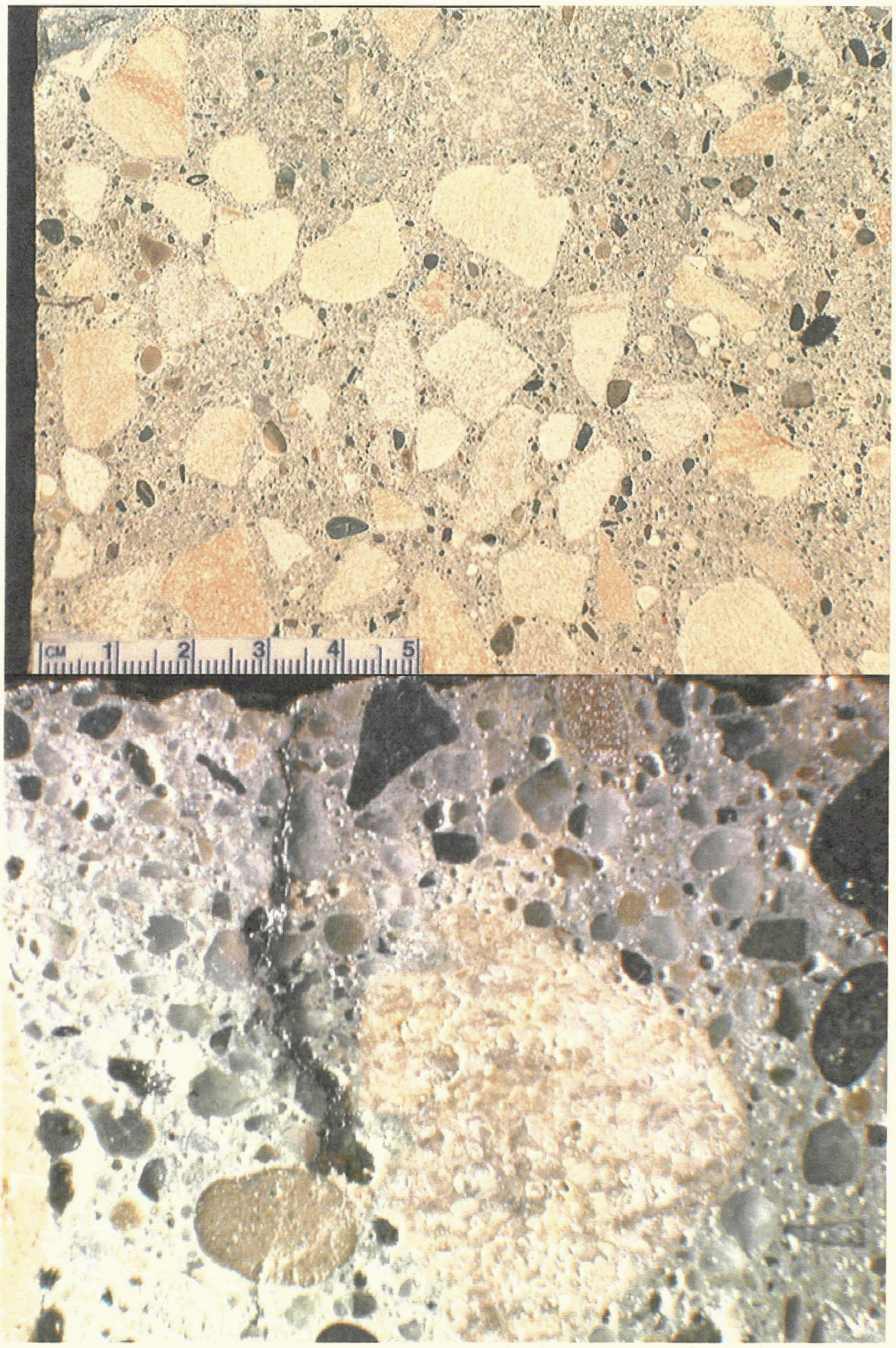

Figure 40. Surface crack in core 12 (approx. center-left) appears to be entirely within the mortar, and the lower image shows the crack plane through mortar highlighted using ink. 8 mm field width.

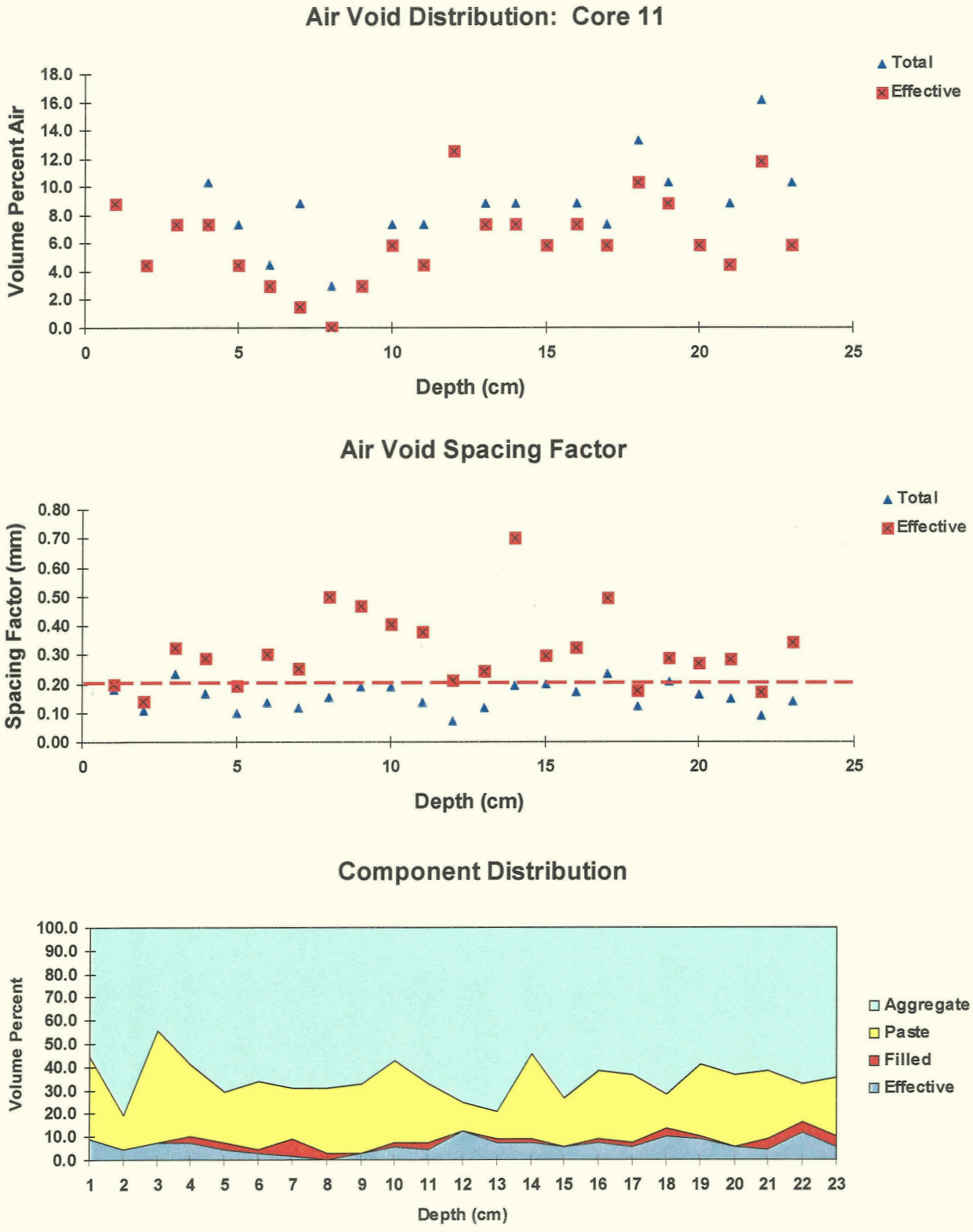

Figure 41: Core 11 air void parameters and component distribution show a loss of air void spacing yet relatively uniform air void volume and materials distribution.

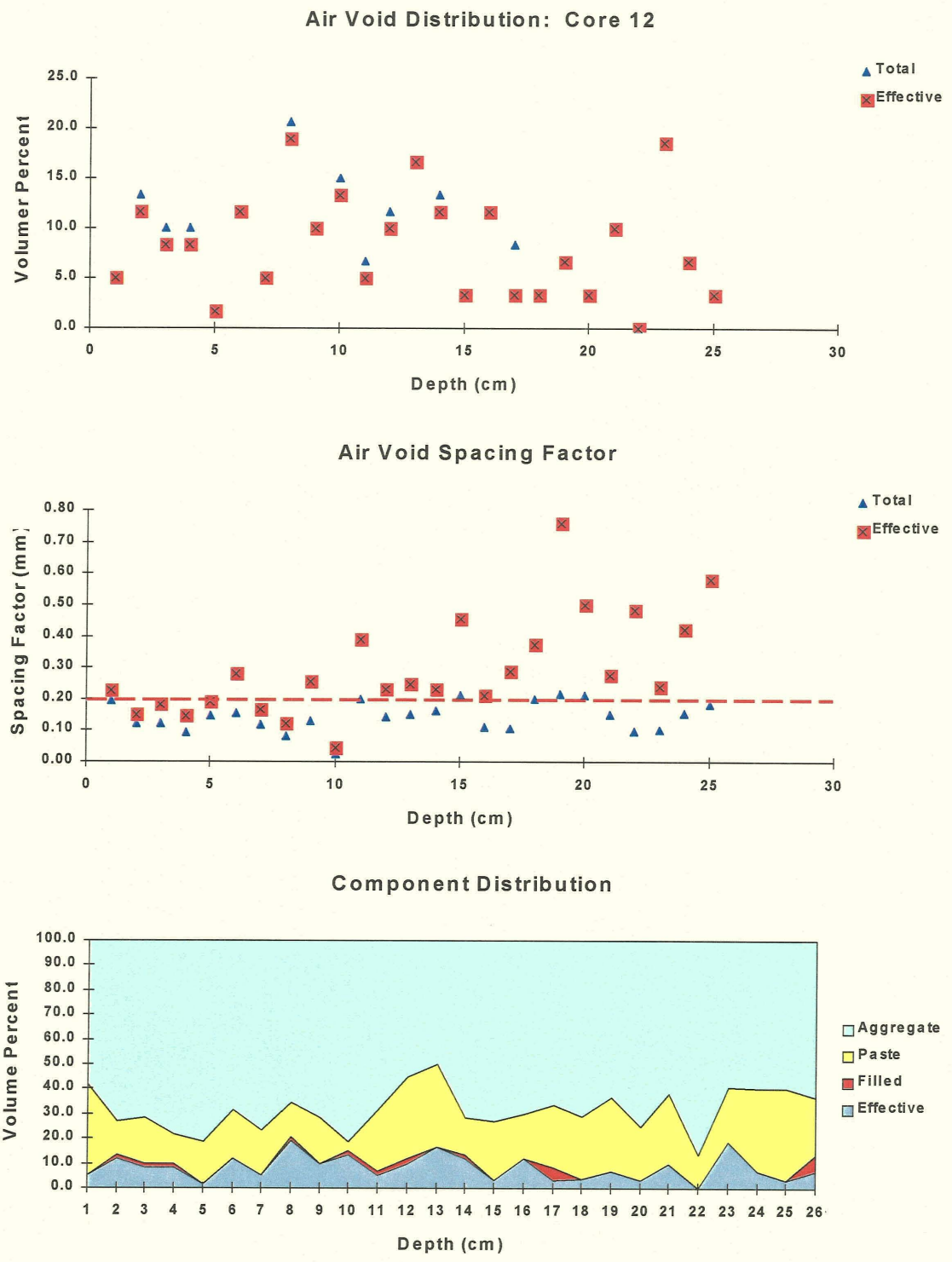

Figure 42. Core 12 air void volume and spacing parameters, and component distribution shows an increased degree of entrained air void filling with depth.

Table 8. I-80, Milepost 210.40: Materials and Properties [28].

	Cement, Type I, SO_3 2.41 %; Equivalent Alkali 0.64 %;	
Coarse Aggregate:	Conklin Quarry, Limestone Freeze-thaw: 5 % loss; LA Abrasion: 39 % loss;	absorption 0.72 %; durability factor 79
Fine Aggregate:	Kimmich Pit (Conklin Quarry)	
Admixtures:	WR; AEA	
Fly Ash:	Class C, 1.97 % SO_3, 1.88 % equivalent alkali 0.25 % loss on ignition	

Concrete Batch Weights:

Cement	299 kg	0.42 w/s	Slump: 76 mm to 19 mm, average- 48 mm Air 10.5 % to 5.4 %,
Water	148		Temps: 37 °C to 12 °C, no rain, clear/warm
Fly Ash	54		CMI SF-550 Slipform paver, hyd. stinger
C.Agg.	900		Mix Characteristics No data located
F.Agg.	896		Strength average 30 MPa
AEA			

Cores:

No.	Mile	Location	Vibrator Trail	Designation	Condition
29	210.40	Midpanel	on	29mb	pattern and longitudinal cracking, distinct vibrator trails.

3.4 Iowa I-80

Core 29 was selected from I-80 to examine microstructural differences of concretes containing distinct vibration trails. Tining appeared uniform on the surface to a depth of about 3 mm. Minor pattern cracking is present along with pronounced vibration trails, and longitudinal cracking along these trails. The pattern cracking density increased close to the longitudinal cracks, running parallel to both the longitudinal cracks and the transverse joints. Core 29 was centered upon one of these cracks and was selected for air void and materials distribution analysis.

Core 29 contains a large surface crack about 0.5 mm wide running parallel to the long axis of the pavement (Figure 43). The crack appears to extend about 40 mm into the core. Other less prominent surface cracks trending vertically extend a few centimeters into the core through the mortar. The plots of air void parameters clearly illustrate the lower half of the core having greater entrained and entrapped air compared to the upper half (Figure 44). These plots also indicate that the spacing factors are substandard the entire depth of the core for both the original and effective air void system. Materials distribution appears fairly uniform with mortar-rich regions common throughout the core. The plot of materials distribution shows a slight increase in paste in the upper half of the core. Cracking observed using optical microscopy appears confined to the upper portions of the core and pass through both the mortar and coarse aggregate. Filling of the entrained air voids occurs in the upper portion of the core and was not seen in the top 4 cm. This may reflect the availability of water along the surface crack. The decrease in filling in the upper-most 4 cm may reflect the zone of drying. The lack of filling in the lower portion of the core may indicate a lack of a microcrack network at depth and / or lack of water at the slab base.

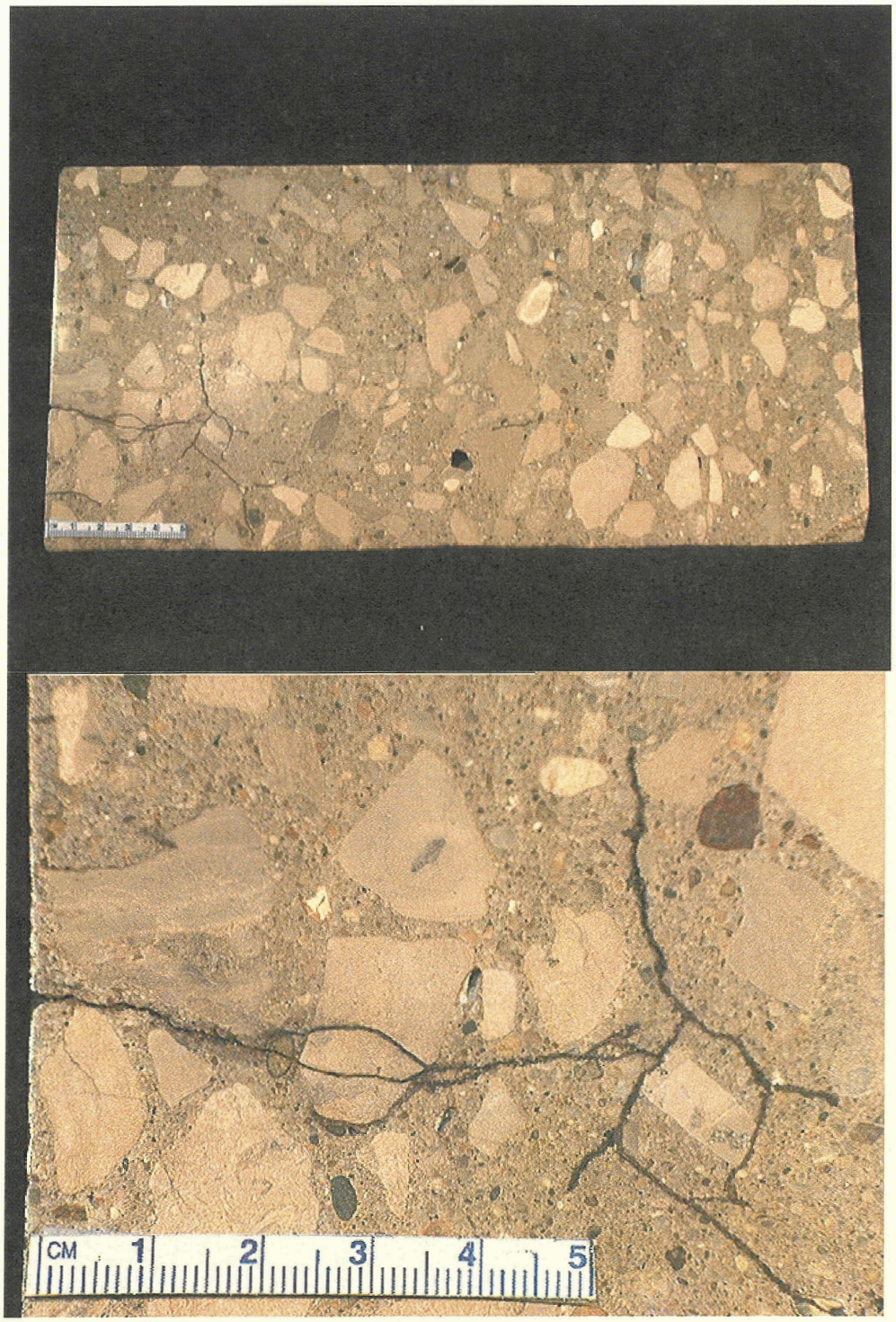

Figure 43. Core 29 cracking near surface passes through both the mortar and coarse aggregate. Cracking also follows close along paste-aggregate interface and is typical of a shrinkage crack. Cracking in aggregate and in the mortar at depth may reflect freeze-thaw damage, as the air void system in the upper half of this core is much poorer than that in the lower half.

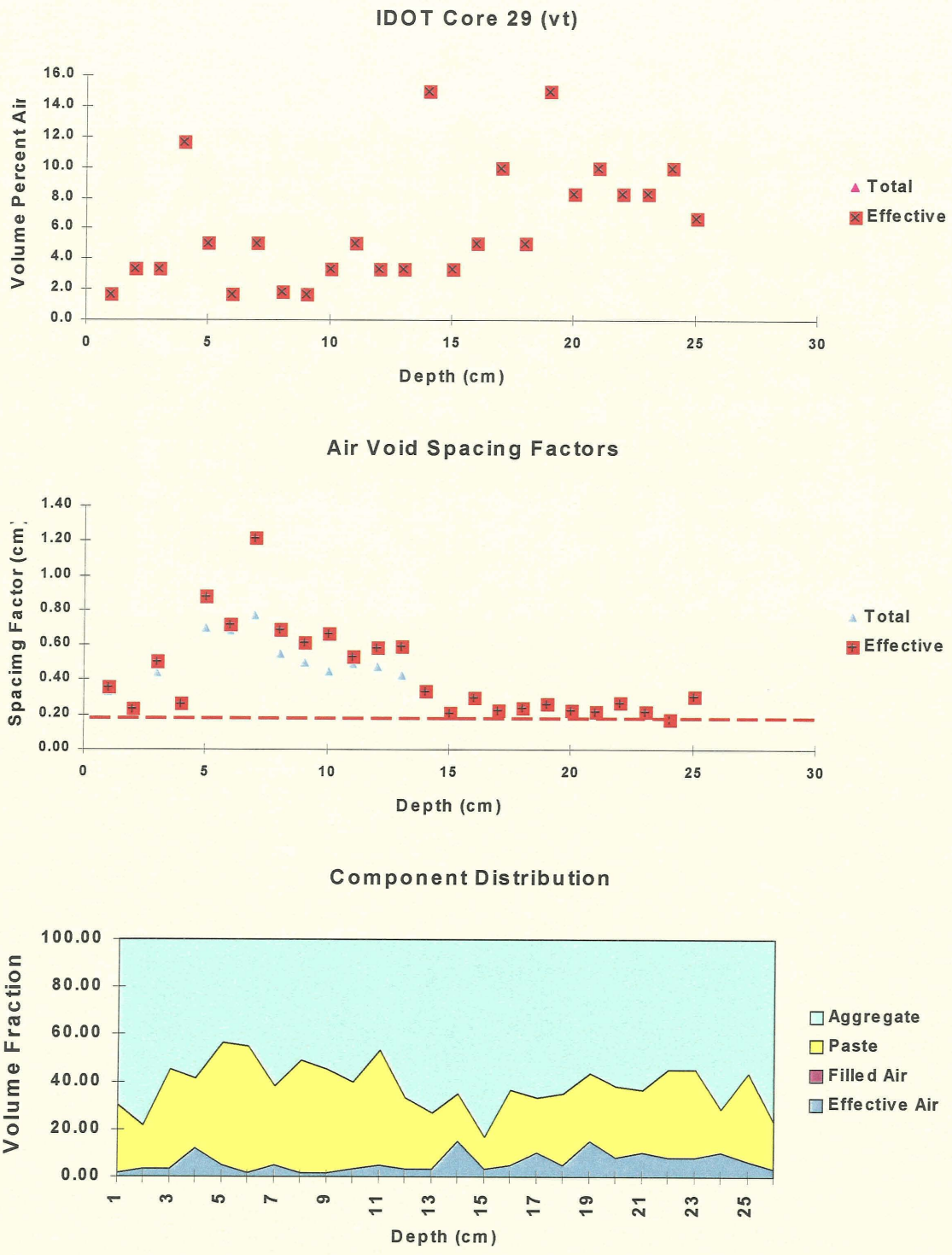

Figure 44. Core 29, centered on a well-defined vibration trail exhibits a significant increase in spacing factor in the upper half. This probably represents the zone of influence of the immersion vibrator probe. Note that the spacing factor is generally not satisfactory at any depth.

4. DISCUSSION AND CONCLUSIONS

4.1 Primary Cause of Pavement Deterioration

Based on visual examinations, petrographic evaluation, and an application of materials models, the deterioration of concrete highway pavements in Iowa appears to be related to a freeze-thaw failure of the coarse aggregate and the mortar. Surface cracks traceable into the coarse aggregate, cracking of coarse aggregate and crack patterns sub-parallel to the concrete surface transecting the mortar fraction and the coarse aggregate are indicative of freeze-thaw damage of these constituents.

The entrained air void system was marginal to substandard, according to recommendations provided in ACI 201. Filling of the finer-sized (<125 μm) entrained air voids by secondary ettringite further degraded the air void system. The filling approaches up to 2 % by volume resulting in an increase in void spacing factor and decrease in specific surface values generally in excess of those considered necessary for freeze-thaw exposure.

4.2 The Significance of Secondary Ettringite

The formation of secondary ettringite within the entrained air voids reflects a relatively high degree of concrete saturation causing the smaller voids to be filled with pore solution when the concrete freezes. Freeze-concentration of dissolved solids in the pore solution and temperature changes may result in a condition contributory to precipitation of secondary ettringite. Over time, the cyclic freezing and thawing accompanied by secondary ettringite precipitation would result in filling of some of the entrained air voids.

The source of material for ettringite formation is probably from dissolution of calcium monosulfoaluminate within the cement paste. The dissolution of these phases (less than 10 % by volume) and subsequent precipitation as ettringite in the air voids may increase permeability of the paste facilitating the deterioration. Calculations on potential volume of ettringite based upon mix design and cement composition estimates indicate that more than sufficient ettringite (8 % to 10%) may be produced as a result of cement hydration to fill the entrained air void system. Therefore, losses of 2 % and less, by volume of the entrained air void system due to secondary ettringite formation, should not be considered to indicate excessive ettringite formation as proposed in some studies [9].

The occurrence of ettringite in concretes is not new, nor unique, and in many cases its presence in voids is attributed to the specimen being from "old concrete". Terzaghi [31] observed secondary ettringite crystallized in air voids in cores extracted from a gate structure of a shipway in Virginia. She considered this to reflect the presence of seawater in the pores of the concrete that provided the conditions necessary for formation of ettringite. Idorn [32] noted that ettringite is a common occurrence in sound, older concretes and will often be found to accumulate in voids and cracks. Trägårdh and Lagerblad [33] examined concretes damaged by a combined alkali-silica reactivity and

freeze-thaw attack. They commonly observed calcium hydroxide and ettringite in air voids and attributed their occurrence to dissolution and leaching caused by water movements during recurrent cycles of freezing and thawing. The dissolved constituents precipitate in cracks and air voids as secondary products.

Taylor [34] examined microstructural and chemical aspects of sulfate reactions in concrete and concluded that the ettringite occurring in cracks and voids in both sound and deteriorated concretes is not necessarily the cause of the cracking but a product of recrystallization in a pre-existing crack or void of some other origin. He states that in early stages of hydration, ettringite is replaced by monosulfate as a result of continued hydration of aluminate. Ettringite is frequently observed in mature concretes, whereas monosulfate is not. Studies using backscattered electron imaging and X-ray diffraction (XRD) at NIST do find monosulfate in mature cement pastes but the XRD data do not exhibit very strong diffraction peaks. This may indicate a poorly-crystalline monosulfate, or changes due to dehydration or relative humidity during powder preparation. Taylor [34] feels that the most likely cause for the presence of ettringite in concretes is from carbonation, resulting in the monosulfate being replaced by a mixture of ettringite and hemicarbonate. He considered the carbonate could come from small amounts of calcite in the gypsum and notes that only 2.4 % (by mass of monosulfate) CO_2 is necessary.

Atkins et al. [35] performed solubility measurements of ettringite ($C_6A\bar{S}_3H_{32}$), hydrogarnet (C_3AH_6), monosulfate ($C_4A\bar{S}H_{12}$), and tetracalcium aluminate hydrate (C_4AH_{13}) and found that dissolution of pure monosulfate lead to the precipitation of ettringite with sucessive dispersions. These findings were in agreement with those of Brown [36] that the tetra-calcium aluminate hydrates are thermodynamically metastable relative to C_3AH_6 and ettringite. C_4AH_{13} was also found to be metastable relative to C_3AH_6.

Ludwig, Stark, and Eckart [37,38,39,40] exposed a suspension of monosulfate in water to freezing and thawing cycles and found monosulfate will transform to ettringite. They considered a change in thermodynamic stability at low temperatures to account for the transformations where formation of ettringite is favored and felt the sulfate required for this reaction was derived through partial decomposition of the monosulfate. They also found that freeze-thaw cycling in 3 % NaCl solution resulted in transformation of monosulfate to Friedel's salt and ettringite. In these experiments, they observed no indications of carbonation, and thought the SO_3 required for ettringite formation may come from the conversion of monosulfate to monochloride. The apparent uniform distribution of Friedel's salt in the Iowa cores would indicate, for these pavements, that either the chloride was present upon mixing or, less likely, that they have been permeated by a road salt solution.

Skalny et al. [41] discuss ettringite formation in concrete as a consequence of an aging via Ostwald ripening. They consider a high moisture content to facilitate this process of dissolution, transport, and recrystallization into the available empty spaces and, that this mode of ettringite formation is non-expansive. Neville [49] also recognizes the role of excess moisture in this process as hydration products may only be formed in water. The

formation of ettringite in the air voids therefore must indicate they are at least partially filled with water.

Detwiler and Powers-Couche [42] examined the effects of sulfates in concrete on its resistance to freezing and thawing through a series of laboratory freeze-thaw tests using both 3 % NaCl and 3 % NaCl and gypsum solutions. They concluded that the freeze-thaw damage precedes the filling of voids with ettringite with deposition occurring in cracks and voids after damage occurred. These data do not explain the occurrence of filled voids in concretes from this study where filled voids may be observed in concretes exhibiting little or no damage, but they do show how easily the formation of secondary ettringite in voids can occur in concretes exposed to cyclic freezing and thawing.

4.3 Freezing and Thawing

Freeze-thaw cracking of aggregate may be related to both the high degree of saturation and the loss of the adjacent air void system as no correlation between aggregate lithology and cracking was noted. Modeling simulations of deterioration processes indicate that cracking may be explained by both aggregate and paste expansions.

Wang et al. [43] found that ice did not completely fill the pores in cement paste and that supercooled water was always present due to alkalinity of the cement paste. Ice propagation in aggregates is faster than in cement paste and at -10 °C, ice was found in large pores but not small ones. Excess water in aggregates is expelled when concrete is frozen. Depending on size, permeability, and aggregate saturation, water flow from the aggregate may be too rapid to diffuse into the surrounding paste creating a pressure that may disrupt the paste at the paste / aggregate interface. Ice formation is from pure water so pore solution becomes increasingly concentrated. This creates an osmotic pressure that may be sufficient to result in failure.

The original air void system parameters generally appear to be uniform from top to base of the concrete. The excessive vibration, considered to be contributory [9], appears to not have adversely affected the entrained air void system for specimens taken away from the direct points of immersion probe vibrator insertion. The single vibrator trail specimen showed a substandard entrained air void system in the upper third of the core, and at the depth of the probe. Joint specimens exhibiting greater filling of the entrained air voids, which may reflect greater water availability to concrete adjacent to joints. The filling of the entrained air void system generally appears uniform with depth, although some mid-panel specimens appear to have increased filling with depth. These observations suggest that the degradation is not a "top down" process by infiltration of gypsum-contaminated road salt solutions. The increased filling at depth of some of the mid-panel specimens indicates a significant influence of surface drying and / or a source of water at the base of the slab. The low-permeability base may actually have facilitated deterioration by wicking water to the base of the pavement or by hindering drainage.

Entrained air affects plastic concrete by providing a potential for improved workability, improved resistance to segregation, settlement, and bleeding. The improvement of these

properties is dependent upon the total air volume, the size distribution and dispersion of the voids, and the material properties of the concrete. However, the primary purpose of the entrained air void system is to facilitate frost resistance in hardened concrete. Air voids, being much larger than the capillary pores, remain open with water filling them only at sub-freezing temperatures, or when under pressure [44].

Early theories of frost damage in concrete were based upon the expansion of ice upon freezing and the subsequent stress increase [45]. Later, consideration that concretes contain enough air space to accommodate this expansion resulted in thoughts that stresses are produced by the flow of the water during freezing. The development of an entrained air void system for protection of concrete allowed room for excess water to migrate upon freezing. Finally, an osmotic pressure theory was developed based upon ice formation in voids leaving an alkali-concentrated supercooled water. Subsequent movement of this unfrozen water toward the air voids may create an osmotic pressure sufficient for concrete disintegration. Other factors in frost damage that must be considered are the availability of water, with the volume of freezable water (the degree of saturation) influenced by initial porosity, concrete age, curing conditions, and environmental exposure [44].

ASTM C 457 [46] provides a means to measure air-void size and size-distribution. Entrained air void bubble sizes range from a few micrometers to one millimeter. Larger-sized voids, while contributing to frost resistance, are considered to be entrapped air. The total paste volume protected by these large voids is much less than that for the smaller voids. The air volume is a measure of the total volume of the air bubbles in the hardened concrete. The spacing factor, considered to be the most significant measure of frost resistance, is defined as the theoretical maximum distance from any point in the paste to the edge of the nearest air void. ASTM C 457 recommends a spacing factor between 0.10 mm to 0.20 mm and notes that these values are for moderate exposures. Concretes in more severe environments, such as pavements that may be exposed to water upon freezing, may require smaller values than those stated here. Specific surface is comparable to "fineness" in cements, and is calculated by dividing the cumulative surface area of the voids by their cumulative volume. This variable is expressed as a surface area per unit volume with higher values indicating a finer size distribution. ASTM C 457 provides acceptable values for typical concrete being 24 mm^2/mm^3 to 43 mm^2/mm^3.

Freezing of water within aggregate pore systems may also pose problems in concrete durablity [45, 47]. Similar to freezing of water in cement paste, saturated aggregate pore systems will expel water during freezing. This may result in a hydraulic pressure induced stress within the aggregate and in the aggregate / cement paste interfacial zone. The 'onion skin'-appearing failure of many of the aggregates may result from this pressure. This effect is increased with aggregate size and is influenced by freezing rate and degree of saturation. T.C. Powers reports that the effects of entrained air in accommodating pressures from freezing of aggregates appear to be minimal [45].

The influence of immersion-type vibrators on the entrained air void system has been shown to have a limited zone of influence. Simon et al. [48] demonstrated that concrete

close to the immersion probe may experience a reduction of 50 % of the total air and a 100% increase in specific surface. They found a decrease in the large entrained air voids at the point of insertion, along with an increase in small air voids. They concluded that some of the larger bubbles are being broken up into smaller bubbles. However, beyond a radius of 125 mm, vibration has little effect on air void systems. For the Iowa concretes, the air void system quality, if judged primarily on spacing factor did not appear to be adversely affected by vibration outside of the vibrator trails, and in many cases was improved near the surface. The core taken directly from a vibrator did exhibit a sub-standard air void system for about half of its depth, roughly the probe immersion depth.

Mehta and Monteiro [47] indicate that aggregate gradation affects the volume of entrained air, whose volume may be decreased by excess sand and the presence of fine-sized mineral admixtures. Mixing, transportation, and placement procedures need to be optimized as insufficient mixing, over mixing, excessive transport and handling time, and over vibration all can reduce the air void system.

Neville [49] also acknowledges the influence of mixing on air content: "the cement should be well dispersed and the mix uniform before the air entraining agent is introduced. If the mixing time is too short, the air entraining agent does not become sufficiently dispersed, but overmixing may expel air - there is an optimum mixing procedure."

Kosmatka and Panarese [50] identify mixing action as one of the most important factors in production of entrained air in concrete. The lack of a suitable entrained air void system in most of these cores indicates a need to examine the effects of production procedures on the development of the entrained air void system.

4.4 Microcracking

Microcracking in the form of drying shrinkage, or freeze-thaw cracks is common in most of the cores as vertical surface cracks extending 10 mm to 20 mm into the core. These cracks may be found both exclusively in the cement paste, and also through the paste and coarse aggregate. Cracks along the vibration trails appear to be drying shrinkage cracks resulting from the greater shrinkage potential of the mortar-rich vibration trail regions and the bulk concrete. The pattern cracking observed on the surface may result from similar phenomena. Cores through vibration trails exhibit a lower entrapped air volume, poor air void distribution in upper half, and appear to be enriched in the mortar fraction due to segregation.

Bakharev and Struble [51] examined microstructural features associated with freeze-thaw deterioration. An early manifestation was microcracking extending vertically several mm into the specimen. Additional freeze-thaw cycles resulted in a horizontal cracking that, when intersecting the vertical cracks, resulted in spalling. They considered the crack development to result from localized expansive shear stresses from hydraulic pressure and localized stresses from differential volume changes. They postulate as the top layer of the concrete is frozen, water is expelled to the surface and to the interior causing

hydraulic pressure. As the permeability of the frozen surface layer is low, water moves inward. Horizontal crack development may be due to development of shear forces at some distance from the surface due to differential volume change of saturated and unsaturated layers, that is, the surface layers are expanding while unsaturated interior layers may be contracting.

4.5 Alkali-Aggregate Reaction

Alkali-silica reaction affects the shale and an occasional quartz sand grain in the fine aggregate, but is not deemed to be significant cause of the deterioration. The field survey found no evidence of permanent expansion such as closure of joints, blowups, nor gel efflorescence. The cement paste pore structure adjacent to the shale grains appears filled with reaction product, with only minor cracking (about the length of the sand grain). The accommodation of reaction products by the cement paste pore structure may have limited expansive stresses created by the reaction of the shale with alkali hydroxides in the pore solution. Significant cracking associated with ASR may occasionally be found when a large (5 mm) shale aggregate is located in the upper-most 20 mm of the concrete.

4.6 Delayed Ettringite Formation

Delayed ettringite formation was not deemed likely as no evidence of a uniform paste expansion away from aggregates was observed, no massive agglomerations of ettringite in the paste, near aggregates, or in cracks, and no filling of the capillary pore system was observed. The lack of a permanent expansion, as mentioned above, is also evidence against this mode of deterioration.

4.7 Fly Ash

The utilization of fly ash does not appear to have significantly affected the deterioration as 1) earlier test pavements (Iowa 175) incorporating fly ash are sound, 2) a US 20 pavement considered sound, around mile post 124, utilized concrete containing fly ash.

Test pavements on I-175, utilizing Class F and C fly ashes and a control section, exhibiting good performance are characterized by a good entrained air void system and some material heterogeneity. Cracking in one core bottom occurs in regions exhibiting filling of the entrained air voids with secondary ettringite. Spacing factors and specific surface estimates in the core base appear adequate, that is, indicates a freeze-thaw resistant concrete. Therefore, this damage indicates the lower portion of the concrete was critically saturated, probably with the water source at its base. US 20 pavements are among some of the best and worst performing pavements in this study. A set of specimens, reportedly containing the same materials (including fly ash) and the same mix design, exhibit opposite performance characteristics. Cores extracted from the undamaged stretch of the road appear to have a smaller coarse aggregate maximum size and a more uniform aggregate gradation. These cores contain an entrained air content almost double, and a spacing factor half that of the failed pavement. The additional air volume may account for the improvement in spacing factor and resulted in an air system

adequate for freeze-thaw protection. Specific surface values for these pavements still indicate a coarse-sized entrained air void system. The change in aggregate gradation may have altered the mix rheology and facilitated development of a more protective entrained air void system.

The influence of the mix design, mixing, and placing must be evaluated with respect to the development of an adequate entrained air void system, concrete homogeneity, long-term drying shrinkage, and microcracking. A high-sand mix may contribute to the field-observed harsh mix characteristics and exacerbate concrete heterogeneity, difficulty in developing an adequate entrained air void system, poor consolidation potential, and increased drying shrinkage and cracking. The availability of moisture, in particular to the base of the pavement slab, must also be considered, as excess water is necessary for these failures.

5. ACKNOWLEDGEMENTS

The support of the State of Iowa, the Portland Cement Association, and the National Institute of Standards and Technology is acknowledged. The assistance of Dr. Steven Forester and Marcia Simon of the Turner-Fairbanks Research Laboratory of the Federal Highway Administration provided access to their air void analysis system. The assistance of Vernon Marks and the Iowa Department of Transportation during the field study and collection of the cores was appreciated. The assistance of the reviewers, James Clifton, Clarissa Ferraris, and Steve Lane is appreciated.

The contents of this report reflect the views of the author, who is responsible for the facts and accuracy of the data presented. The contents do not necessarily reflect the views of Iowa DOT or the Portland Cement Association.

Appendix A

Estimate of Potential Ettringite Formation in Concrete

I. Physical Properties of Cementitious Materials Relevant to Ettringite Formation.

Phase	Molar Volume (cm^3/mole)	Molecular Weight (g/mole)	Specific Gravity (g/cm^3)
Ettringite	735.0	1249.5	1.70
C_3A	89.1	269.9	3.03
C_4AF	128.0	477.4	3.73
Gypsum	74.2	172.1	2.32

To determine the potential volume fraction of ettringite in concrete, we find:

$$(1)\quad \frac{m^3\ ettringite}{m^3\ concrete} = \frac{Mg\ ettringite}{1.7 \times m^3\ concrete}$$

Assuming each mole of C_3A or C_4AF forms one mole of ettringite we can write:

$$(2)\quad = \frac{\frac{1249.5}{269.97} \times MgC_3A + \frac{1249.5}{477.44} \times MgC_4AF}{1.7 \times m^3 concrete}$$

$$(3)\quad = \frac{\left(\frac{1249.5}{269.97} \times C_3Acontent + \frac{1249.5}{477.44} \times C_4AFcontent\right) \times Mgcement}{1.7 \times m^3\ concrete}$$

$$(4)\quad = \frac{\left(\frac{1249.5}{269.97} \times C_3Acontent + 1.5395 \times C_4AFcontent\right) \times Mgcement}{m^3\ concrete}$$

Examples using median values of Iowa concrete cements

US 20: C_3A= 0.0864, C_4AF 0.0541, Air = 7 %
Cement content calculated at 0.2906 Mg cement/m^3 concrete
Substituting into equation 4, the potential ettringite volume fraction of 0.0926 m^3 ettringite / m^3 concrete is greater than the 0.07 (7%) air void content

US 218: C_3A = 0.066, C_4AF = 0.0541, Air Content = 6.5 %
Cement Content = 0.3362 Mg cement / m^3 concrete
Potential ettringite volume fraction of 0.0957 m^3 ettringite / m^3 concrete is greater than the .0065 (6.5%) air void content.

The potential ettringite volumes exceed that of the air void system. This suggests that the entire entrained air void system could potentially be filled by ettringite (if sufficient sulfate is available) and so, the 2 % maximum volume filling observed in the cores does not necessarily indicate an external sulfate source.

6. REFERENCES

[1] Jones, K., "Evaluation of Deterioration on US 20 in Webster County," Iowa Department of Transportation Project MLR-91-1, 1991, 28 pp.

[2] Ouyang,C., " Possible Reasons for Pavement Cracking of Highway US-20," Iowa Department of Transportation Project. Iowa DOT Internal Report, April 26, 1994.

[3] J.M. Pitt, M.C. Schluter, D-Y. Lee, and W. Duberkee, "Sulfate impurities from deicing salt and durability of portland cement mortar," Transportation Research Record 1110 (1987) pp. 16-23.

[4] D. Stark, "Investigation of Pavement Cracking in US 20 and I 35, Central Iowa," Report to Iowa Concrete Paving Association, 1992, 20 pp.

[5] N. Thalow, "Petrographic analysis of 6 concrete cores, highway 520, Iowa," G.M. Idorn Consultants final report, Job 960734, Ref. No. 960734r.001, August, 1996, 21 pp.

[6] D. E. Kofoed,Report on Project 793-587 to the Iowa Concrete Paving Association, "Highway 520 IDOT Materials Task Group," 1993, 48 pp.

[7] V.J. Marks, "Characteristics of Iowa Fine Aggregate," Final Report for Research Project MLR-92-6, Iowa Department of Transportation, April 1996

[8] ASTM C 1260, Standard Test method for Potential Alkali Reactivity of Aggregates (Mortar-Bar Method), Annual Book of ASTM Standards, 4.02, Concrete and Aggregates, American Society for Testing and Materials.

[9] V.J. Marks and W.G. Dubberke, "A Different Perspective for Investigation of PCC Pavement Deterioration," Paper No. 960414, 75th Annual Meeting, Transportation Research Board, Washington, D.C., January 7-11, 1996.

[10] Von J. Stark and H.-M.Ludwig, "Die rolle von phasenumwandlungen im zementstein beim frost- und frost- tausalz-angriff auf beton, Zement Kalk Gips International.

[11] S. Schlorholtz and J. Amenson, "Evaluation of Microcracking and Chemical Deterioration in Concrete Pavements," Iowa DOT Project HR-358, ERI Project 3711, Final Report, October 31, 1995, 90 pp.

[12] D. Gress, "Recommendations for mitigating early distress in concrete pavements," Presentation to the ASR Committee, June 26, 1996

[13] C. Ouyang and O.J. Lane, "Freeze-Thaw Durability of Concretes With and Without Class C Fly Ash," in Materials for the New Millennium, Vol. 2, ed. K.P. Chong, American Society of Civil Engineers, New York, 1996, pp. 939-948

[14] C. Ouyang and O.J. Lane, "Freeze-thaw durability of concretes with infilling of ettringite in voids," Final report for MLR-94-9 - Phase 2, Iowa Department of Transportation, April, 1997, 48 pp.

[15] Northwestern University Pooled Fund Study of Premature Rigid Pavement Deterioration, 1997

[17] Distress Identification Manual for the Long-Term Pavement Performance Project, Strategic Highway Research Program Publication No. SHRP-P-38, 1993, 147 pp.

[18] F. Lallard, LCPC Personal Communication.

[19] J.M. Shilstone, Sr., Personal Communication.

[20] J.M. Shilstone, "Optimizing Concrete Mixtures," Concrete International, pp. 33-38, June, 1990

[21] V.J. Marks, Engineer, Iowa Department of Transportation, personal communication.

[22] H.F.W. Taylor, Cement Chemistry, Academic Press, San Diego, CA, 1990 475 pp.

[23] ASTM C 856, "Standard Practice for Petrographic Examination of hardened Concrete," Annual Book of ASTM Standards 4.02, Concrete and Aggregates

[24] H.N. Walker, "Petrographic Methods of Examining Hardened Concrete: A Petrographic Manual," FHWA/VA-R14 report, 286 pp., May, 1992

[25] ASTM C 457, "Standard Test Method for Microscopical Determination of Parameters of the Air-Void System in Hardened Concrete," Annual book of ASTM standards Vol. 4.02, The American Society for Testing and Materials,

[26] A.B. Poole and A. Thomas, "A staining technique for the identification of sulphates in aggregates and concretes," Mineralogical Magazine, September 1975, Vol. 40, pp. 315-16

[27] Simon, M., MS-Bubble instruction manual. Federal Highway Administration Turner-Fairbanks Laboratory, McLean, VA.

[28] Northwestern Pooled Pavement study

[29] E.J. Garboczi, " Stress, displacement, and expansive cracking around a single spherical aggregate under different expansive conditions," Cem. Conc. Res. 27, 495 (1997).

[30] E.J. Garboczi, "Finite element and finite difference programs for computing linear electric and elastic properties of digital images of random materials, NIST Tech Note, in press, (also http://ciks.cbt.nist.gov/garboczi/, Chapter 2.

[31] R.D. Terzaghi, "Concrete deterioration in a shipway," Jour. Am. Concrete Inst. Vol. 19, No. 10, June 1948, pp. 977-1005

[32] G.M. Idorn, "Durability of concrete structures in Denmark," Dissertation, pp. 208, Technical University of Denmark, Copenhagen 1967.

[33] J. Trägårdh and B. Lagerblad, "Influence of ASR cracking on the frost resistence of concrete," Swedish Cement and Concrete Research Institute CBI Report 1:96

[34] H.F.W. Taylor, "Sulfate Reactions in Concrete – Microstructural and Chemical Aspects," in Ceramic Transactions Vol. 40, Cement Technology, eds. E.M. Gartner and H. Uchikawa, American Ceramic Society, 1994, pp. 61-78

[35] M. Atkins, D. Macphee, A. Kindness, and F.P. Glasser, "Solubility properties of ternary and quaternary compounds in the CaO-Al2O3-SO3-H2O system," Cement and Concrete research, Vol. 21, pp. 991-998, 1991

[36] P.W. Brown and J.V. Bothe, Jr., "The Stability of Ettringite," Advances in Cement Research, 1993, **5**, No. 18, pp. 47-63.

[37] H.-M.Ludwig and J. Stark, "Effects of low temperature and freeze-thaw cycles on the stability of hydration products," 9th International Congress on Chemistry of Cement FINISH THIS REF

[38] J. Stark, A. Eckart, and H.-M. Ludwig, Influence of C_3A content on frost and scaling resistance," *in* Frost Resistance of Concrete, eds. M.J. Setzer and R. Auberg, E & FN Spon, London.,

[39] J. Stark and H. -M. Ludwig, "Die rolle von phasenumwandlungen im zementstein beim frost- und frost-tausalz-angriff auf beton," Zem. Kalk Gips 49, No. 11, pp. 648-663.

[40] J. Stark, Frost resistance with and without deicing salt - a purely physical problem?," *in* Frost Resistance of Concrete, ed. M.J. Setzer and R. Auberg, 1997 E & FN Spon, pp. 83-99.

[41] J. Skalny, V. Johansen, N. Thalow, A. Palomo, "DEF: As a form of sulfate attack," Materiiales De Construccion, Vol. 46 no. 244 Dec. 1996.

[42] R.J. Detwiler and J.J. Powers-Couche, "Effect of sulfates in concrete on its resistance to freezing and thawing," PCA R & D Serial No. 2128b, 25 pp., 1997.

[43] K. Wang, P.J.M. Monteiro, B. Rubinsky and A. Arav, "Microscopic study of ice propogation in concrete," ACI Materials Journal, Jul-Aug. 1996 pp. 370-377.

[44] K.C. Hover, "Air content and unit weight of hardened concrete," in ASTM STP 169c, Significance of Tests and Properties of Concrete and Concrete-Making Materials, P. Klieger and J.F. Lamond, eds, pp. 296-314.

[45] T.C. Powers "Freezing Effects in Concrete," Durability of Concrete, ACI SP 47, 1975 pp. 1-11

[46] Standard Test Method for Microscopical Determination of Parameters of the Air-Void System in Hardened Concrete, ASTM C 457 - 90, American Society for Testing and Materials Annual Book of Standards, Vol. 4.02.

[47] P.K. Metha and P.J.M. Monteiro, Concrete, Prentice Hall, Englewood Cliffs NJ 1996.

[48] M.J. Simon, R.B. Jenkins, and K.C. Hover, "The influence of immersion vibration on the void system of air entrained concrete," ACI AP 131-4 pp. 99-126.

[49] A.M. Neville, "Properties of Concrete, 4th ed., Wiley, New York, 1997 844 pp.

[50] S. H. Kosmatka and W.C. Panarese, Design and Control of Concrete Mixtures, Portland Cement Association 1994.

[51] T. Bakharev and L.J. Struble, "Microstructural features of freeze-thaw deterioration of concrete," Mat Res. Soc. Symp. Proc. Vol 370, 1995 MRS, pp. 83-88.